NTNU

Norwegian University of
Science and Technology

Study of the Effect of Added Soil Mass on Earthquake Response of Subsea Structures on Closed Caisson Foundations

Anders Stensløkken

Civil and Environmental Engineering
Submission date: June 2016
Supervisor: Gudmund Reidar Eiksund, BAT
Co-supervisor: Corneliu Athanasiu, Multiconsult ASA

Norwegian University of Science and Technology
Department of Civil and Transport Engineering

NORWEGIAN UNIVERSITY OF SCIENCE AND TECHNOLOGY
DEPARTMENT OF CIVIL AND TRANSPORT ENGINEERING

Report Title:	Date: June 10, 2016			
Study of the Effect of Added Soil Mass on Earthquake Response of Subsea Structures on Closed Caisson Foundations	Number of pages (incl. appendices): 117			
	Master Thesis	X	Project Work	

Name:

Anders Stensløkken

Professor in charge/supervisor:

Professor Gudmund Reidar Eiksund, NTNU

Other external professional contacts/supervisors:

Dr. Corneliu Athanasiu, Multiconsult ASA

Abstract:

Earthquake related design activities of subsea closed caisson foundations require analyses of intricate soil-structure interaction effects. The complexity give rise to both advanced and simplified analytical tools. Today numerical approaches such as the finite element method are most commonly used. Although many analytical and simplified methods have been developed, no standardized approach is established for caisson foundations.

At the ISFOG-conference held in Oslo 2015, the Simplified Modal Non-linear Analysis was introduced. The method use springs to represent the subgrade in a two degree of freedom system. Based on force-displacement and moment-rotation relations from external soil-caisson analyses, secant spring stiffness are used. An iterative modal analysis procedure is then conducted, giving non-linear properties to the springs. Relevant accelerations are retrieved from an acceleration response spectrum. Dynamic force and overturning moment are calculated with corresponding lateral displacement and rocking motion.

Foundation mass and soil added mass have been neglected in previous studies of the SMNA-method. This work is a parametric study to further develop the method studying inertial effects. Numerical analyses are first conducted in PLAXIS 3D, which provide indicative results. The simplified model is then calibrated based on consistency with the numerical model.

The initial SMNA-results show very low dynamic forces and excessively large moments, when soil added mass are introduced. The divergent tendencies indicate too high ratio of rotation to translation stiffness. In order to achieve compliance in the results a reduction in mass, mass moment of inertia and soil stiffness are needed.

Keywords:

1. Earthquake
2. Soil-structure interaction
3. Added mass
4. PLAXIS 3D
5. Caisson foundations

Preface

The work presented is my Master's thesis conducted at the Norwegian University of Science and Technology. The thesis represents the end of my five years at the MSc programme in Civil and Environmental Engineering in Trondheim. The work was carried out during the spring semester in 2016 after a preliminary literature study completed the fall of 2015.

The problem formulation was proposed by Dr. Corneliu Athanasiu at Multiconsult in Oslo, who also served as my supervisor alongside Professor Gudmund R. Eiksund at NTNU. The work is part of a larger research project under development aiming at a more effective earthquake design of subsea structures and their foundations.

Courses within geotechnical engineering and structural dynamics has influenced my academic interest towards earthquake related subjects over the last two years. I am therefore thankful that I got the opportunity to conduct a thesis within these fields. The work has been challenging but provided useful knowledge in both numerical modelling and analytical methods. I hope that my work can contribute to further development within the research and that my experiences will be useful in the future.

Trondheim, 2016-06-10

Anders Stensløkken

Acknowledgment

First of all I would like to thank Dr. Corneliu Athanasiu and Dr. Steffen Giese at Multiconsult for providing the problem formulation and continuous guidance along the way. From the very beginning you have been very welcoming and facilitated a good collaboration.

I also want to thank my main supervisor Professor Gudmund R. Eiksund for daily counseling at the university. Your contributions has given me a better insight in my problems and pushed my work forward in stagnant periods.

Last but not least, thanks to Professor Steinar Nordal, Professor Gustav Grimstad and Adjunct Professor Amir M. Kaynia for good advice and providing useful literature during this process.

A.S.

Summary

Skirted caissons are frequently used as foundations in the offshore industry. It was first introduced as a gravity based foundation in the early 1980's related to the development of the first oil platforms in the North Sea. Over the last two decades the concept has shown applicability in deepwater manifolds, jackets and offshore wind turbines.

Dynamic soil-structure interaction are traditionally analyzed numerically, analytically or a combination of the two. Analytical methods can either evolve from advanced mathematics or rather simple physical spring models. Simplified methods are generally more efficient than numerical models. They also provide useful insight and a better understanding of the underlying physical concepts. Although a great number of substructure methods has been developed, no distinctive approach towards closed caisson foundation has yet been established.

As part of an ongoing research project Multiconsult have developed the *Simplified Modal Non-linear Analysis*. This is a simplified method estimating earthquake induced loads and displacements on a superstructure founded on a closed caisson. The method is based on a two degree of freedom system with a lumped mass representing the superstructure. The subgrade is represented through non-linear translational and rotational springs. Non-linearity is maintained through externally obtained backbone curves from static soil-caisson analyses. Modal analyses are conducted on the system, for each iteration the spring stiffness are updated giving rise to new natural frequencies. Dynamic loads and displacements are then retrieved from an acceleration response spectrum. The procedure aims to become an efficient alternative to numerical analyses.

A case study is performed comparing a numerical model and the *Simplified Modal Non-linear Analysis* on a deepwater manifold structure. Assuming that the numerical model is responding correctly, a parametric study is conducted to calibrate amount and distribution of mass used in the simplified analysis. The scope of this work is limited to study one specific structure subjected to one particular earthquake. All numerical earthquake analyses are conducted using linear elastic perfectly plastic Mohr-Coulomb model. Material damping is introduced to the soil using Rayleigh-damping. Hydrodynamic effects and water added mass in the manifold are not considered in this thesis.

The numerical analyses are conducted in PLAXIS 3D and involve three parts: *(1) free-surface analysis, (2) kinematic interaction analysis* and *(3) full analysis.* The free-surface analysis is done by applying accelerations to the bottom of a soil layer and record surface response. Kinematic interaction analysis is done by introducing a massless caisson and record resulting motion at the top plate. Recordings later serve as the foundation input motion in the simplified method.

Then the superstructure is set in place before applying the same accelerations. In this analysis accelerations, displacements and rocking are recorded.

The numerical soil model gave adequate results through correct amplification and reasonable filtering of high frequencies in initial analyses. Kinematic interaction also showed good compliance with theory. Slightly lower accelerations than free-surface and more high frequency filtering was observed. The full model analysis gave maximum responses of 4.9 cm and 0.0010 radians in lateral displacement and rocking respectively. Equivalent loads were calculated to be 1 227.9 kN and 8 598.1 kNm in horizontal force and overturning moment, working at the base of the manifold.

To establish the non-linear spring stiffness relations (backbone-curves), static soil-caisson interaction analyses are carried out using PLAXIS 3D. Horizontal force and overturning moment are applied to the foundation top. The loads are increased at a constant ratio while translation and rotation of the caisson are recorded. Force-displacement and moment-rotation relations are accordingly plotted.

The simplified analyses are carried out using MODAN, a code developed at Multiconsult performing the modal analysis procedure in the *Simplified Modal Non-linear Analysis*. First massless foundation and no added mass are analyzed. Further analyses are done introducing soil added mass stepwise inside the caisson. The results show very low forces and excessively large moments. The divergent tendencies observed indicate a too high ratio of rotation to translation stiffness.

In order to achieve comparable results from the two models reduction in mass, mass moment of inertia and spring stiffness are needed. Best results suggest only to consider manifold mass, and reduce mass moment of inertia with a factor of 0.33. Soil stiffness are reduced accordingly by factors of 0.25 and 0.33 in translation and rotation respectively. The results then give $Q_{dyn} = 2003\ kN$, $M_{dyn} = 9749\ kNm$, $\delta_{dyn} = 0.039\ m$ and $\theta_{dyn} = 0.0019\ radians$, which provide best compliance with numerical results.

Contents

Chapter 1

Introduction

1.1 Background

Earthquakes impose many challenges to the design of subsea strucures and their foundations. Since the development of the first oil platforms in the North Sea in the 1980's a huge effort has been done in the field, leading way for new technology and foundation designs. Gravity based offshore foundations require high demands to seismic resistance, whether to protect sensitive equipment, or prevent disastrous events. The introduction of the closed caisson foundation in 1982 was a breakthrough in the industry due to reliability and easy installation. Today the closed caisson is a frequent choice of seabed foundation for jackets, templates, manifolds and offshore wind turbines.

Traditionally geotechnical earthquake engineering and soil-structure interaction use both analytical methods and simplified models. Some analytical approaches involve advanced mathematics while others simplifies the subgrade using springs such as the Winkler-model, see for example Gerolymos and Gazetas (2006). Hybrid approaches combining numerical and analytical methods are often called substructure methods, such as the multi-step method presented in Kausel et al. (1978). Due to complex geometry and 3D effects, limited efforts has been done to develop good analytical solutions for closed caisson foundations.

Technological development in recent years has led to an increased use of sophisticated numerical tools such as the *finite element method* (FEM). Easy access to powerful computers and well developed software makes this the most commonly used tool in analysing dynamic response today. However, these analyses are often time consuming, expensive and require good insight by the user.

A study conducted by Transparency Market Research (2015) predicts that oil recovery from more complex offshore reservoirs in the years to come will boost the subsea manifold market. Also offshore wind farms will continue to develop. Today more than one hundred

offshore wind farms are planned world wide according to Offshore Center Danmark (2016). These forecasts suggest a high demand of gravity based subsea structures in the future and suggests that more specialized analysis tools could be beneficial.

At the ISFOG-conference held in Oslo 2015, Corneliu Athanasiu at Multiconsult presented the *Simplified Modal Non-linear Analysis* (Athanasiu et al., 2015). The method is presented in chapter 3, and will hereafter be abbreviated as the SMNA-method. The method is based on modal analysis and a simplified spring model, which provide good physical insight to the user. The method intend to be an alternative to numerical analyses and has already shown adequate results, despite significant simplifications of the mass matrix.

Problem Formulation

Analytical soil-structure interaction analyses of subsea structures founded on closed caissons require realistic input of soil added mass inside and around the caisson. This work is a further step in developing the SMNA-method by applying foundation mass and study the effects of soil added mass. The thesis is part of a larger research project in Multiconsult aiming to create more effective design activities related to subsea foundations in the years to come.

The first step of the thesis is to perform numerical analyses in PLAXIS 3D of a manifold structure founded on a closed caisson. Acceleration response spectrum from kinematic interaction analyses will serve as foundation input motion in the SMNA-method. Results from the full analysis is assumed to be the correct dynamic behavior of the structure.

A modal analysis parametric study will then be conducted in MODAN, a software executing the SMNA-procedure. The effects of mass and its distribution will then be studied by varying relevant parameters. The study is aimed to recommend appropriate amount and distribution of mass to be used in modal analyses. The correct combination will be based on similar results as with finite element analyses.

Literature Survey

The thesis originates from a best practice report and the paper by Athanasiu et al. (2015) published and presented at the International Symposium on Frontiers in Offshore Geotechnics III, (Meyer, 2015). The paper introduce the SMNA-method which is a proposed simplified method handling non-linear behavior of closed caisson foundations in earthquake loading. Chapter 3 in this thesis is entirely based on the report by Athanasiu et al..

Although no widely used practical procedure has been established for dynamics analyses of closed caisson foundations, similarities can be found in many well known publications. In the *multi-step method* presented by Kausel et al. (1978) embedded foundations are analysed stepwise making use of superposition. Kinematic and inertial interaction gives foundation input while the subgrade are represented as a simplified spring model. Dynamic soil stiffness and damping are in these cases represented as frequency dependent impedance functions. Traditionally these functions have been found using analytical half space solutions. Numerous of closed form solutions has been obtained for common foundation designs, see for example Richart et al. (1970) and Luco and Wong (1987).

Due to the complexity of dynamic soil-structure interaction problems the use of simplified methods has been important to understand the main physical effects. A good presentation of spring models used in soil-structure interaction are found in the book *Foundation Vibration Analysis Using Simple Physical Models* (Wolf, 1994). In the Winkler-model the subgrade are represented as a series of independent springs and dashpots connected to the foundation. The model is used in both static and dynamic analyses, see for example Gerolymos and Gazetas (2006). For comprehensive overview of simplified models and their importance, the reader is refered to Dobry (2014).

The theory presented in chapter 2 are based on a study of literature and backround theory towards this thesis. The study was conducted as a student project and focused on theory and methods in geotechnical earthquake engineering, structural dynamics and soil-structure interaction. A brief historical introduction of skirted foundations is also included. The theory are found in well known books within the field, e.g. *Geotechnical Earthquake Engineering* (Kramer, 1996), *Dynamics of Structures* (Chopra, 2007), *Dynamic Soil-Structure Interaction* (Wolf, 1985).

1.2 Objectives

The thesis has four objectives of which the last is considered to be the primary objective. The first three objectives are considered to be secondary objectives.

1. Analyze the dynamic response of a subsea manifold structure founded a closed caisson, subjected to earthquake induced loads, using a numerical time domain analysis performed in PLAXIS 3D.
2. Study inertial effects by varying mass parameters in analyses conducted at the same structure, using the simplified SMNA-approach in frequency domain.
3. Obtain comparable estimations of maximum dynamic displacement, rotation, force and overturning moment from the two different methods.

4. Propose an adequate amount and distribution of mass, including soil added mass, to be considered using the simplified SMNA-method, based on similarity with numerical analysis.

1.3 Limitations

Obtaining a properly functioning numerical model for dynamic earthquake analysis has proven to be a time consuming activity. The scope of this research is therefore limited to involve only one manifold structure subjected to one particular earthquake. Also the calculation time in PLAXIS 3D had to be restricted. This involved use of the linear-elastic perfectly-plastic Mohr-Coulomb soil model and artificial Rayleigh-damping. These simplifications bring some uncertainties to a realistic behavior of the model.

Comparing two fundamentally different approaches require some simplifications in collecting comparable output. In the SMNA-approach a modal analysis decouples two mode shapes an looses time dependency. To estimate maximum response the *square root of the sum of squares* (SRSS) are used. This is a then a statistical approximation of maximum modal response from the two modes at the same time.

Uncertainties are also related to retrieval of dynamic loads from time domain analysis. Inertial considerations was used in this study. Both analysis are conducted assuming the water table to be at seabed level. Hydrodynamic effects and water added mass are therefore not considered.

1.4 Approach

This thesis present a quantitative study in which two conceptually different models are set up against each other. By the assumption that one model gives correct response the other method is adapted based on comparable output from both models.

First the numerical analysis is carried out and assumed to be correct. A parametric study are then conducted on the simplified model calibrating previously neglected mass parameters based on consistency with the numerical results.

Conclusive estimates of inertial parameters to be used in the simplified method are then established.

1.5 Structure of the Report

The report is hereafter divided into two parts structured as follows.

- **Part 1: Theory**
  - Chapter 2: Theoretical Background and Analytical Methods
    The chapter gives an introduction to the theory and well known analytical and numerical approaches related to earthquake engineering.
  - Chapter 3: The SMNA-method
    The chapter presents the basic concept and calculation procedures in the simplified method.
- **Part 2: Case study**
  - Chapter 4: Descripton of Analyses
    The chapter gives a review of the all the analyses conducted in the case study.
  - Chapter 5: Results and Discussion
    The chapter presents the results of all analyses and a discussion of the findings.
  - Chapter 6: Conclusions and Further Work
    The conclusions are made and recommendations for further work are given.

Part I

Theory

Chapter 2

Theoretical Background and Analytical Methods

2.1 Background

Earthquakes involve complicated mechanisms to be analysed by structural and geotechnical engineers. It is necessary to understand wave propagation through soils, soil-structure interaction and resulting structural response. These cases require insight in dynamic differential equations, eigenanalysis and non-linear considerations, concepts that constitutes the majority of the mathematical basis in relevant analytical methods. This chapter first give a brief introduction of the closed caisson foundation, before presenting the fundamental background theory and some of the methods used in earthquake engineering. The chapter is based on a preliminary literature survey conducted towards this thesis.

2.2 Closed Caisson Foundations

A closed caisson foundation is a skirted foundation consisting of a steel cylinder of varying length-diameter and a closing top plate, see figure 2.1. The foundation is penetrated into the ground using gravity and suction from pumping water out of the caisson during installation. The foundation acts as a hybrid between traditional piles and gravity based foundations. The concept was first introduced in the offshore industry by Senpere et al. (1982) in early 1980's. The technology wasn't really accepted at first, due to complications installing the first suction anchors in the Gorm field in 1980 (Tjelta, 2001).

In 1985 the largest offshore penetration test was carried out in the Gullfaks field where 22 meter steel cylinders got penetrated into the seabed at 200 meter depth by suction and submerged weight (Tjelta et al., 1986).

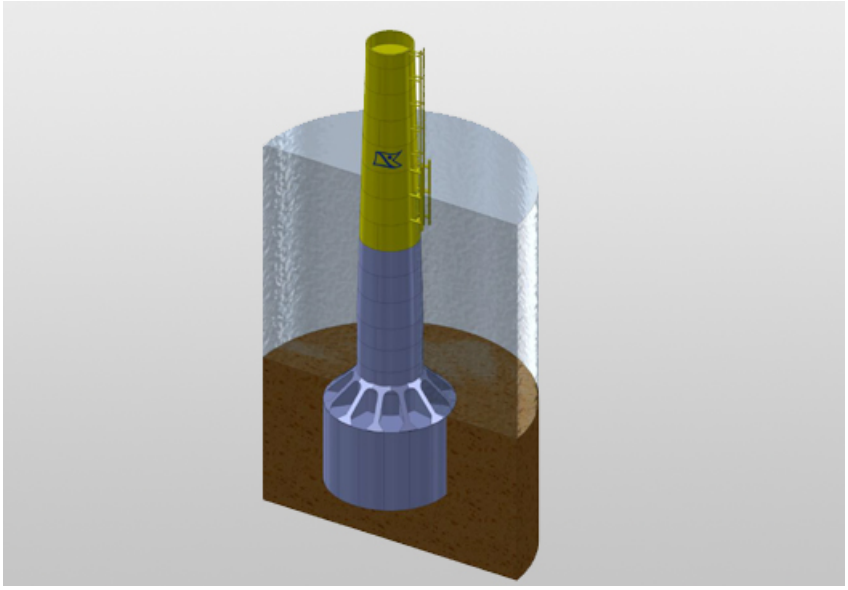

Figure 2.1: Bucket foundation. Figure from SubseaWorldNews.

When Statoil in 1989 started the construction of their platform for the Gullfaks C platform the concept finally got its appreciation. Suction caissons is today a frequent choice of subsea foundations due to reliability, material use, cost efficiency and relatively simple installation procedure. The technology is applicable in most soil conditions and requires little or no preparation on the seabed.

2.3 Seismic Wave Propagation

Seismic waves are devided into body waves and surface waves. Body waves propagates through the interior of the earth and consists of primary waves and secondary waves, see figure 2.2. Primary waves or p-waves are compressional waves with particles travelling in the longitudinal direction of the wave. Secondary waves, or s-waves, has particles moving perpendicular to the travelling direction. S-waves are generally more destructive to surface structures although they propagates in about half the speed of p-waves.

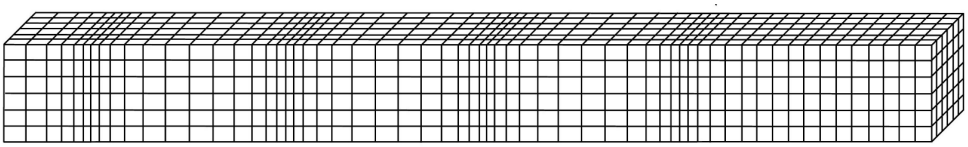

(a) p-waves

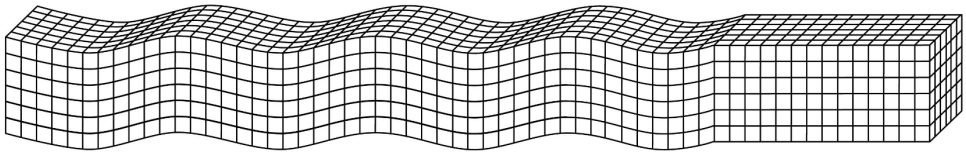

(b) s-wave

Figure 2.2: Seismic body waves.

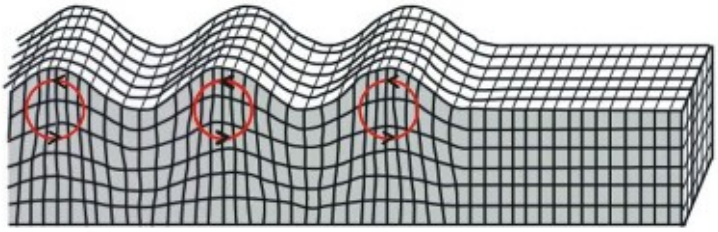

(a) Rayleigh wave

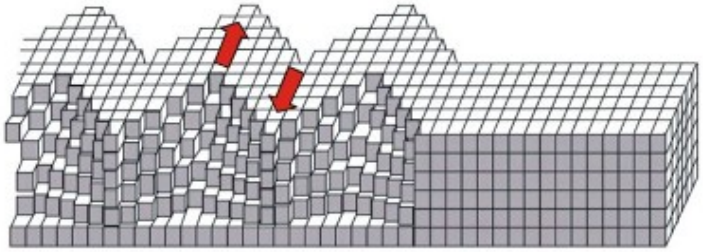

(b) Love wave

Figure 2.3: Seismic surface waves

Surface waves consists of Rayleigh waves and Love waves, see figure 2.3. These waves travel along the earth surface. Rayleigh waves have particle motion in circles like ocean waves while the Love waves travels with side wise particle motion like a snake. Surface waves travels slower than body waves but has predominant amplitudes at great distances.

The travelling motion of body waves can be expressed by the following differential equations derived from the stress equilibrium of an infinitesimal part of a constrained infinite rod, illustrated in figure 2.4, (Kramer, 1996).

$$\frac{\partial^2 u}{\partial t^2} = \frac{M}{\rho}\frac{\partial u}{\partial x^2}$$
$$\frac{\partial^2 v}{\partial t^2} = \frac{G}{\rho}\frac{\partial v}{\partial x^2} \tag{2.1}$$

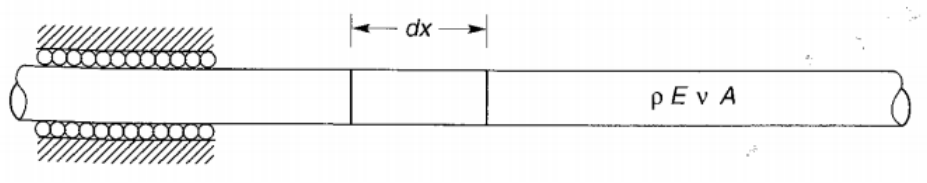

Figure 2.4: Constrained infinite rod (Kramer, 1996).

Where u and v is the longitudinal and perpendicular particle motion respectively, as functions of time and location along the rod. M and G is the constrained and shear modulus while ρ is the material mass density.

Compressional and shear wave velocities can be expressed as follows:

$$V_p = \sqrt{\frac{M}{\rho}} \quad \text{and} \quad V_s = \sqrt{\frac{G}{\rho}} \tag{2.2}$$

Which gives the following simplified differential equations for p-waves and s-waves:

$$\frac{\partial^2 u}{\partial t^2} = V_p^2\frac{\partial u}{\partial x^2}$$
$$\frac{\partial^2 v}{\partial t^2} = V_s^2\frac{\partial v}{\partial x^2} \tag{2.3}$$

2.4 Site Response Analysis

Determination of local effects due to an earthquake some distance away is called site response analysis. Prediction of local ground motion is necessary to obtain useful response spectres, investigating soil strains and estimate earthquake induced forces on structures (Kramer, 1996). Historically it is observed crucial consequences of local soil amplification effects, such as the Mexico City earthquake in 1985, where a selection of structures were especially vulnerable to destruction.

One Dimensional Approach

Site response effects depends on the layering and geometry of the soil deposit at the site. The principles is briefly presented to establish the basis for an approach calculating a simple case of uniformly layered, undamped elastic soil over rigid rock. The approach can be extended to account for more complicated cases including non-linear soil and damping effects.

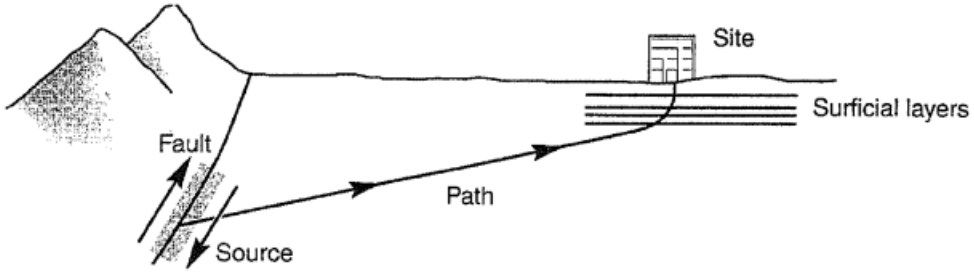

Figure 2.5: Wave propagation from hypocenter to surface (Kramer, 1996).

When earthquake energy is released from the location of a rupture, seismic waves propagate in all directions of which some reaches the surface. Due to increasingly stiffer medium with depth, waves tend bend upwards transmitting into softer layers, according to Snell's law, see figure 2.5. It is therefore common to analyze vertically propagating shear waves in site response analysis. The aim is to determine the surface response of a soil deposit, and the problem narrows down to how the incoming waves amplifies through the soil layer, see figure 2.6.

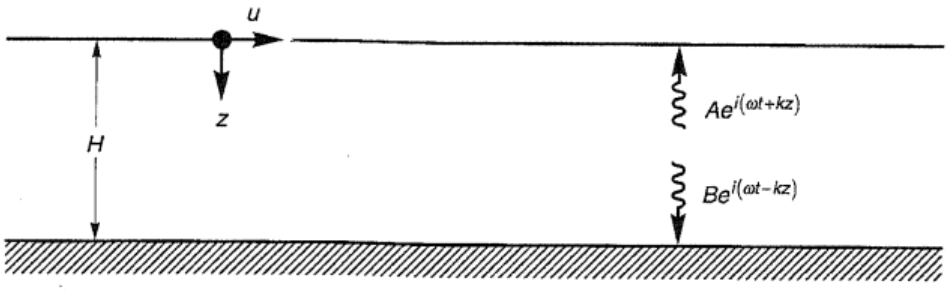

Figure 2.6: Incoming and reflected wave in uniform soil layer (Kramer, 1996).

Propagating incidental and reflected waves are expressed in terms of horizontal harmonic particle oscillation. Resulting displacement are found by the sum of the two.

$$u(z,t) = Ae^{i(\omega t+kz)} + Be^{i(\omega t-kz)} \tag{2.4}$$

Where A and B are the incidental and reflected wave amplitudes, t is the time, ω is the frequency in radians per second, z is soil depth, $i = \sqrt{-1}$ is the imaginary constant and

$k = \omega/V_s$ is the wave number, where V_s is the shear wave velocity in the homogeneous soil.

The shear strains in the soil layer are found differentiating the displacement with respect to the soil depth.

$$\gamma(z,t) = \frac{\partial u}{\partial z} \tag{2.5}$$

Shear stresses do not occur on the surface which provide an useful boundary condition.

$$\tau(0,t) = G \cdot \gamma(0,t) = G \cdot \frac{\partial u}{\partial z} = 0 \tag{2.6}$$

The boundary condition reformulates the wave equation to:

$$u(z,t) = 2A\frac{e^{ikz} + e^{-ikz}}{2}e^{i\omega t} = 2A\cos(kz) \cdot e^{i\omega t} \tag{2.7}$$

Equation 2.7 represents a standing wave used to establish ratio between surface motion and bedrock motion called the transfer function.

$$F_1(\omega) = \frac{u_{max}(0,t)}{u_{max}(H,t)} = \frac{2A \cdot e^{i\omega t}}{2A\cos(kH) \cdot e^{i\omega t}} = \frac{1}{cos(kH)} = \frac{1}{\cos\left(\frac{\omega H}{V_s}\right)} \tag{2.8}$$

Amplification of the soil layer is then determined by the mode of the transfer function called the amplification function.

$$|F_1(\omega)| = \sqrt{\mathrm{Im}(F_1(\omega))^2 + \mathrm{Re}(F_1(\omega))^2} = \frac{1}{\left|\cos\left(\frac{\omega H}{V_s}\right)\right|} \tag{2.9}$$

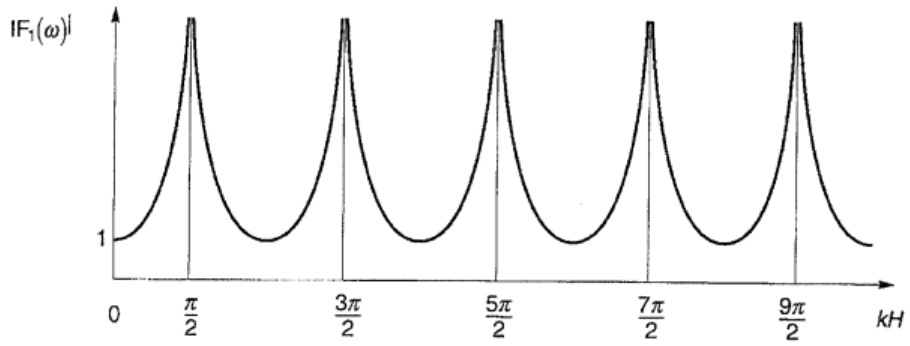

Figure 2.7: Amplification of a undamped soil layer (Kramer, 1996).

The amplification function show that the soil layer is only able to amplify, not de-amplify the incoming motion and in this undamped case could cause infinitely large amplifications as shown by the asymptotes in figure 2.7. The phenomenon is called resonance and occurs when the incoming oscillations coincides with the natural frequencies of the soil layer.

In a damped case the frequency dependent amplification will look like figure 2.8.

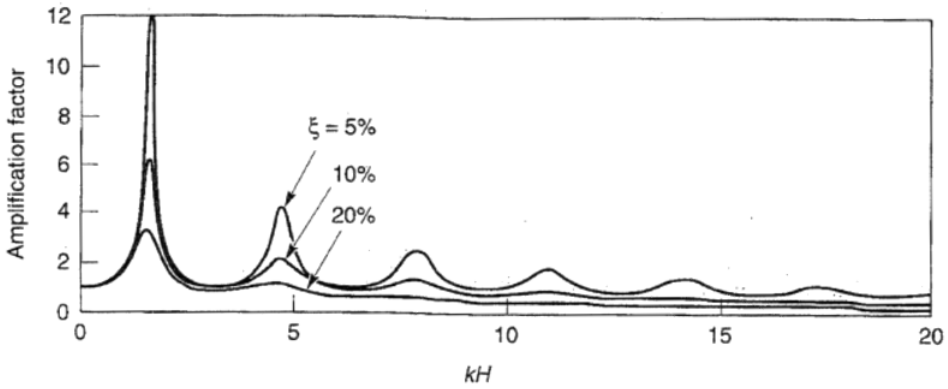

Figure 2.8: Amplification of a damped soil layer (Kramer, 1996).

By inspecting the resulting deformations of the soil layer at resonance the natural mode shapes can be found, see figure 2.9.

It is important to emphasize that the amplification function (2.9) is defined in the frequency domain. This means that in order to use the amplification function it is necessary to perform a Fourier transformation on the time series before amplifying the response. Then perform an inverse Fourier transformation to obtain desired time series at the surface. This procedure is well illustrated in figure 2.10 by Kramer (1996) on the bext page, where the surface amplification of Gilroy No. 2 is considered.

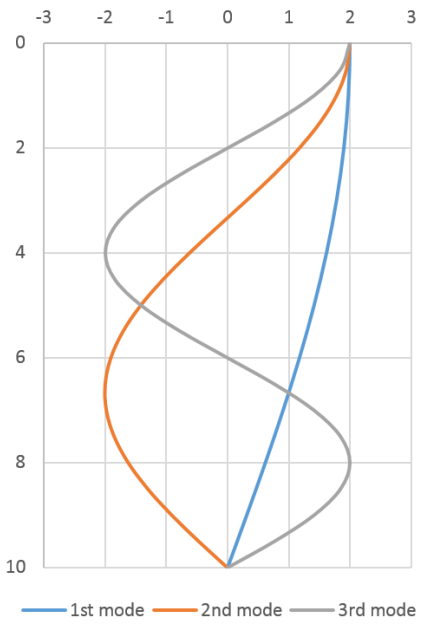

Figure 2.9: Mode shapes of a 10 meter deep soil layer with shear wave velocity of $V_s = 10m/s$ oscillating at $\omega_1 = \frac{\pi}{2}$, $\omega_2 = \frac{3\pi}{2}$ and $\omega_3 = \frac{5\pi}{2}$

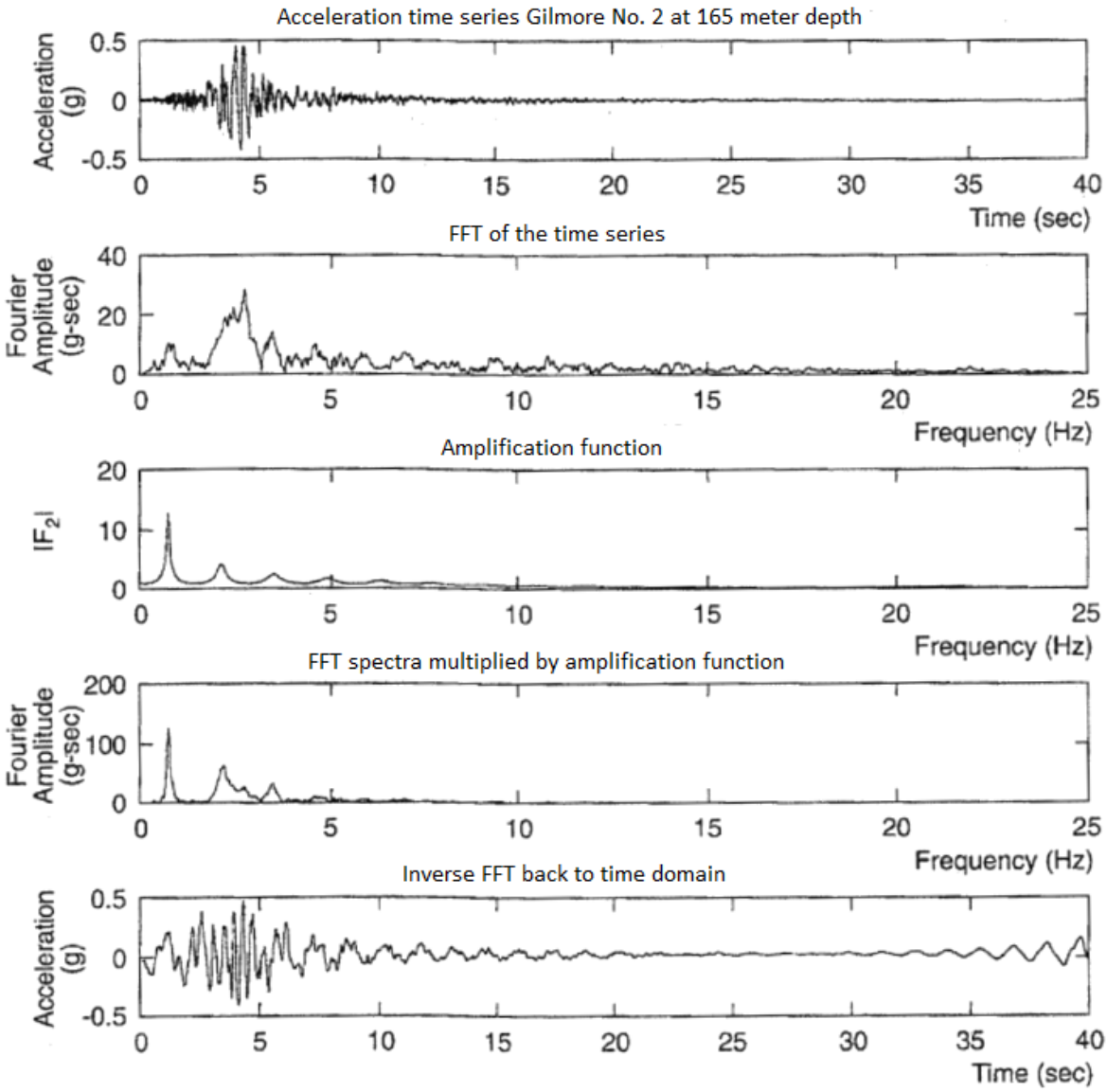

Figure 2.10: Amplification of time series (Kramer, 1996)

2.5 Response Spectrum Analysis

Evaluating single degree of freedom (SDOF) systems and their frequency dependent behavior is a convenient tool in dynamic analysis and is the basis in obtaining the response spectrum.

2.5.1 Single Degree of Freedom Model

The lollipop model is a simple way describing dynamic behavior of a SDOF-mechanism. It is convenient to use a massless column, providing stiffness and damping, and a lumped mass on top, see figure 2.11. In earthquake analysis the system is exited by an acceleration at the base and response at the lumped mass is measured.

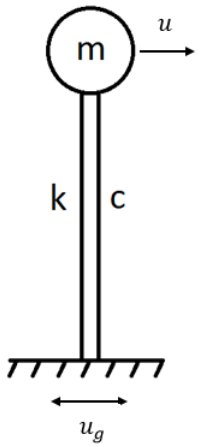

Figure 2.11: The single degree of freedom lollipop model.

Equations of motion

The dynamic equilibrium condition of the SDOF-system excited by the ground acceleration $\ddot{u}_g(t)$ is given by the equation.

$$m \cdot \big(\ddot{u}(t) + \ddot{u}_g(t)\big) + c \cdot \dot{u}(t) + k \cdot u(t) = 0 \tag{2.10}$$

Where m, c and k is the mass, damping and stiffness of the structure, and $u(t)$ is the relative displacement of the mass to the ground motion. The stiffness and damping are only dependent on the relative displacement in the structure. It is then possible to move the ground motion term over to the right hand side and consider it as an equivalent force acting on the structure.

$$m \cdot \ddot{u}(t) + c \cdot \dot{u}(t) + k \cdot u(t) = -m \cdot \ddot{u}_g(t) \tag{2.11}$$

Natural Frequency

Considering the homogeneous equation without damping provides the following dynamic equation.

$$m \cdot \ddot{u}(t) + k \cdot u(t) = 0 \tag{2.12}$$

By the technique of Fourier transformation the response can always be expressed as the sum of harmonic oscillations of all frequencies with corresponding amplitudes, hence.

$$u(t) = Re\left(\sum_{n=1}^{\infty} A_n \cdot e^{i\omega_n t} \right) \tag{2.13}$$

For the homogeneous conditions it is only one frequency dominating the response.

$$u(t) = Re(A_1 \cdot e^{i\omega_1 t}) \tag{2.14}$$

Substituting 2.14 into 2.12 gives.

$$(k - \omega_1^2 \cdot m) \cdot A_1 = 0 \tag{2.15}$$

since $A_1 \neq 0$ we get the natural frequency of the system.

$$\omega_1 = \sqrt{\frac{k}{m}} \tag{2.16}$$

2.5.2 The Response Spectrum

In creating the response spectrum, SDOF-oscillators of all natural frequencies are considered. All of them are subjected to the same dynamic input and maximum response is measured in each case. The response spectrum is then obtained by plotting this response against the fundamental periods. In figure 2.12 the colored time series represent the response of six different oscillators and the black graph is the obtained response spectra.

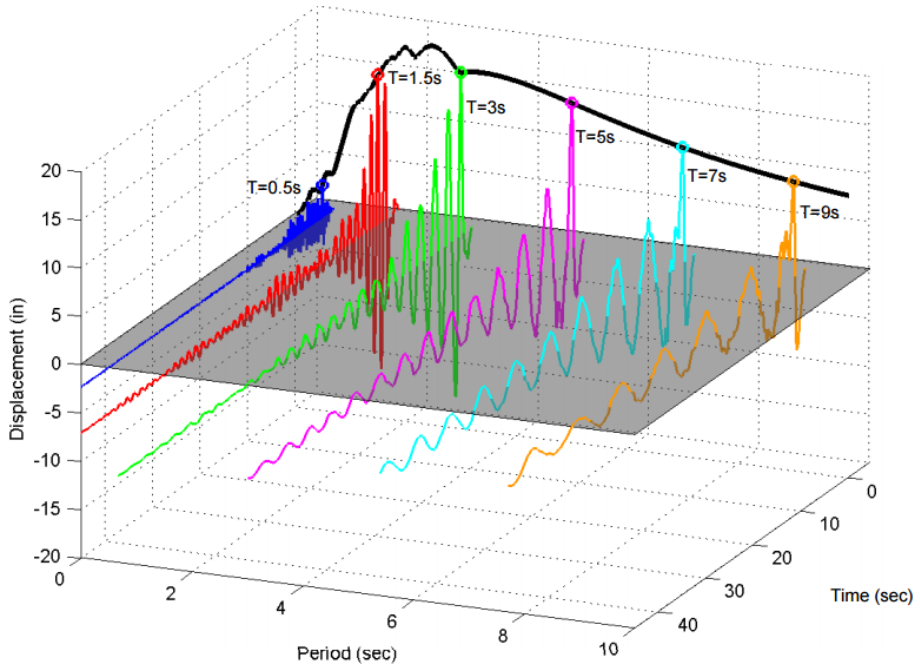

Figure 2.12: Construction of the response spectrum. Figure from QuakeManager (2015).

It is common to create response spectres for both displacement and acceleration. The acceleration response is convenient to use calculating earthquake induces forces. Figure 2.13 and figure 2.14 shows the acceleration time series from the Imperial Valley 1979 earthquake and the corresponding response spectra for this ground acceleration.

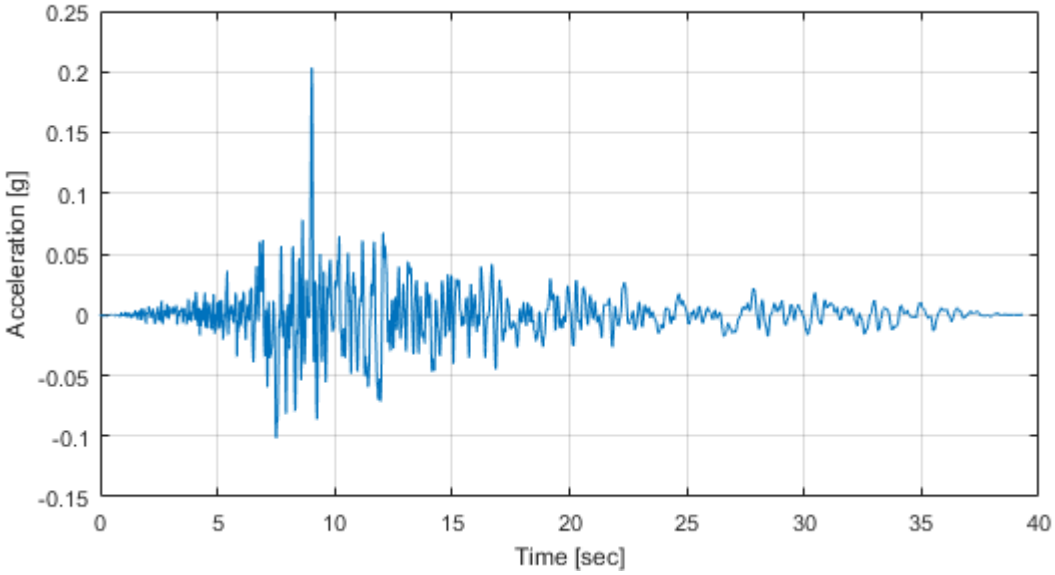

Figure 2.13: Acceleration time series from the Imperial Valley earthquake in 1979.

The Fourier spectrum probably gives a more accurate illustration of the frequency content of an earthquake, but the response spectrum gives important information about which natural frequencies to avoid when designing structures. By inspecting figure 2.14 we see

that the critical situation occurs in a structure with fundamental period of about 0.2 seconds, which gives the acceleration:

$$S_A(0.2) = 0.49\ g$$

And the equivalent base shear at a simplified 1000 kg structure:

$$F_{eq} = 4.8\ m/s^2 \cdot 1000\ kg = 4.8\ kN$$

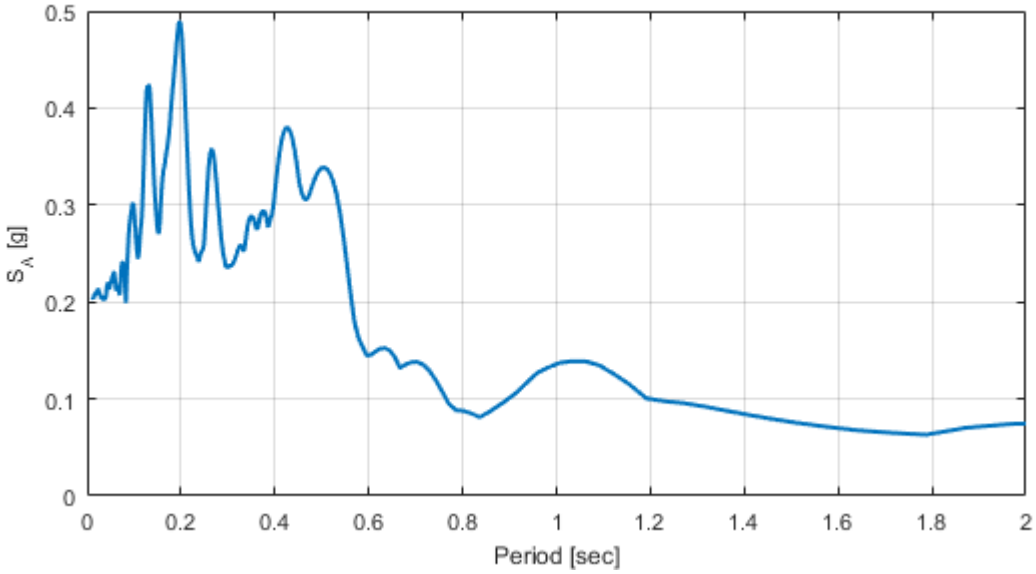

Figure 2.14: Acceleration response spectrum for the Imperial Valley earthquake 1979.

In practice several time series are taken into account when obtaining a response spectrum. The time series should be in relevant magnitude for the geographical area and give an adequate range in frequency content. This can be taken care of by seismic zonation maps, giving expected acceleration for a given return period of an area. Through proper scaling of the considered time series it is established simplified methods used in building codes, for example Eurocode 8 (Norge, 2004).

2.6 Dynamic Soil-Structure Interaction

A foundation on the surface or embedded in a soil layer causes deviation in the surrounding soil motion compared to the free field motion. This effect is called soil-structure interaction (SSI) and it is able to change expected response in a system considerably from a fixed base analysis. The phenomenon is dependent on the foundation geometry, embedment and dynamic properties of the soil. In general the SSI effects will always cause softer behavior and increase the natural periods. A fixed base analysis will therefore be

more conservative regarding overturning moments and base shear, but the effects of foundation rocking can contribute to much larger displacements of a structure. SSI-analysis is necessarily of great importance in dense areas with high rise buildings or motion in sensitive connection devices such as manifolds. Economic considerations suggest that a SSI-analysis are beneficial in design activities due to the reduction in induced forces (Wolf, 1985).

The theory of dynamic soil-structure interaction is complex and will only be discussed briefly in this thesis. For more detailed derivation of the subject see for example Wolf (1985). Traditionally dynamic SSI analysis can be divided into two groups: the direct methods in time domain and the substructure methods in the frequency domain.

2.6.1 Direct Methods

Direct methods involve analyzing both soil and structure directly integrating numerically through the time domain. The advantage of this approach is that it is performed in one step and copes with non-linearity directly. The *discrete element methods* constitutes the family of direct methods including the *finite element method* (FEM). The methods use small elements coupled together to build up a calculation model and is the most general methods used in geotechnical engineering today. In dynamic analyses large models are required to radiate out unwanted boundary reflected waves. This has traditionally been an issue due to excessive calculation time and has lead to development of other techniques, such as the *substructure methods*.

2.6.2 Substructure Methods

The *substructure methods* are based on the general superposition theorem that permits breaking the problem into parts that later are added together. The different steps include *kinematic interaction* analyses and *internal interaction* analyses which are only valid for linear and equivalent linear system. The methods are therefore less accurate analysing highly non-linear soil in strong ground motion, but provides a remarkable agreement with a full direct analysis in most cases (Kausel et al., 1978). The technique is in general reliable, economic and less time consuming than numerical methods.

To illustrate the principles of a substructure method a very brief stepwise description of the *Three-Step Method* from Elsabee (1975) is presented.

The Three-Step Method

The *Three-Step Method* illustrates well how the concept of superposition is used and also explain the different steps in the analysis, see figure 2.15.

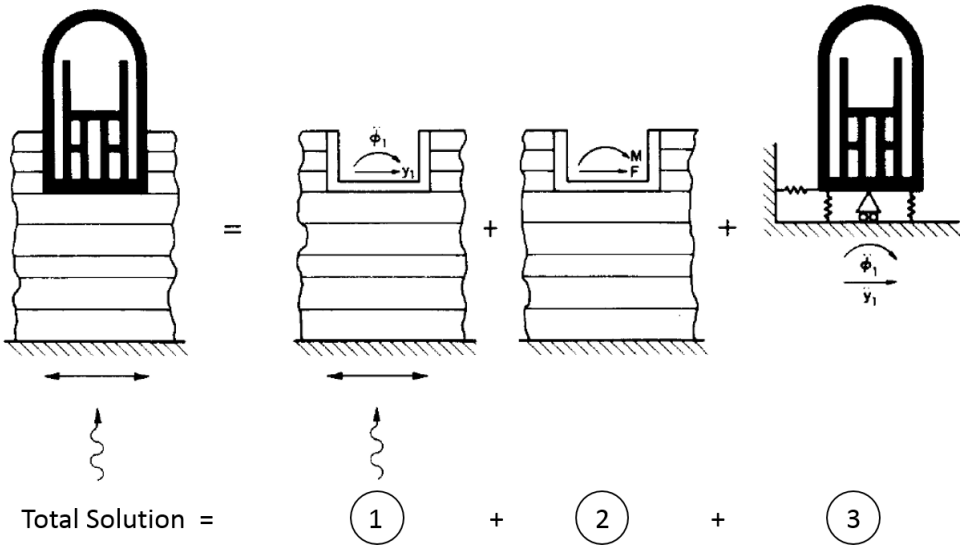

Figure 2.15: Three-step method (Kausel et al., 1978).

1. **Step 1, Kinematic Interaction:** Assume a massless rigid foundation embedded in a soil deposit subjected to ground motion. A stiff foundation cannot necessarily follow the free field motions and a dynamic analysis will generate the *foundation input motion*.

2. **Step 2, Dynamic Impedance:** The frequency dependent soil properties are determined. These properties are expressed through the dynamic *impedance function*, a complex frequency dependent function related to soil stiffness and damping. This step requires finite element or finite difference analysis. Numerous of closed form solution has been tabulated for conventional foundation designs.

3. **Step 3, Inertial Interaction:** Inertial forces from the foundation input motion is applied to the structure founded on springs representing the soil properties through the *impedance function*. The response of the structure including SSI-effects can then be analysed in both frequency and time domain.

2.7 The Normal Mode Method

A fundamental discipline in dynamic calculations is linear (matrix) algebra and eigenanalysis. The *normal mode method* is an approach based on eigenanalysis that uncouples any dynamic motion into independent modes. A mode is a particular dynamic motion

of a system oscillating at a natural frequency. The modal superposition property ensures capability of representing any motion by adding up mode shapes with their respective modal amplitudes. This method also requires the use of Fourier transformations. The fundamental concepts in using the normal mode method will now be presented on a multi degree of freedom system. Starting with the undamped equation of motion.

$$\mathbf{M\ddot{u}(t)} + \mathbf{Ku(t)} = \mathbf{Q(t)} \tag{2.17}$$

Where $\mathbf{M}$ and $\mathbf{K}$ is the mass and stiffness matrix, $\mathbf{Q}$ is the corresponding load vector and $\mathbf{u}$ is the degrees of freedom. By Fourier transformation we can express the degrees of freedom by a sum of harmonic oscillations:

$$\mathbf{u}(t) = Re\Big(\sum_{n=1}^{\infty} \mathbf{A}_n \cdot e^{i\omega_n t}\Big) \tag{2.18}$$

We will now consider the homogeneous case and apply 2.18 into equation 2.17, which simplifies to:

$$\begin{gathered}\Big(\mathbf{K} - \omega_n \mathbf{M}\Big)\mathbf{A}_n e^{i\omega_n t} = \mathbf{0} \\ \big(\mathbf{K} - \omega_n^2 \mathbf{M}\big) = \mathbf{0}\end{gathered} \tag{2.19}$$

Now the eigenfrequencies or natural frequencies can be retrieved from the determinant of the assembled matrix.

$$\det\big(\mathbf{K} - \omega_n^2 \mathbf{M}\big) = \mathbf{0} \tag{2.20}$$

For every eigenfrequency, ω_n, there is a corresponding eigenvector, $\boldsymbol{\varphi_n}$, that solves the system, thus:

$$\big(\mathbf{K} - \omega_n^2 \mathbf{M}\big)\boldsymbol{\varphi_n} = \mathbf{0} \tag{2.21}$$

These eigenvectors constitutes the mode shapes of the dynamic response to a natural frequency. Modal superposition now states that every mode shape can be multiplied by a corresponding modal degree of freedom and summed up to get the physical response:

$$\mathbf{u}(t) = \sum_{n=1}^{N} \boldsymbol{\varphi}_n \cdot q_n(t) \tag{2.22}$$

Where q_n is the modal degrees of freedom. Substitute into 2.17 and premultiply by the transposed mode shapes gives n equations of the form:

$$\boldsymbol{\varphi}_n^T \mathbf{M} \boldsymbol{\varphi}_n \ddot{q}_n + \boldsymbol{\varphi}_n^T \mathbf{K} \boldsymbol{\varphi}_n q_n = \boldsymbol{\varphi}_n^T \mathbf{Q}\ \mathbf{l} \tag{2.23}$$

Where $\mathbf{l} = \begin{bmatrix} 1 & 1 \end{bmatrix}^T$. The equation can further be simplified to:

$$\tilde{M}_n \ddot{q}_n + \tilde{K}_n q_n = \tilde{Q}_n \tag{2.24}$$

Where $\tilde{M}_n$, $\tilde{K}_n$ and $\tilde{Q}_n$ is the modal mass, modal stiffness and modal load respectively. The system is now fully uncoupled and we have n linearly independent SDOF-equations. The modal degrees of freedom is now found solving the differential equations. By modal superposition (equation 2.22) the physical degrees of freedom can be back calculated.

2.8 The Finite Element Method

The *finite element method* (FEM) is an approximate technique of solving boundary value problems originated from the field of aerospace engineering. Today the method are widely used in several fields of engineering including structural engineering, geotechnical engineering, thermodynamics and bio-mechanics, to mention a few. The method is based on discretization of a continuous system into a finite number of elements. By prescribing node displacements or stresses in the boundary nodes (boundary conditions) it is possible to solve the system for nodal degrees of freedom inside the discretized model.

The method has become very popular over the last decades due to the easy access to powerful computers. However, the method also represents a danger if the user don't have sufficient knowledge. The advanced tool then can be used as a "black box", resulting in good looking output that can cause engineering decisions with great consequences (Liu and Quek, 2013). The user should therefore have good understanding of the theoretical background and also make use of simplified methods to make quick comparable estimates.

2.8.1 Basic FEM-theory

In recent times there has been done a lot in the field of finite element technology and a thoroughly description of the theory will be too comprehensive for the purpose of this thesis. A very brief description without any derivation of equations will rather be of priority. Overall the *finite element method* can be be summarized in the following concepts:

- Discretization of a physical model into smaller elements.
- Establish local set of equations in terms nodal quantities in each element.
- Interpolate between nodes using shape functions.
- Establish global set of equations assembling all elements.
- Determine sufficient amount of boundary conditions and ensure compatibility.
- Solve the global set of equations.

The finite element method is an approximate numerical solution. It can either aim to find the highest possible accuracy of a solution by using small sized elements and many iterations costing computational time. Or prioritize fast calculations including large sized elements and fewer iterations on the cost of accuracy. A coarse mesh generally gives less accurate solutions due to fewer nodes and a higher degree of interpolation between nodes. Figure 2.16 shows a FEM-model of a symmetric half of a soil medium used in dynamic closed caisson analysis (Brandt, 2014).

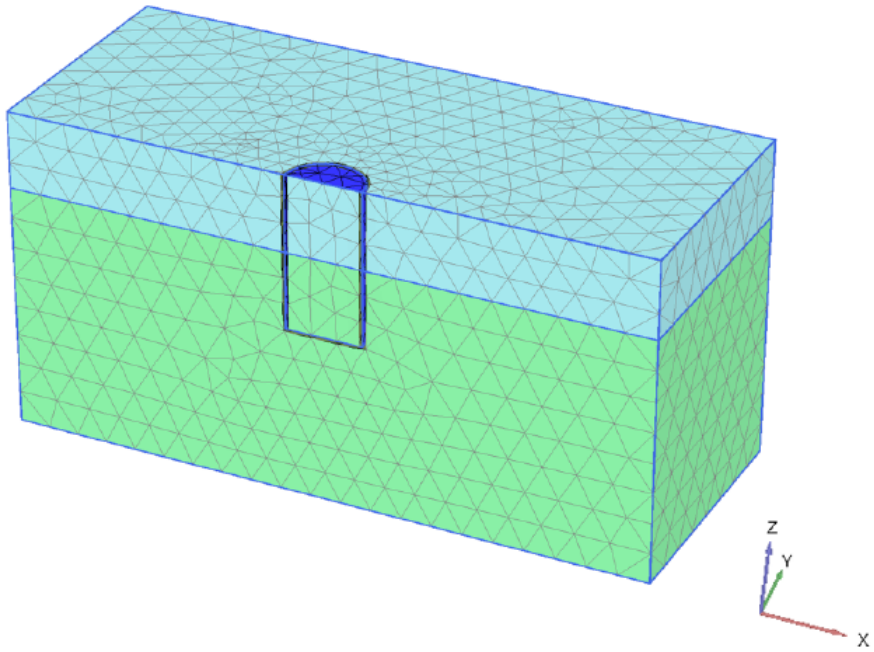

Figure 2.16: FEM-model used in dynamic analysis of closed caisson foundation. Figure from Brandt (2014).

The choice of element type used in the model is another issue when it comes to accuracy and CPU time. Many different types of elements, each with their pros and cons, have been developed. The basic element types are beam elements, plate elements and volumetric elements. Generally the elements are determined by the distribution of nodes and Gaussian stress points. Each element has a specific number of nodes distributed along its boundary ensuring continuity with neighbouring elements. Figure 2.17 shows an example of a 10-noded tetrahedral element with nodes and stress points.

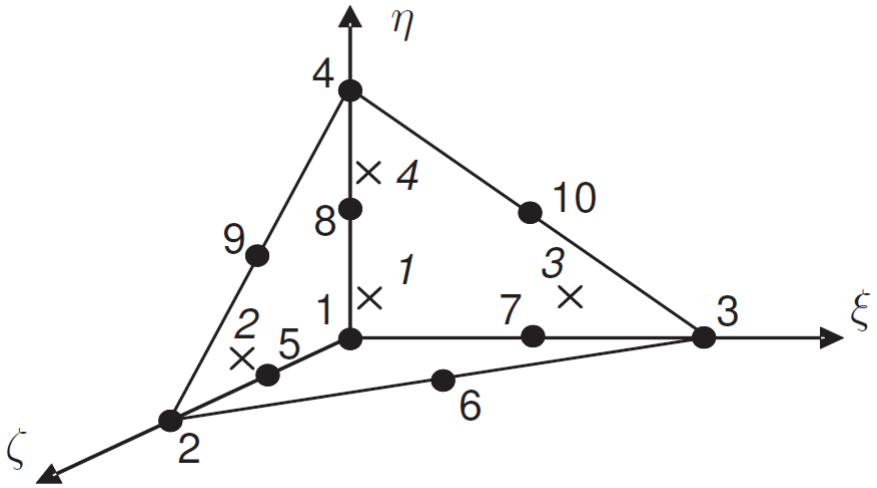

Figure 2.17: 10-noded tetrahedral element. Nodes marked as black dots and stress points as x.

Nodal quantities, like forces and displacements, are calculated in each node and makes number of equations and CPU time proportional to number of nodes. Shape functions provide an appropriate interpolation of the discrete nodal quantities in between nodes. The order of the shape functions also influences accuracy and calculation time. Typically, low order polynomials or linear shape functions gives sufficient results.

2.8.2 Challenges in Dynamic FEM-Analyses

Boundary Issues

In geotechnical earthquake engineering it is common to model a soil deposit over bedrock using volumetric elements, see figure 2.16. This makes number of nodes exponentially increasing with the size of the model and cause excessive calculation time. With this in mind, small models are desirable. However, in dynamic analyses propagating waves eventually hits vertical boundaries that represents a continuous soil medium. From basic wave propagation theory it is known that waves gets reflected back when hitting a boundary. This also happens when waves propagates inside an element model. Unfortunately, this causes trapped energy that in nature would dissipate through continuous soil.

There are two ways to solve this problem. *(1)* create a sufficiently large model so that the wave energy dissipates in damping. This will increase the computational time significantly. Or *(2)* introduce viscous boundaries that absorbs wave energy. These boundaries typically work properly on perpendicularly incoming waves, but tend to generate unwanted boundary effects otherwise, see for example Brandt (2014).

Although the first absorbing boundaries was invented by Lysmer and Kuhlemeyer already in 1969, there is still a huge challenge adapting these in a general manner. The best absorbing boundaries developed is by Lindman (1975), but are only applicable in finite difference calculations.

Time Stepping

In dynamic FEM-analyses numerical time integration is used, such as the Newmark Method (Newmark, 1959). In numerical integration a global set of equations are solved at a particular time (t_i) before stepping one time step (Δt) ahead and solve the equations once again and so on.

Both explicit and implicit formulations of the time integration scheme are used in FEM. Explicit methods calculate next step based on current step while implicit methods solve an equation based on both current and the next time step. Explicit methods are generally easier to formulate but are very sensitive to time stepping. Implicit methods are more advanced but provide robust integration and are therefore suitable for dynamic calculations.

Essentially the time step should be set to be smaller than a critical value. This value is roughly said to be the time a wave use to travel over an element. Too large time steps could skip the smallest elements and cause less accurate solutions and unstable numerical behavior.

2.9 Soil Stiffness and Damping

2.9.1 Soil Stiffness Parameters

Soils are highly non-linear which has a significant impact on the shear stiffness. The shear stiffness is essential in wave propagation due to the shear wave velocity relation:

$$V_s = \sqrt{\frac{G}{\rho}} \tag{2.25}$$

From laboratory tests it is widely proven that the shear stiffness is dependent on shear strain. Soils subjected to incoming shear waves will experience cyclic shear which simplified can be illustrated as a hysteretic loop, see figure 2.18 below.

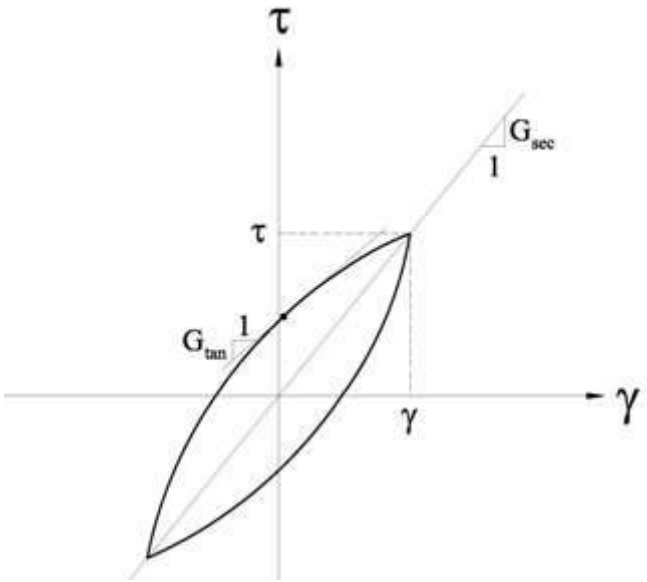

Figure 2.18: Equivalent linear cyclic shear hysteresis. Figure from BuildingResearchInstitute.

The shear stiffness can be determined by the inclination of the loop in every point at the curve, G_{tan} in the figure. However, a convenient simplification is to look at the mean shear stiffness over one cycle, namely the secant shear stiffness, G_{sec} (Kramer, 1996). This provide the foundation for an equivalent linear approximation of non-linear response much used in earthquake engineering. However, the method cannot be used when plastic deformations or failure occurs, these cases require a more realistic path of the hysteresis loop, see figure 2.19.

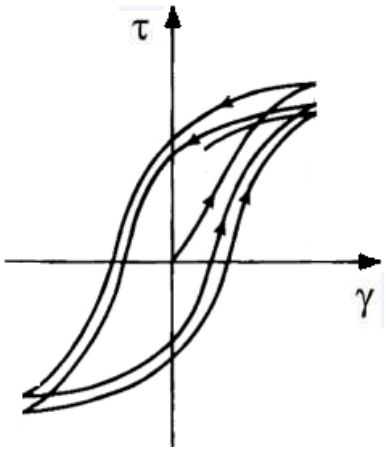

Figure 2.19: Non-linear degrading hysteresis loop. Figure from BuildingResearchInstitute.

The figure clearly illustrates how the secant stiffness degrades with shear strains and number of cycles. This can be illustrated by the stress-strain curve running through the

origin and each of the tips in every loop, called the back-bone curve, illustrated in figure 2.20. The inclination of the backbone curve at the origin will provide the maximum shear stiffness, G_{max}. The secant stiffness are now found as a straight line from the origin to a point on the back-bone curve at current shear strain. The ratio between the secant stiffness and the max stiffness can graphically be shown using a modulus reduction curve, figure 2.21.

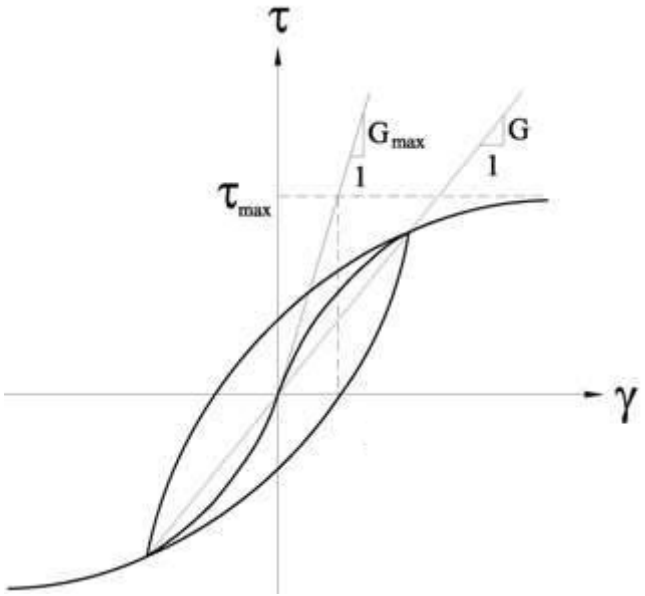

Figure 2.20: Backbone curve. Figure from BuildingResearchInstitute.

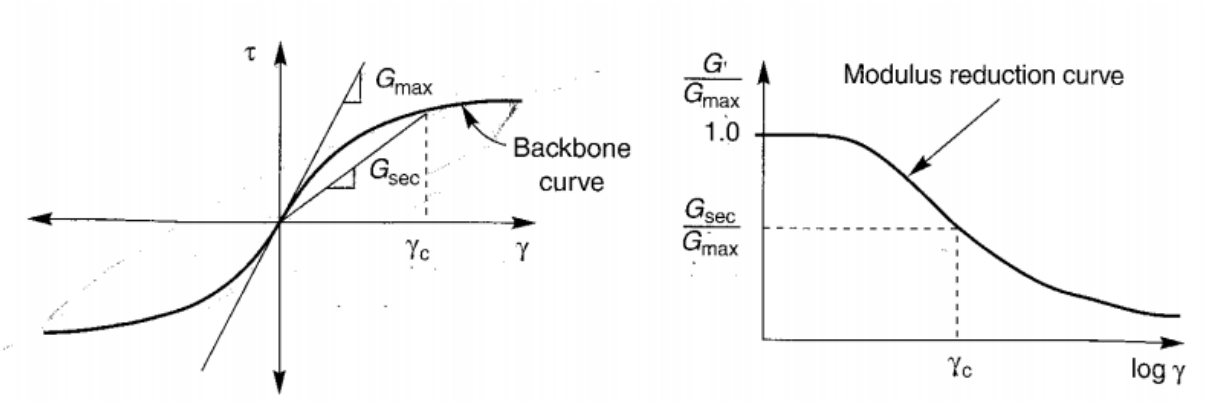

Figure 2.21: Backbone curve and modulus reduction curve. Figure from Kramer (1996).

2.9.2 Damping in Soil

Damping effects is present in all natural dynamic mechanisms. When waves propagates through a soil medium energy will dissipate through friction and heat generation before the waves eventually dies out. The phenomenon of damping is difficult to quantify and there is developed many crude techniques removing energy from a dynamic system.

Damping Ratio

Damping is often quantified as the ratio between the actual damping coeffecient and a critical damping defined as the minimum damping necessary to prevent the system to oscillate, see figure 2.22. The damping ratio is used as a helpful parameter frequently used in techniques of describing damping.

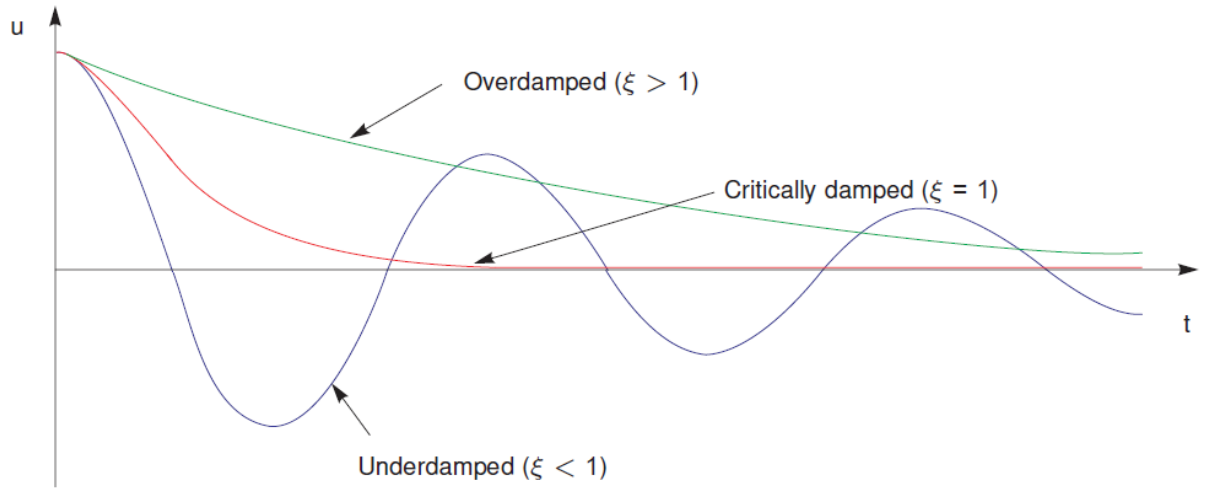

Figure 2.22: Effect of damping ratios on a system, figure from PLAXIS 3D reference manual.

$$\xi = \frac{c}{c_{critical}} \tag{2.26}$$

It can be shown that:

$$c_{critical} = 2m\omega_0 \quad \Rightarrow \quad \xi = \frac{c}{2m\omega_0} = \frac{c\omega_0}{2k} \tag{2.27}$$

Where m and k are the mass and stiffness of the system and ω_0 represents the natural frequency.

Hysteretic Damping

In relation to soil stiffness degradation presented in the previous section (2.9) there are also equivalent-linear and non-linear techniques of describing damping, Kramer (1996). The basic idea is to evaluate the amount of work from the area inside one hysteretic loop. This is the total work done over one cycle and can be expressed as the force times deformation of a infinitesimal soil element integrated over one cycle, hence:

$$W_D = \int_{t_0}^{t_0+T} F\frac{du}{dt}dt = \pi c\bar{\omega}u_0^2 \tag{2.28}$$

Where F is the induced force on a soil element deformed, u. u_0 is the maximum displacement, $\bar{\omega}$ is the frequency of the applied force and c is the damping coefficient from the dynamic equilibrium equations. W_D then expresses the dissipated energy over one cycle. The stored energy at maximum displacement can be expressed as:

$$W_S = \frac{1}{2}ku_0^2 \tag{2.29}$$

Where k is representing the soil stiffness. Assuming $\bar{\omega} = \omega_0$ the equation 2.28 and 2.29 can be reformulated and combined to give the damping ratio:

$$\xi = \frac{W_D}{4\pi W_S} = \frac{1}{2\pi}\frac{A_{loop}}{G_{sec}\gamma_c^2} \tag{2.30}$$

This strain based damping ratio is then to be used in non-linear computational tools. The strain dependent damping ratio can be graphically illustrated the same way as the shear stiffness reduction curve, see figure 2.23 below.

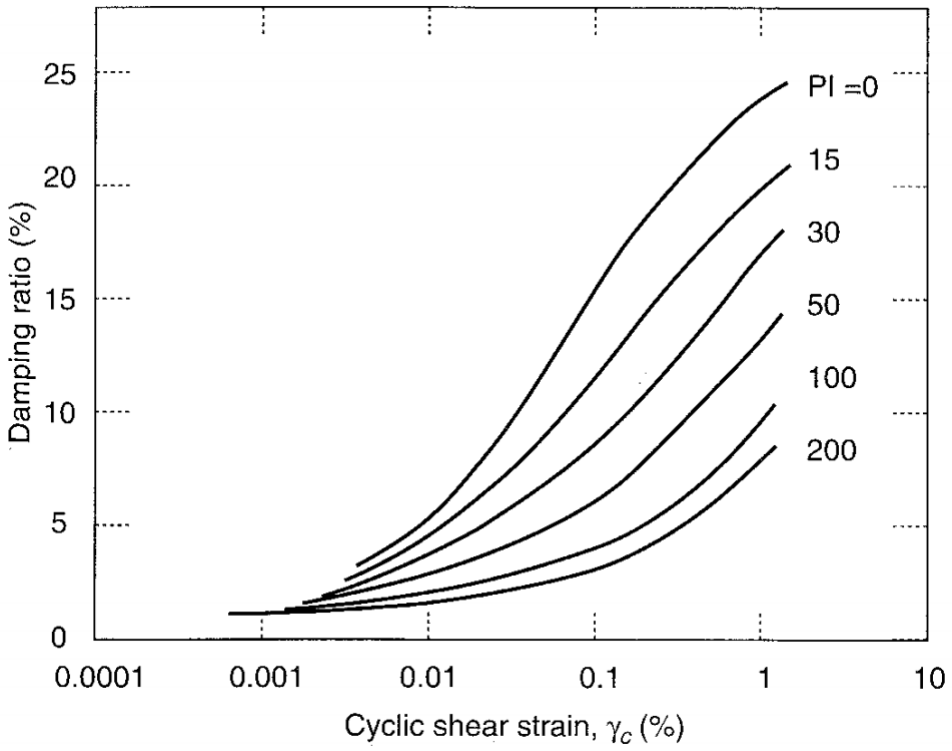

Figure 2.23: Strain dependent damping ratio. Figure from Kramer (1996).

Rayleigh Damping

Rayleigh damping is a simplified method of imposing energy dissipation to a dynamic system. The damping consists of a mass proportional and a stiffness proportional term, both frequency dependent.

$$\mathbf{C} = \alpha\mathbf{M} + \beta\mathbf{K} \tag{2.31}$$

α and β are the Rayleigh coefficients used to tune the damping ratio ξ into relevant frequency band between f_1 and f_2 and are obtained by the following set of equations.

$$\begin{aligned} \xi_1 &= \frac{\alpha}{4\pi f_1} + \beta\pi f_1 \\ \xi_2 &= \frac{\alpha}{4\pi f_2} + \beta\pi f_2 \end{aligned} \tag{2.32}$$

Here ξ_1 and ξ_2 represents the desired damping ratios at the two target frequencies. Within the frequency band the damping gets below ξ_1 and ξ_2 whereas outside the damping ratios increase quickly, see figure 2.24. It is crucial to pick the target frequencies wisely to avoid artificial over damping. There are several techniques of finding f_1 and f_2, see for example Hashash and Park (2002).

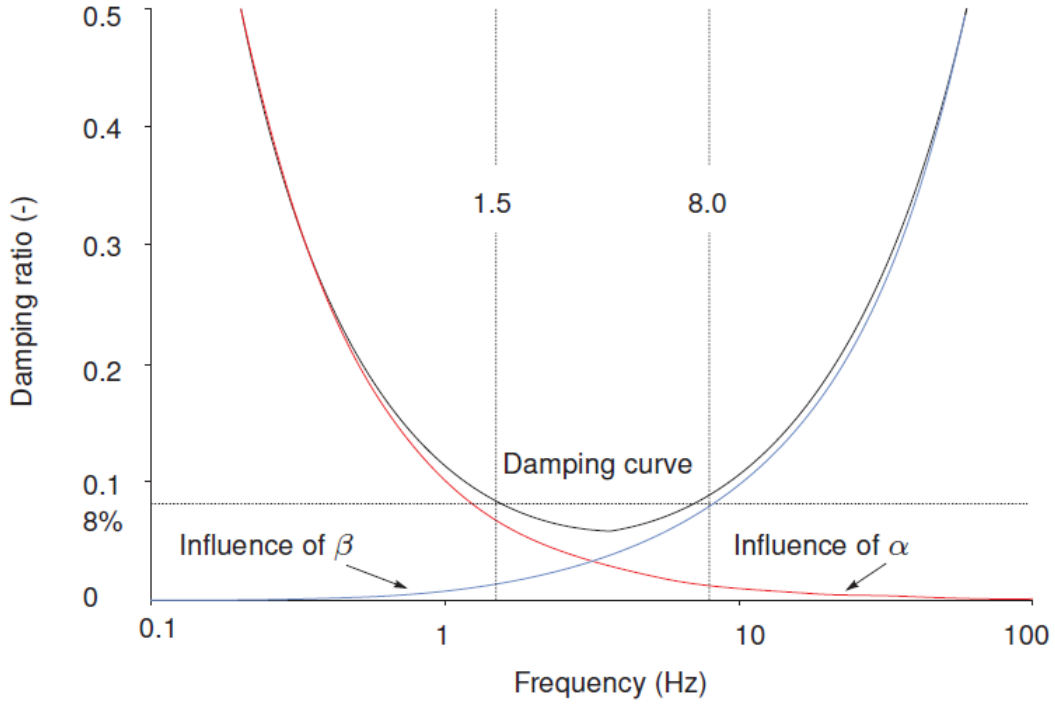

Figure 2.24: Rayleigh damping, red line is the mass proportional part, blue line is the stiffness proportional part. $f_1 = 1.5$ Hz, $f_2 = 8$ Hz, $\xi_1 = \xi_2 = 8\%$.

Chapter 3

The Simplified Modal Non-Linear Analysis

3.1 Background

The *Simplified Modal Non-linear Aanalysis* is a method calculating earthquake induced loads and response of a subsea superstructure founded on a closed caisson. The method was developed by Athanasiu et al. (2015) and presented at the ISFOG conference held in Oslo June 2015. The desire to develop a robust approach giving reasonable estimates of dynamic response avoiding time consuming numerical analyses is the motivation behind the method. This chapter is based on the paper published in Meyer (2015).

3.2 Model

The simplified physical model creating the basis of the method is a two degree of freedom model illustrated in figure 3.1. The model illustrates a foundation embedded in the seabed with a mass lumped at the center of gravity. Pure lateral displacement and rotation are prevented by two non-linear springs representing the soil-stiffness.

The model has translational and rotational degrees of freedom at the base of the structure given by δ and θ. These can be expressed in terms of δ_m and θ_m, which is the corresponding degrees of freedom at the center of gravity in the structure. Hence:

$$\begin{aligned} \delta &= \delta_m - \theta_m \cdot h_c \\ \theta &= \theta_m \end{aligned} \tag{3.1}$$

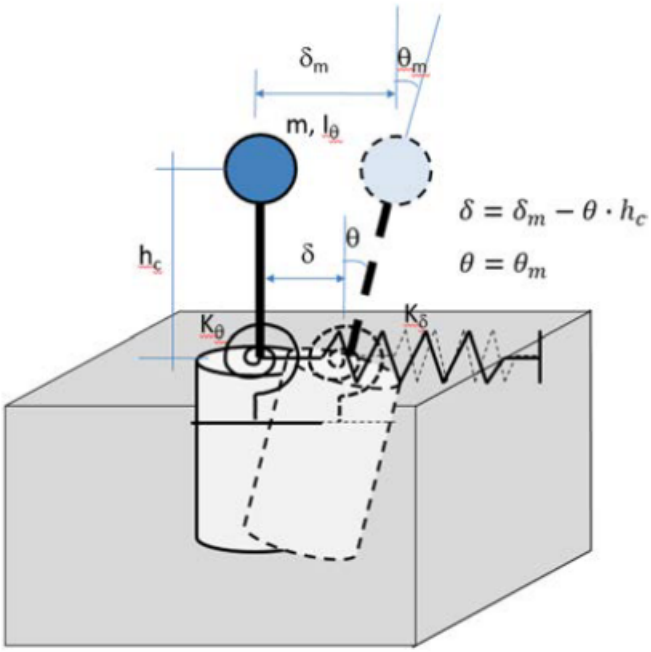

Figure 3.1: The SMNA-model. Figure from Athanasiu et al..

The equivalent force and overturning moment on the system can then be expressed as:

$$\begin{aligned} Q_0 &= K_\delta \cdot \delta + K_{\delta\theta} \cdot \theta \\ M_0 &= K_{\theta\delta} \cdot \delta + K_\theta \cdot \theta \end{aligned} \tag{3.2}$$

Where $K_{\delta\theta}$ and $K_{\theta\delta}$ are the off-diagonal entries in the stiffness matrix.

3.3 Input

The set of input used can be segmented into three groups separately obtained. The different input segments are briefly explained in this section.

Physical Parameters

Physical parameters for the caisson and superstructure are combined into total mass, center of gravity and total mass moment of inertia. These parameters constitutes the mass matrix in the dynamic equation of motion.

Back-Bone Curves

An external soil-caisson interaction analysis are conducted to consider non-linear properties of the soil. The analysis can be done in a discrete element program or a finite element program such as PLAXIS 3D.

The analysis involves modelling relevant caisson geometry and soil conditions before applying lateral force and overturning moment at the top plate of the caisson. The load increases incrementally at a constant load ratio, $h = \frac{M}{Q}$, illustrating different eccentricities. Failure are gradually reached and $Q - \delta$ and $M - \theta$ relations are obtained. The plots from these relations are called back-bone curves, see figure 3.2. Note that different load ratios represents different stiffness conditions.

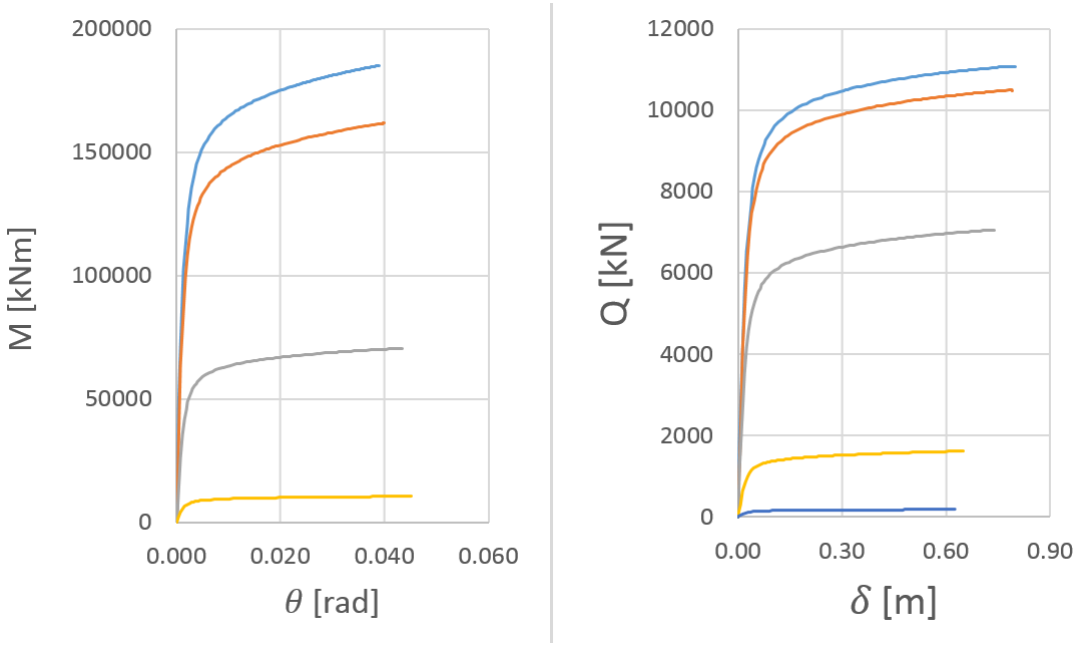

Figure 3.2: Example of back-bone curves obtained in PLAXIS 3D.

From the ultimate loads found in the analysis the yield-surface can be expressed through following equation:

$$\left(\frac{Q_{ult}}{Q_{ult,0}}\right)^{\alpha} + \left(\frac{M_{ult}}{M_{ult,0}}\right)^{\beta} = 1 \tag{3.3}$$

Where $Q_{ult,0}$ and $M_{ult,0}$ are ultimate loads for h_{min} and h_{max} respectively. α and β are curve fitting parameters. Equation 3.3 are further developed using the degree of mobilization, *f*.

$$\left(\frac{Q}{f \cdot Q_{ult,0}}\right)^{\alpha} + \left(\frac{M}{f \cdot M_{ult,0}}\right)^{\beta} = 1 \tag{3.4}$$

The $Q - M$ space are den constructed assembling different load ratios and degrees of mobilization.

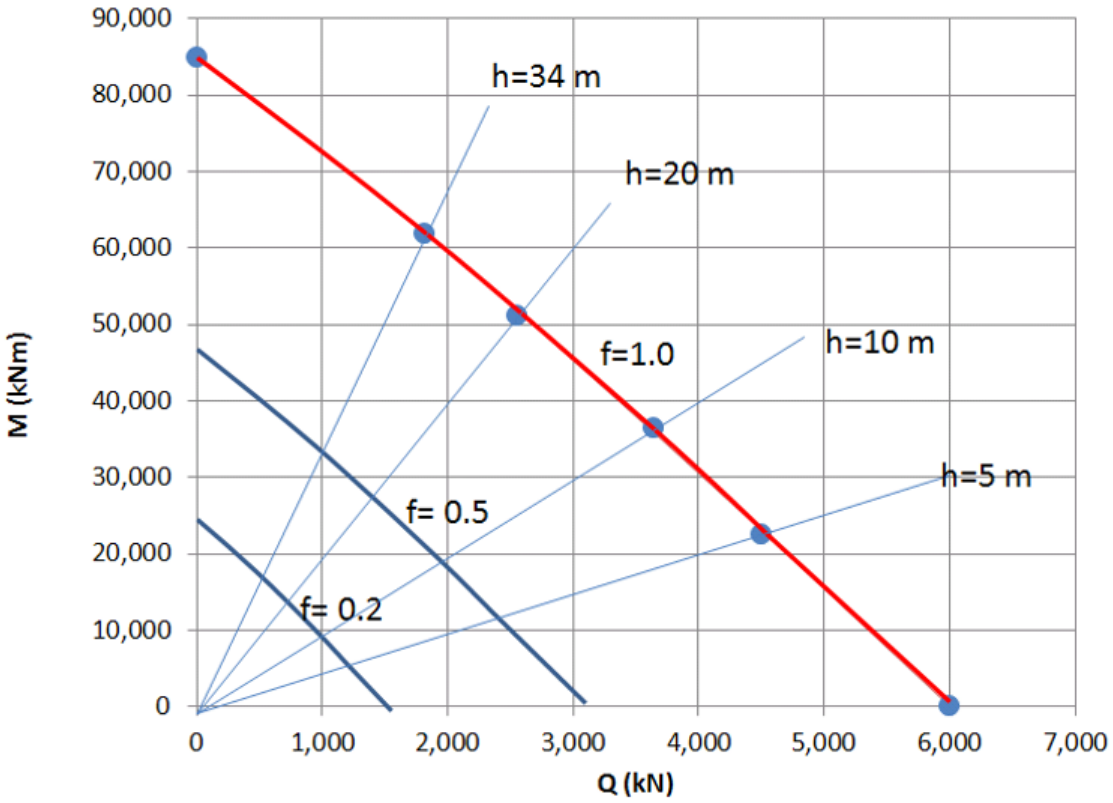

Figure 3.3: Q-M space. Figure from Athanasiu et al.

Acceleration Response Spectrum

The acceleration response spectrum is constructed from a foundation input motion subjected to the structure. Due to soil-structure interaction effects this motion deviate from a free surface motion. The input motion can be found from a kinematic-interaction analysis.

It is convenient to normalize the spectrum such that the response is averaged over a certain frequency band width, see figure 3.4.

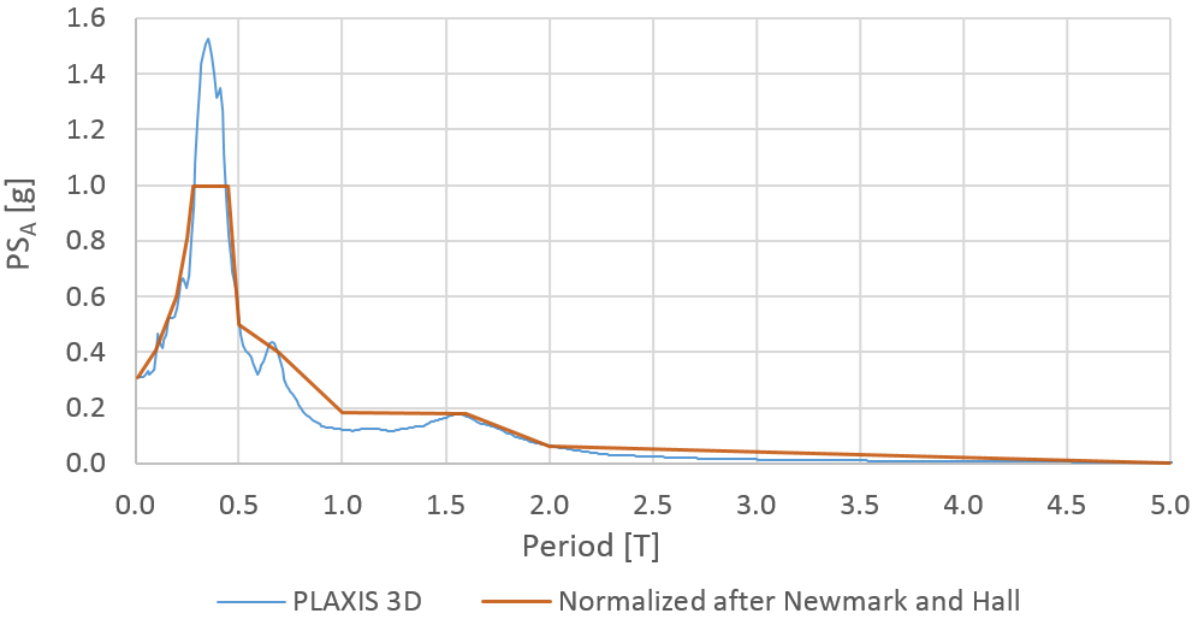

Figure 3.4: Acceleration response spectrum from foundation input motion.

3.4 Method of Solution

Executing the SMNA-method are done in a modal analysis iteration procedure called the *variable secant stiffness procedure*, which implies that the stiffness properties are changing each iteration. In this section a review of the modal analysis and given before the iteration procedure and convergence criteria are explained.

3.4.1 Modal Analysis

Equations of Motion

The undamped homogeneous equations of motion for the two degree of freedom system are:

$$\mathbf{M\ddot{u}} + \mathbf{Ku} = \mathbf{0} \tag{3.5}$$

Where:

$$\mathbf{M} = \begin{bmatrix} m & 0 \\ 0 & I_\theta \end{bmatrix} \quad \mathbf{K} = \begin{bmatrix} K_\delta & -K_\delta h_c \\ -K_\delta h_c & K_\delta h_c^2 + K_\theta \end{bmatrix} \quad \mathbf{u} = \begin{Bmatrix} \delta_m \\ \theta_m \end{Bmatrix} \tag{3.6}$$

$$\begin{aligned} m \cdot \ddot{\delta}_m + K_\delta \cdot (\delta_m - h_c \cdot \theta_m) = 0 \\ I_\theta \cdot \ddot{\theta}_m - K_\delta \cdot (\delta_m - h_c \cdot \theta_m) \cdot h_c + K_\theta \cdot \theta_m = 0 \end{aligned} \tag{3.7}$$

Hence:

$$\begin{bmatrix} m & 0 \\ 0 & I_\theta \end{bmatrix} \begin{Bmatrix} \ddot{\delta}_m \\ \ddot{\theta}_m \end{Bmatrix} + \begin{bmatrix} K_\delta & -K_\delta h_c \\ -K_\delta h_c & K_\delta h_c^2 + K_\theta \end{bmatrix} \begin{Bmatrix} \delta_m \\ \theta_m \end{Bmatrix} = \begin{Bmatrix} 0 \\ 0 \end{Bmatrix} \tag{3.8}$$

Where δ_m is the lateral displacement of the lumped mass, m, of the structure and foundation. θ_m is the rotation at the base, I_θ is the mass moment of inertia of the foundation and superstructure combined. h_c is the height to center of gravity in the structure and K_δ and K_θ are the translation and rotation stiffnesses representing the subgrade.

Natural Frequencies and Mode Shapes

By assuming harmonic response in both degrees of freedom and perform a Fourier transformation (see 2.13) on the two, substitution of the transformed expression will result in equation 3.9. Solving the equation in terms of ω_n will give the system's natural frequencies:

$$det \left(\begin{bmatrix} K_\delta & -K_\delta h_c \\ -K_\delta h_c & K_\delta h_c^2 + K_\theta \end{bmatrix} - \omega_n^2 \begin{bmatrix} m & 0 \\ 0 & I_\theta \end{bmatrix} \right) = 0 \tag{3.9}$$

Where ω_n is the natural frequencies, $n = 1, 2$ on this case. Both natural frequencies has corresponding mode shapes, $\boldsymbol{\varphi_1}$ and $\boldsymbol{\varphi_2}$, solving the equation:

$$\begin{bmatrix} K_\delta - \omega_n^2 m & -K_\delta h_c \\ -K_\delta h_c & (K_\delta h_c^2 + K_\theta) - \omega_n^2 I_\theta \end{bmatrix} \begin{Bmatrix} \varphi_{1,n} \\ \varphi_{2,n} \end{Bmatrix} = 0 \tag{3.10}$$

Modal Decoupling

The two modes are linearly independent of each other and makes it possible to decouple the system into two distinct modes. The modal degrees of freedom are expressed as:

$$\mathbf{u(t)} = \boldsymbol{\varphi_n} \cdot \mathbf{q_n} \tag{3.11}$$

Substitute into 3.5 and pre-multiply by the the modeshape gives:

$$\boldsymbol{\varphi_n^T}\mathbf{M}\boldsymbol{\varphi_n} + \boldsymbol{\varphi_n^T}\mathbf{K}\boldsymbol{\varphi_n} = \mathbf{0} \tag{3.12}$$

Introducing the modal mass and modal stiffness:

$$\tilde{M}_n = \boldsymbol{\varphi_n^T}\mathbf{M}\boldsymbol{\varphi_n} \qquad \tilde{K}_n = \boldsymbol{\varphi_n^T}\mathbf{K}\boldsymbol{\varphi_n} \tag{3.13}$$

The decoupled equations of motion for $n = 1$ and $n = 2$ are then established:

$$\tilde{M}_n\ddot{q}_n(t) + \tilde{K}_n q_n(t) = 0 \tag{3.14}$$

Where $q(t)_n$ is the modal coordinates, $\tilde{M}_n$ and $\tilde{K}_n$ is are the modal mass and stiffness for the two modes. The response can also be back calculated to real degrees of freedom:

$$\begin{Bmatrix}\delta(t)_m \\ \theta(t)_m\end{Bmatrix} = \begin{Bmatrix}\varphi_1 \\ \varphi_2\end{Bmatrix}_1 q_1(t) + \begin{Bmatrix}\varphi_1 \\ \varphi_2\end{Bmatrix}_2 q_2(t) \tag{3.15}$$

3.4.2 System Response and Dynamic Loads

Response

From the modal equations obtained above, response to a given earthquake can now be computed using the response spectra. First the modal excitation factor are introduced:

$$L_n = \boldsymbol{\varphi}_n^T \cdot \mathbf{M} \cdot \mathbf{l} \tag{3.16}$$

Where

$$\boldsymbol{l} = \begin{Bmatrix}1 \\ 1\end{Bmatrix}$$

This gives the modal distribution of the earthquake induced loads from $\ddot{u}_g$, hence:

$$\tilde{M}_n\ddot{q}_n(t) + \tilde{K}_n q_n(t) = -\boldsymbol{\varphi}_n^T \cdot \mathbf{M} \cdot \mathbf{l} \cdot \ddot{u}_g(t) \tag{3.17}$$

Dividing by the modal mass and simplify:

$$\ddot{q}_n(t) + \omega_n^2 q_n(t) = -\frac{L_n}{\tilde{M}_n}\ddot{u}_g(t) \tag{3.18}$$

Solving the differential equation 3.18 it can be shown that the maximum modal response can be expressed as:

$$q_{n,max} = \frac{L_n}{\tilde{M}_n} \cdot S_d(\omega_n) \tag{3.19}$$

Where S_d is the displacement response spectrum of the given time series. From now the frequency will be expressed in periods, $T_n = \frac{2\pi}{\omega_n}$. It is also possible to express modal maximum acceleration in the terms of pseudo spectral acceleration $PS(T_n) = \omega_n^2 \cdot S_d(T_n)$:

$$\ddot{q}_{n,max} = \frac{L_n}{\tilde{M}_n} PS_A(T_n) \tag{3.20}$$

Maximum response for a given earthquake can now be expressed through equation 3.15. However, since there is no longer any time dependency and the modes are independent of each other it is necessary need to use SRSS (Square Root of the Sum of Squares) to obtain a statistical approximation for the combined modal response.

$$\begin{Bmatrix} \delta_m \\ \theta_m \end{Bmatrix}_{max} = \sqrt{\left(\boldsymbol{\varphi}_1 q_{1,max}\right)^2 + \left(\boldsymbol{\varphi}_2 q_{2,max}\right)^2} \tag{3.21}$$

Equivalent Forces

The earthquake induced loads on the system can be expressed as equivalent dynamic forces using the spectral acceleration. These equivalent forces are given in terms of the maximum SRSS acceleration.

$$\begin{aligned} F_n &= m \cdot \frac{L_n}{\tilde{M}_n} \cdot S_A(T_n) \cdot \varphi_{1,n} \\ M_n &= I_\theta \cdot \frac{L_n}{\tilde{M}_n} \cdot S_A(T_n) \cdot \varphi_{2,n} \end{aligned} \tag{3.22}$$

and

$$F_{dyn} = \sqrt{F_1^2 + F_2^2}$$
$$M_{dyn} = \sqrt{M_1^2 + M_2^2} \tag{3.23}$$

3.4.3 Variable Secant Stiffness Procedure

From the previous sections all necessary tools to begin the iteration procedure are presented. Each step of the iteration process will here be presented, including the convergence criterion.

- **Step 1**
  Initial loading ratio, h_0 is assumed, represented by the dotted line in the $M - Q$-diagram. Corresponding back-bone curves are constructed and initial stiffnesses values are found.

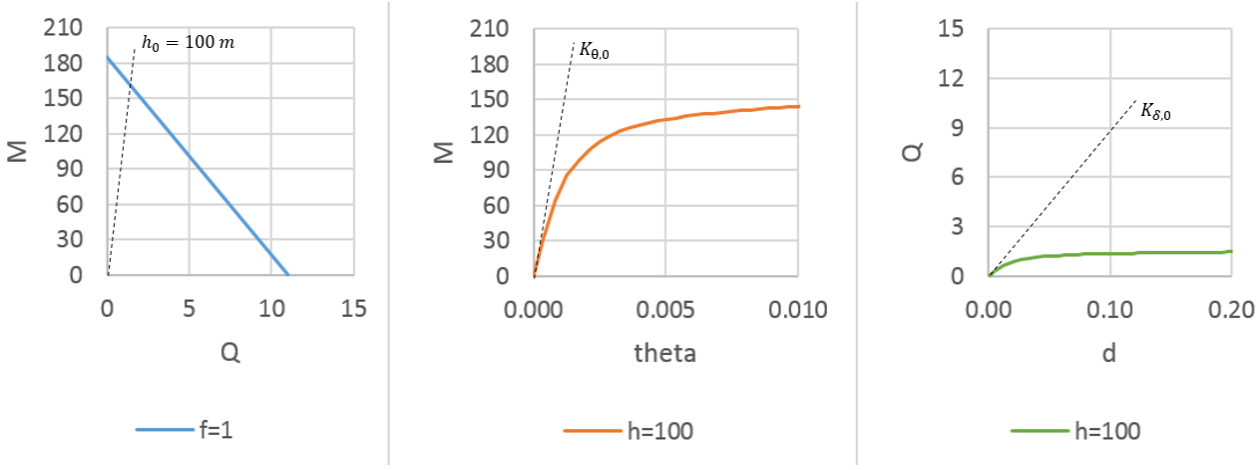

Figure 3.5: SMNA: Iteration step 1

- **Step 2**
  First modal analysis is conducted using the initial stiffnesses, $K_{\delta,0}$ and $K_{\theta,0}$. Equivalent load, Q_{dyn} and M_{dyn}, from the analysis are illustrated by the red dots in figure 3.6. The loads are then projected onto the back-bone in order to find the displacement based loads, Q and M, whence the displacement based mobilization is found:

$$f_M = \frac{M}{M_{ult}} \qquad f_Q = \frac{Q}{Q_{ult}}$$

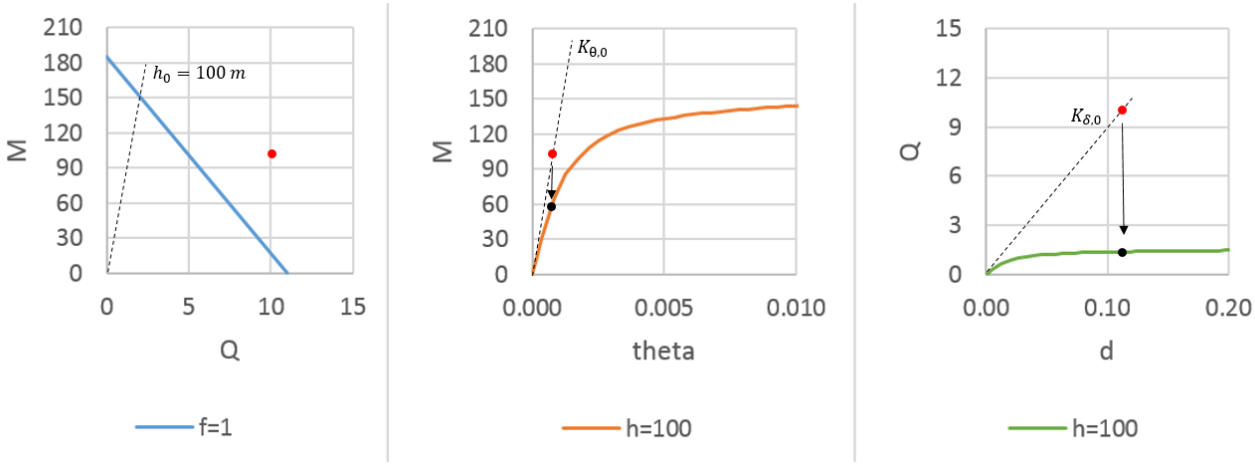

Figure 3.6: SMNA: Iteration step 2

- **Step 3**
  The loading ratio is updated (h_1) according to the load response from previous step, and new back-bone curves are drawn. Mobilization degrees are plotted onto the load ratio line and average degree of mobilization is represented by the yellow dot. Secant stiffnesses are determined from f_{ave} in the newly obtained back-bone curves.

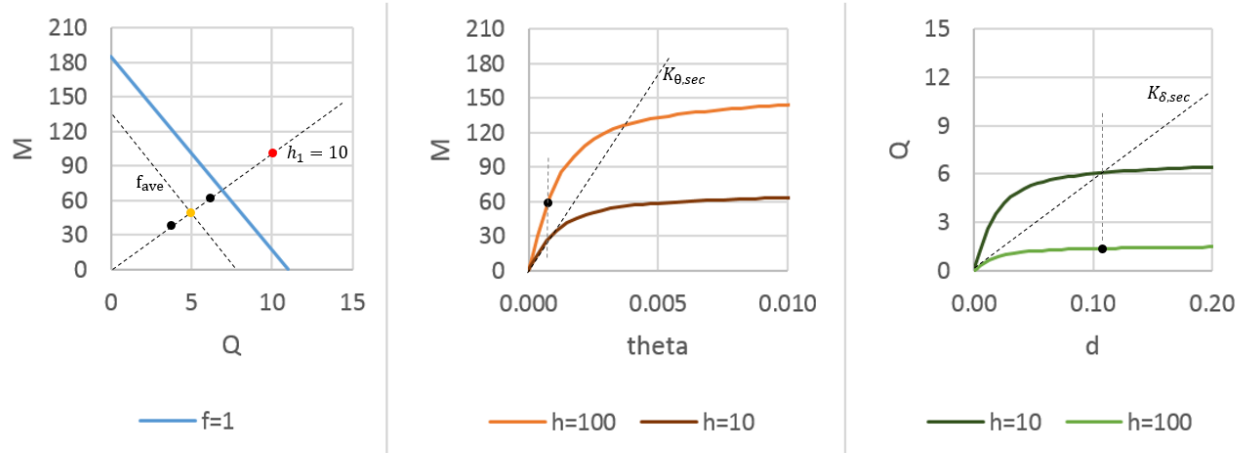

Figure 3.7: SMNA: Iteration step 3

- **Step 4**
  Then step 2 is repeated using updated secant stiffnesses. The procedure are repeated until convergence is obtained from the following criteria:

  – Dynamic stiffness is compatible to the soil-caisson response stiffness.

  – Loading ratio are the same over the iteration step, $h_i = h_{i-1}$.

  – The ratio between dynamic displacement and rotation, $\theta_{dyn}/\delta_{dyn}$, is the same as the response ratio obtained in soil-caisson interaction analyses.

– The same mobilization degree is obtained for both resulting moment and resulting force, $f = \frac{Q_{dyn}}{Q_{ult}} = \frac{M_{dyn}}{M_{ult}}$

3.4.4 Assumptions and Simplifications

Hysteretic Damping of Soil

As discussed in chapter 2.9.2 there is never any simple way to account for damping. In the SMNA-method it is assumed that the equivalent damping of the system can be expressed as the sum of structural and soil damping.

$$\tilde{\xi} = \xi_0 + D \tag{3.24}$$

Where $\tilde{\xi}$ is the equivalent damping, ξ_0 is the structural damping (usually set to 5%) and D is the hysteretic damping in the soil. It is necessary to introduce equivalent damping as a reduction factor in the response spectrum analysis in order to get proper output for the response. Starting by expressing hysteretic damping in terms of the secans stiffnesses ratio K_0/K_{max}.

$$D = D_0 + (D_{max} - D_0) \cdot \left(1 - \left[\frac{K}{K_{max}}\right]^{\beta_0}\right) \tag{3.25}$$

Where D_0 and D_{max} is the damping ratios at $K/K_{max} = 1$ (low damping) and $K/K_{max} = 0$ (high damping) respectively. β_0 is an empirical factor, here set to 0.6.

Damping ratios may also be determined numerically by integrating the back-bone curve (Ishihara, 1996):

$$D = \frac{1}{4\pi} \cdot \frac{\Delta W}{W} \tag{3.26}$$

For each modal analysis a new period, T_n, is obtained from the secant stiffness ratios. The corresponding damping ration will den produce the reduction factor, η:

$$\eta = \sqrt{(a + \xi_o)/(a + \xi_0 + D)} \tag{3.27}$$

Where a is a frequency dependent coefficient assumed to be 5% in this case. The reduced response acceleration can finally be calculated:

$$PS_{A,d}(T_n) = PS_A(T_n) \cdot \eta \tag{3.28}$$

Added Mass

Until now there has not been considered any foundation mass or soil added mass in the SMNA-calculations. This assumption is justified due to a stiffer behavior and increase in overturning moment, thus a conservative decision regarding safe design.

Part II

Case Study

Chapter 4

Description of Analyses

4.1 Introduction

A hypothetical case study of a deepwater manifold subjected to earthquake loads will be presented in this chapter. The manifold is founded on a closed caisson penetrated 20 meters into the seabed. The structure is illustrated in figure 4.1, geometry and physical data are given in appendix B.2. The seabed consists of a 60 meter deep layer of soft North Sea clay with linear increasing shear stiffness. Soil parameters was provided from preliminary research at Multiconsult.

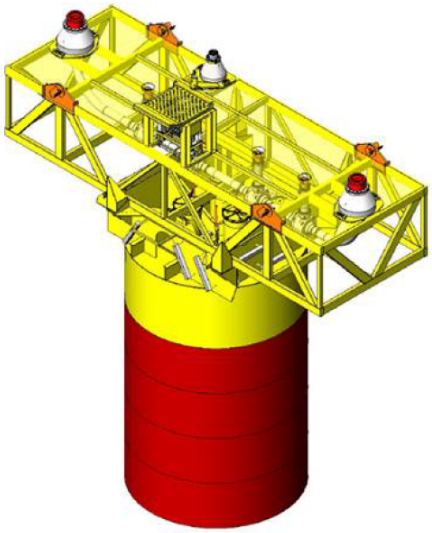

Figure 4.1: Illustration of a subsea manifold founded on closed caisson.

In this case study the dynamic response from in comprehensive numerical model was compared to the simplified SMNA-model. The following sections present methods and

procedures of how the different analyses were built up, verified and carried out. Explanation of how input was retrieved and chosen are considered when necessary. The analyses are presented in the order they where conducted.

Software

All FEM-analyses were done in PLAXIS 3D (AE.01), a software developed especially for deformation and stability problems in geotechnical engineering. The dynamic add-on module was used to apply and analyze the dynamic responses throughout each analysis.

The SMNA-analyses were done in MODAN, a software developed by Multiconsult in Oslo. MODAN carries out the variable secant stiffness procedure, presented in section 3.4.3. Foundation input motion and back-bone curves were obtained using PLAXIS 3D before implementing relevant parameters into MODAN.

Dynamic Input

Acceleration time series from the Upland (CA) earthquake in 1990 was used as dynamic input for this case study. The earthquake has a Richter magnitude of 5.4 and a peak ground acceleration of 0.245 g. The acceleration recordings are plotted in figure 4.2.

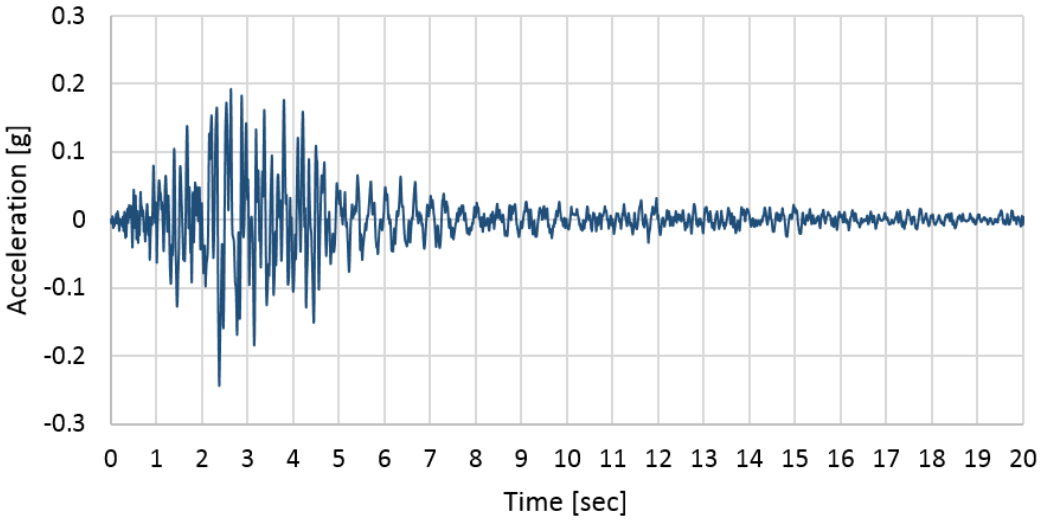

Figure 4.2: Acceleration time series, Upland (CA), 1990

4.2 FEM Analyses

4.2.1 Background Information

The FEM-analyses are the most comprehensive of the analyses conducted and will in this study serve as "the correct solution". Despite this assumption the model include some simplifications and will not necessarily give the complete picture of the physical behavior. The FEM-analyses are done in three parts serving different purposes listed in the table below 4.1.

Analysis	Objective
Free Surface	Soil model verification
Kinematic Interaction	Foundation motion input to SMNA-method
Full Analysis	Analyse earthquake response of the subsea manifold

Table 4.1: FEM-analyses and objectives.

4.2.2 Soil Model

Geometry

The soil was modelled as a 15 meter wide slice of a 60 meter deep soil deposit of soft clay over rigid bedrock, see figure 4.3. To save computational time only one symmetric half was modeled. The extent of the model is 160 meters in the x-direction, parallel to the direction of the applied dynamic load. This was done to avoid unwanted boundary effects. Boundary effects from the y-boundaries were assumed not to be significant. The soil model dimensions are presented in table 4.2.

Soil Model Dimesions					
x_{min}	x_{max}	y_{min}	y_{max}	z_{min}	z_{max}
-80 m	80 m	0 m	15 m	-60 m	0 m

Table 4.2: Soil model measurements used in FEM-analyses.

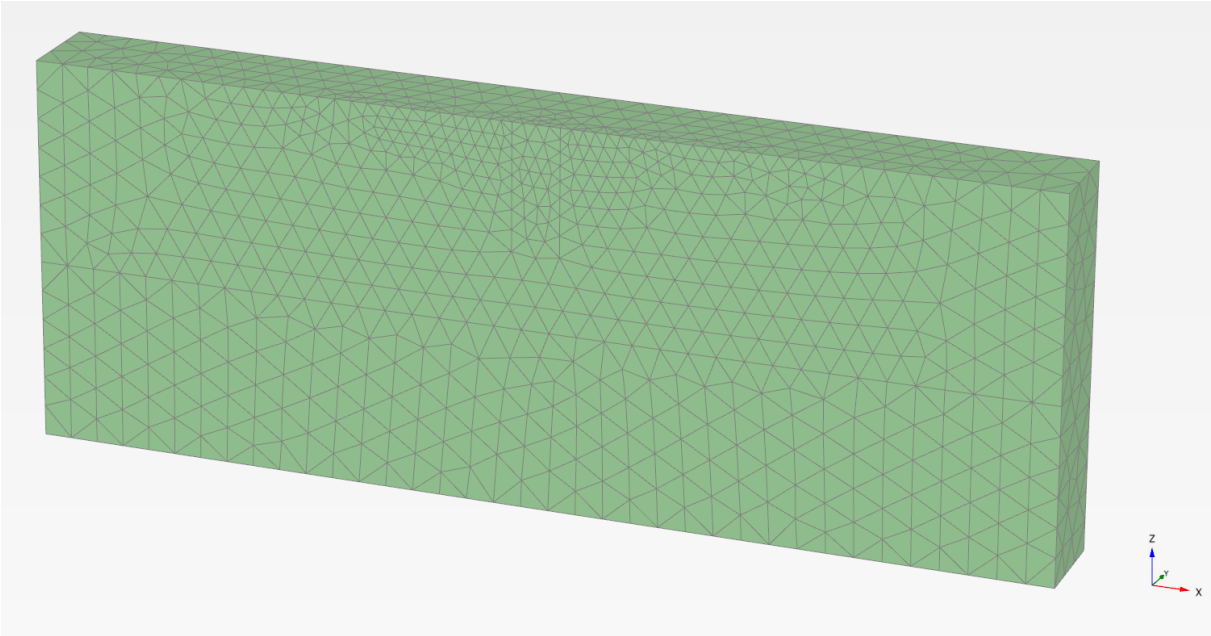

Figure 4.3: PLAXIS 3D soil model

Mesh Refinement

The soil volume was modelled using 10-noded tetrahedral elements. Mesh refinement was set to medium using a coarseness factor of 0.7 on the whole soil volume, in order to maintain an evenly distributed element size. For more detailed mesh information see appendix C.

Material Model

The soil material used was an undrained linear elastic perfectly plastic Mohr-Coulomb model. The material represent soft North Sea clay with increasing shear modulus with depth. To account for strain based modulus reduction a stiffness approximately equal to E_{50} was used. Energy dissipation in the soil material was considered using Rayleigh damping. A damping ratio of $\xi = 5\%$ was tuned over the critical frequencies f_1 and f_2. The target frequencies was calibrated after the principles of Hashash and Park (2002). Soil parameters are listed in table 4.3. For soil profiles and additional information see appendix A.

Soil Model	
Depth	0-60 meters
Water Table	0 m
Material Model	Mohr-Coulomb
Drainage	Undrained B
Unit Weight	$\gamma = 16.4$ kN/m^3
Poisson's Ratio	$\nu' = 0.35$
Youngs Modulus	E' = 2575 kPa
	E_{inc}' = 2788 kPa/m $\cdot$ z
Shear Modulus	G = 953.7 kPa
Shear Strength	S_u = 1.87 kPa
	$S_{u,inc}$ = 2.025 kPa/m $\cdot$ z
Rayleigh Damping	$\alpha = 0.2377$
	$\beta = 2.151 \cdot 10^{-3}$

Table 4.3: Soil parameters

Boundary Conditions

Allowing correct dynamic behavior and avoiding unwanted boundary effects required important considerations choosing boundary conditions. Due to material damping and a sufficiently large model, it was not necessary to assess viscous boundaries in this case. Proper displacements was ensured using vertically fixed x-boundaries and fixed motion in the y-direction. To keep the model from collapsing sideways and at the same time allow dynamic motion in situ horizontal stresses was applied to the x-boundaries working together with to the hydrostatic pressure, see equation 4.1 and figure 4.4.

$$\sigma'_{inc} = \gamma' \cdot K'_0 \tag{4.1}$$

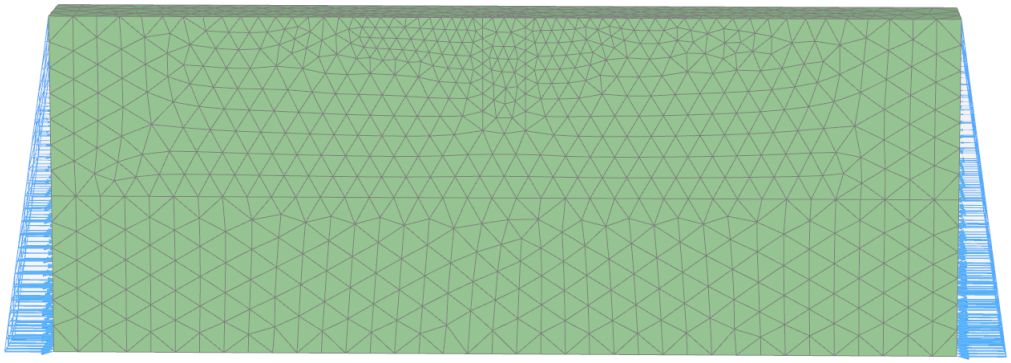

Figure 4.4: Application of in situ horizontal stresses to the numerical soil model.

The boundary conditions used are listed in table 4.4 below.

Boundary	Displacement	Dynamic	Incremental In Situ Stresses
x_{min}	*vertically fixed*	-	3.84 kPa/m $\cdot z$
x_{max}	*vertically fixed*	-	-3.84 kPa/m $\cdot z$
y_{min}	*normally fixed*	-	-
y_{max}	*normally fixed*	-	-
z_{min}	*prescribed motion*	-	-
z_{max}	*free*	-	-

Table 4.4: Boundary conditions used in FEM-analyses.

4.2.3 Free-Field Analyses

In order to verify the model there were initially conducted a series of free-field tests. Both harmonic motion and earthquake acceleration were considered.

Harmonic Free-Field Analysis

Harmonic displacements were applied to the bottom boundary of the soil model. Then the surface displacements at steady state were recorded at a control node and compared with theory, see figure 4.5 . In these analyses linear elastic soil with constant shear wave velocity of $V_s = 150\frac{m}{s}$ was used. Although this is not always a proper material model for soils, it was satisfactory for the purpose of verifying the boundary conditions and wave propagation properties.

Twelve different frequencies were tested. Expected amplification of shear waves propagating through the soil was found from site response theory, discussed in chapter 2.4. The natural frequencies and amplification function were found by the equations 4.2, where ω_n represents the n'th natural frequency and $|F(\omega)|$ is the amplification function.

$$\omega_n = \frac{V_s}{H}\left(\frac{\pi}{2} + n\pi\right)$$
$$|F(\omega)| = \frac{1}{\sqrt{cos^2\left(\frac{\omega H}{V_s}\right) + \left(\xi\frac{\omega H}{V_s}\right)^2}} \tag{4.2}$$

Earthquake Free-Field Analysis

The main focus of this analysis was to see how the soil amplifies and filters out frequencies resulting in a output acceleration time series on the surface. Dynamic input acceleration was applied at the bottom boundary and the surface acceleration was recorded in the control node. Additional information is presented in appendix C.

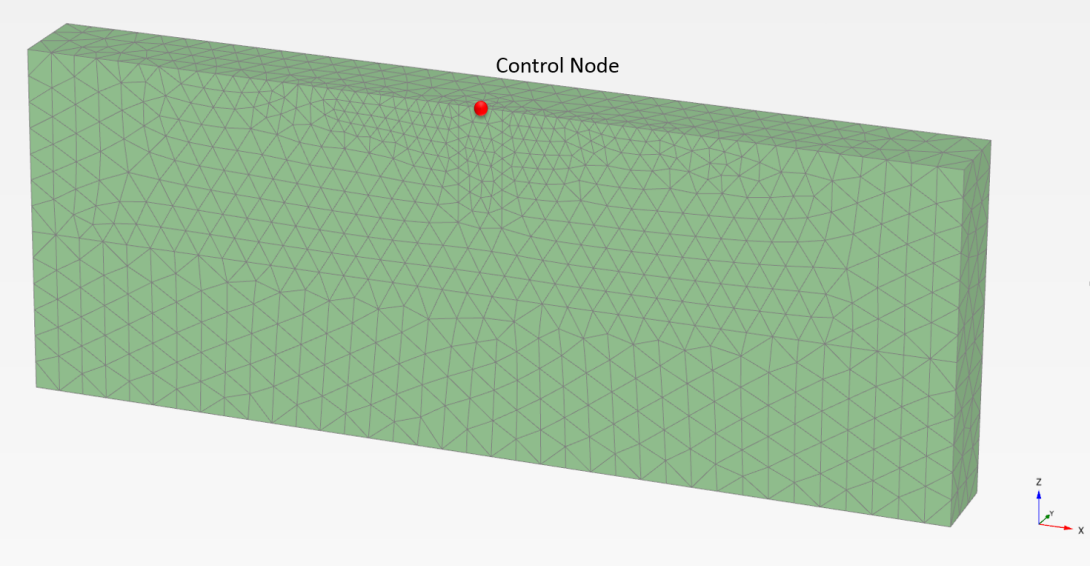

Figure 4.5: Soil model with control node.

4.2.4 Kinematic Interaction Analysis

The kinematic interaction analysis was carried out introducing a massless closed caisson foundation into the soil, before applying earthquake loading, see figure 4.6. The main objective was to obtain the foundation input motion for the SMNA-method, but it was also of interest to see how the stiffness of the foundation constrained the soil motion.

Foundation geometry and material properties are presented in table 4.5 and 4.6. The caisson was modelled using 6-node triangular plate elements. Mesh refinement was set to medium using a coarseness factor of 0.5, see figure 4.7. For a more detailed element information see appendix C. Interface elements were introduced to the outside of the caisson allowing slip between soil and structure, roughness was set to R=0.5.

	Caisson		**Top Plate**	
Diameter	$D_{caisson} =$	7.50 m	$D_{plate} =$	7.50 m
Skirt length	$L_{caisson} =$	20.00 m		-
Wall thickness	$t_{caisson} =$	0.03 m	$t_{plate} =$	0.04 m

Table 4.5: Geometry of caisson

Plate Material	
Young's Modulus	$E = 210\ 000$ GPa
Unit Weight	$\gamma = 0$ kN/m^2
Poisson's Ratio	$\nu = 0.3$
Roughness	$R = 0.5$

Table 4.6: Caisson plate material properties.

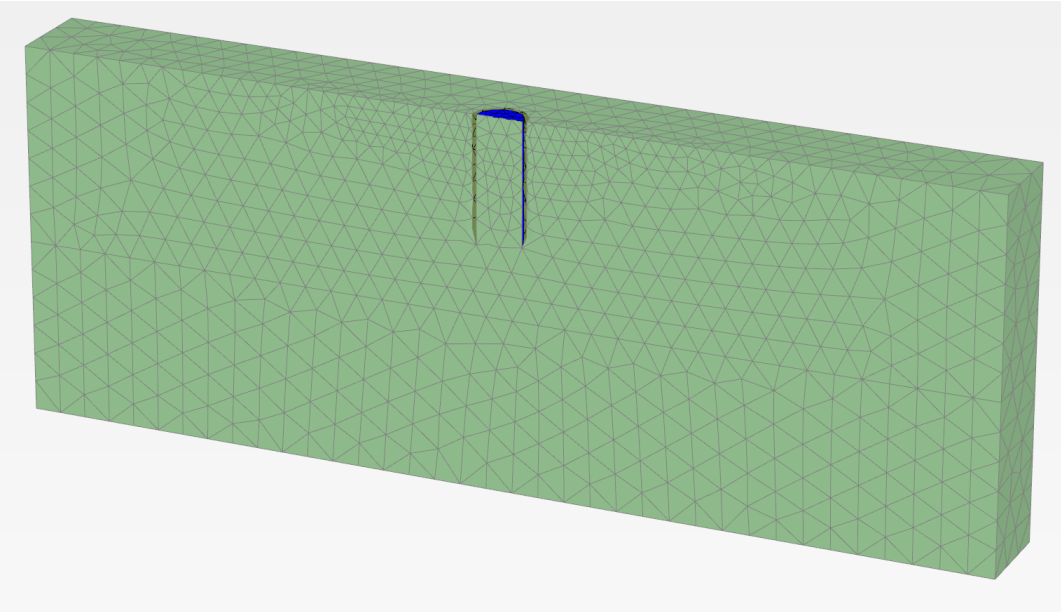

Figure 4.6: Mesh used in the kinematic interaction analysis

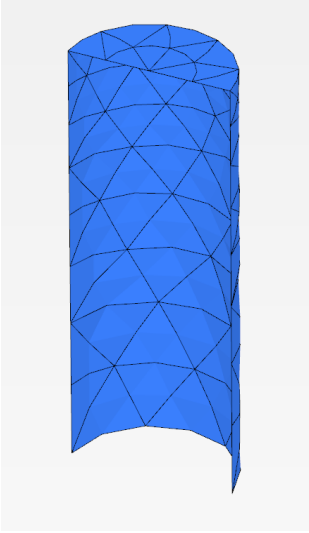

Figure 4.7: Caisson model, medium mesh

4.2.5 Full Model Analysis

The full model analysis was carried out in the same soil model used for the previous analyses. Mass was applied to the foundation and the manifold was installed on top of the foundation supported by a massless column, see figure 4.9. The objective in this analysis was to study the response and equivalent forces acting on the base of the superstructure.

For simplification the manifold structure was modelled as a solid volume with evenly distributed mass, see figure 4.8. Mesh refinement was set to medium, for detailed information see appendix C.4. Geometry and material properties were set to give correct mass, center of gravity and mass moment of inertia as the real structure. The materials and physical properties used the the PLAXIS-model are presented in 4.7. Note that these quantities are for the full geometry of the structure while only one symmetric half is modelled in PLAXIS 3D.

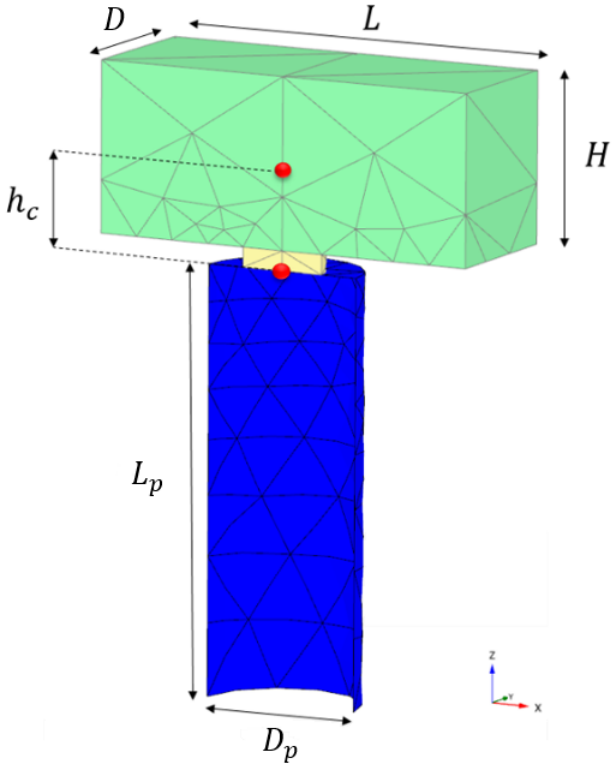

Figure 4.8: Simplified geometry of the manifold structure installed on the caisson foundation.

Once more acceleration was applied to the bottom boundary. During the analysis acceleration and displacement were recorded in control nodes seen in figure 4.9. From these recordings translation and rotation was found. Full PLAXIS setup for the analysis are given in appendix C.4.

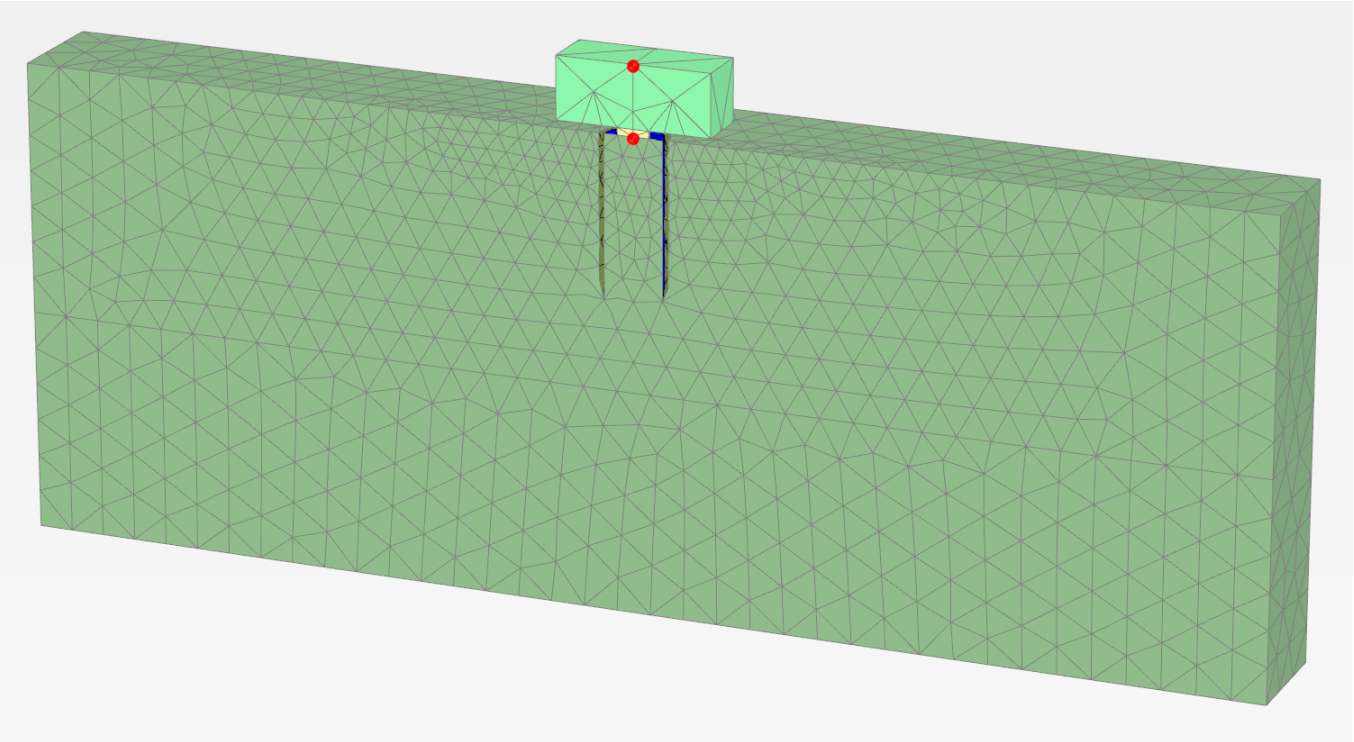

Figure 4.9: Full PLAXIS 3D model used in analyses.

Structure Data			
Manifold geometry			
Length	L	18.9	m
Depth	D	14.2	m
Height	H	8.0	m
Material			
Young's modulus	$E_{manifold}$	$210 \cdot 10^9$	kPa
Unit weigth	$\gamma_{manifold}$	1.62	kN/m^3
Poisson's raitio	ν	0.3	
Physical data			
Weigth	$W_{manifold}$	4 041.0	kN
	$W_{caisson}$	1 240.5	kN
	W_{total}	5 281.5	kN
Moment of inertia	$I_{manifold}$	15 599.3	tm^2
	$I_{caisson}$	4 530.9	tm^2
	I_{total}	39 904.9	tm^2
Center of gravity	h_c	1.68	m

Table 4.7: Properties of the simplified structure modelled in Plaxis 3D.

4.3 SMNA-analyses

4.3.1 Backround Information

In this section analyses conducted using the SMNA-method are presented. The software MODAN was used to perform the analyses. External analyses obtaining necessary MODAN-input parameters were carried out in PLAXIS 3D and will also be presented in this section. The objectives for the analyses presented are divided into primary and secondary objectives.

- **Primary Objective**
  - Perform SMNA-analyses with varying mass parameters to study effects of soil added mass parameters.
- **Secondary Objective**
  - Obtain back-bone curves by static analyses to retrieve necessary MODAN-input parameters.
  - Construct normalized acceleration response spectrum from kinematic interaction record.

4.3.2 MODAN-input

The different segments of input used in MODAN will be presented in this section. Method of how the parameters are obtained are presented if necessary.

Structure Data

The physical parameters used in MODAN constitutes the mass matrix used in the modal calculations. A total mass, mass moment of inertia and center of gravity are calculated externally before put into MODAN. The structure geometry is only used for basic visual purposes in MODAN. Rigid behavior of all structural components is assumed ($E \rightarrow \infty$). Structure data including foundation mass are presented in table 4.8.

Back-Bone Curves

Non-linear soil stiffness is considered using back-bone curves, externally obtained by static load-displacement analysis in PLAXIS 3D. The analyses were done in the same soil material used in the dynamic analyses. In the analyses both symmetric halves was modelled,

STRUCTURE DATA MODAN		
Geometry		
Manifold length	18.9	m
Manifold depth	14.2	m
Manifold height	9.86	m
Caisson diameter	7.5	m
Caisson length	20.0	m
Caisson thickness	0.03	m
Inertial Parameters		
W_{total}	5 281.5	kN
I_{total}	39 881.1	tm^2
h_c	1.68	m

Table 4.8: Initial structure data used in MODAN calculations

seen in appendix C.5. First the massless foundation was installed in the soil, then following steps were performed:

1. Horizontal force and overturning moment were applied in the center of the caisson top lid, see figure 4.10.
2. Loads were increased incrementally at constant load ratio, $h = \frac{M}{Q}$, until failure.
3. $Q - \delta$ and $M - \theta$ curves were plotted for the different load ratios.

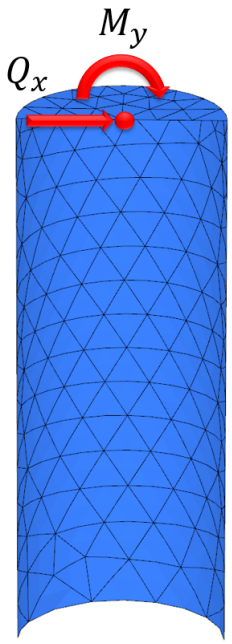

Figure 4.10: Loads applied to foundation in the soil-caisson interaction analyses.

In total five analyses at different load ratios were performed. The lateral displacement, δ was measured at the center of the caisson top lid while θ was measured as the relative

vertical displacements of the edges of the lid divided by the diameter, see equation below and figure 4.11. Load ratios and applied target loads are listed in table 4.9. Load increments were controlled by $\sum M_{stage}$ and adjusted automatically by PLAXIS. Ultimate state criteria was defined manually from the curvature of the plot. A well defined failure state is unavailable in such numerical analyses.

From the back-bone curves necessary stiffness and ultimate state parameters can be extracted. In table 4.10 all parameters used in MODAN is tabulated. Note that MODAN only uses maximum initial stiffness parameters. From the ultimate load and ultimate displacement MODAN interpolates and generate all possible back-bone curves.

$$\theta = \frac{\delta_{z,x=-D/2} - \delta_{z,x=D/2}}{D} \tag{4.3}$$

SOIL-CAISSON INTERACTION ANALYSES			
Test, #	Load ratio, h	Q_{target} [kN]	M_{target} [kNm]
1	0.001	15 000	15
2	1	20 000	20 000
3	10	10 000	100 000
4	100	5 000	500 000
5	1000	2 000	2 000 000

Table 4.9: Load ratios and target loads from static analyses.

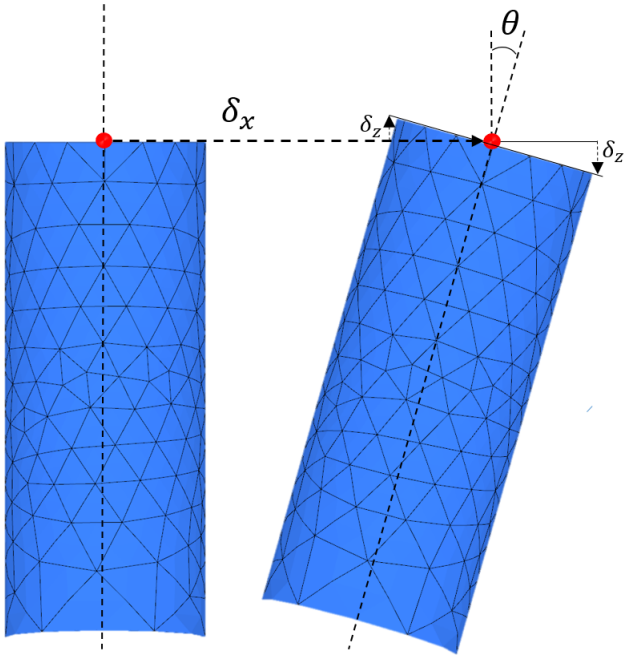

Figure 4.11: Measured displacements of the caisson during static analyses.

Stiffness and Ultimate Parameters		
Parameter	Load Ratio	Description
$K_{x,max,max}$	h_0	maximum initial displacement stiffness
$K_{\theta,max,max}$	h_{ult}	maximum initial rotation stiffness
$Q_{ult,0}$	h_0	ultimate lateral force resistance
$M_{ult,0}$	h_{ult}	ultimate moment resistance
$\delta_{ult,max}$	h_0	ultimate lateral displacement
$\delta_{ult,min}$	h_{ult}	ultimate lateral displacement
$\theta_{ult,max}$	h_{ult}	ultimate lateral rotation
$\theta_{ult,min}$	h_0	ultimate lateral rotation

Table 4.10: MODAN-parameters found from back-bone curves. $h_0 = 0.001$ and $h_{ult} = 1000$ in the analyses.

Failure Surface

From the results found in the soil-caisson interaction analyses the ultimate loads at failure was plotted against each other in a $Q - M$-diagram. Throughout the variable secant stiffness iteration forces and moments from each iteration can be used to find the average degree of mobilization within the yield surface making use of equation 3.4.

Earthquake Loads

As discussed in section 3.3, the modal analysis procedure uses an acceleration response spectrum as an equivalent dynamic input. The input can be interpreted as a foundation input motion and was obtained creating a normalized response spectrum from the acceleration time series obtained in the kinematic interaction analysis.

From the time series the acceleration response spectrum was generated using the curve manager option in PLAXIS 3D.

4.3.3 MODAN-analyses

The MODAN-analyses were initially conducted in five stages, gradually adding more soil mass inside the foundation. Based on the initial results, a parametric study was further carried out varying selected parameters. Effects of reducing response spectrum and stiffness relations were studied in addition to inertial effects. The initial five analyses are summarized in table 4.11. Corresponding mass distributions are illustrated in figure 4.12.

MODAN-Analyses				
Mass Components		**Input**		
Initial-Analyses		m $[t]$	I_θ $[tm^2]$	h_c $[m]$
1	Manifold	411.9	15599.3	4.93
2	Manifold+Caisson+1/7 soil	749.0	52132.0	0.81
3	Manifold+Caisson+3/7 soil	1171.0	65796.0	-1.54
4	Manifold+Caisson+5/7 soil	1593.0	98302.0	-4.16
5	Manifold+Caisson+7/7 soil	2016.0	156719.0	-6.87

Table 4.11: Setup for initial MODAN-analyses.

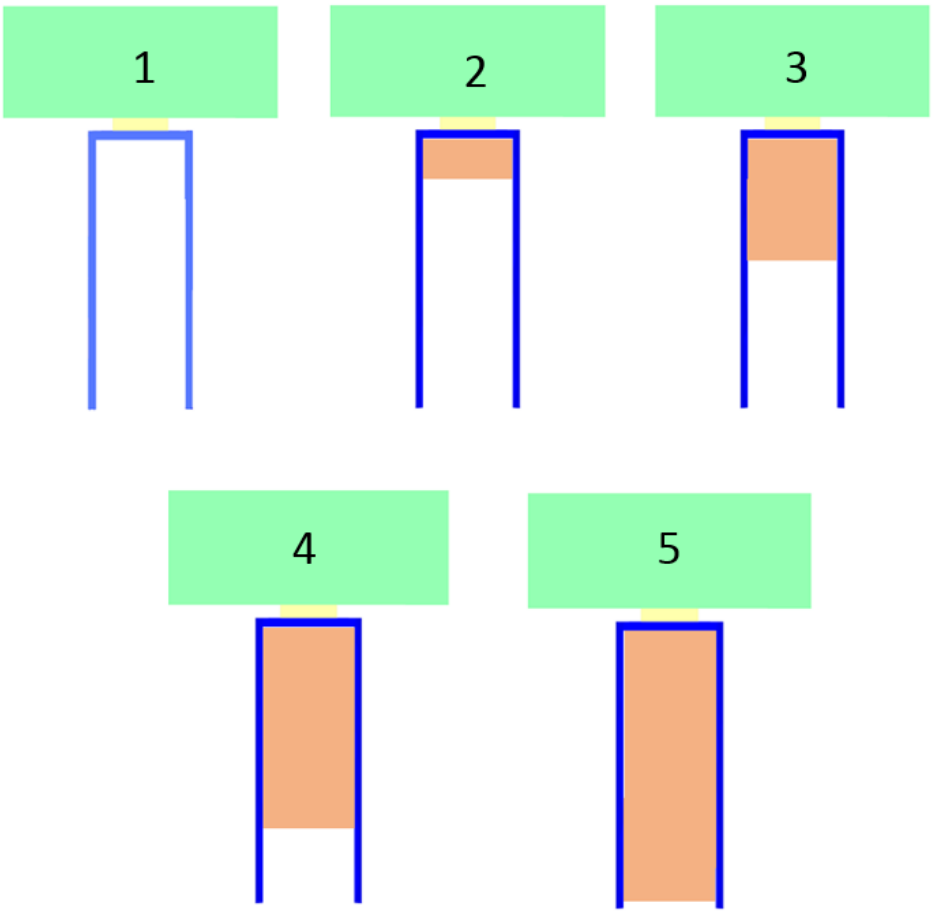

Figure 4.12: Added mass distribution in MODAN-analyses.

Chapter 5

Results and Discussion

5.1 PLAXIS 3D Analyses

5.1.1 Free-Field

Harmonic Results

Harmonic input of twelve different frequencies were tested. Input frequency and amplification results are tabulated in table 5.1 and plotted together with theoretical amplification factor in figure 5.1. The four mode shapes included in the bandwidth are shown in figure 5.2.

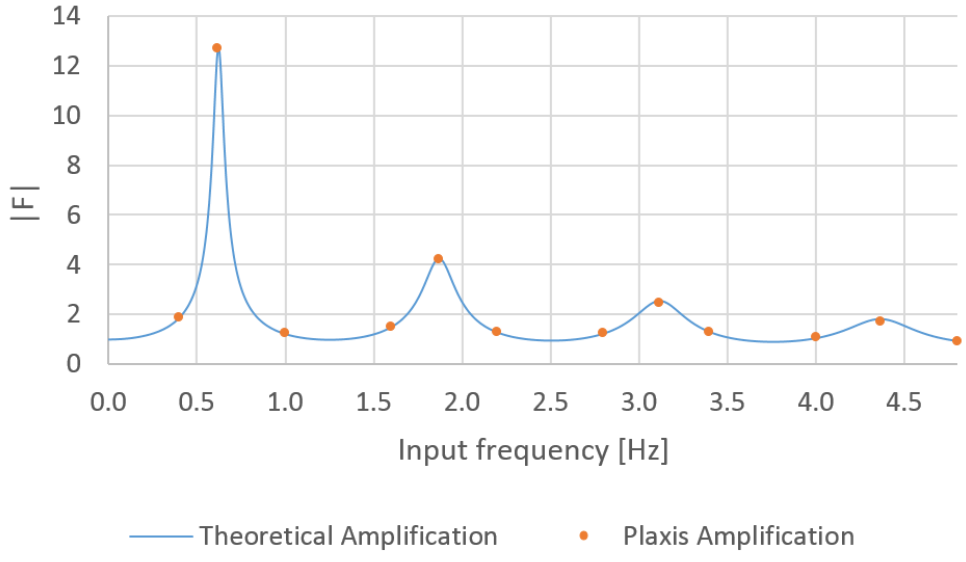

Figure 5.1: Verification of soil amplification.

Harmonic Free-Field Testing				
		$\lvert F(f_n)\rvert$		
n	f_n	Theoretical	Plaxis 3D	Error [%]
1	0.400	1.86	1.86	0.0
2	0.625	12.73	12.68	0.4
3	1.000	1.22	1.22	0.0
4	1.600	1.50	1.50	0.0
5	1.870	4.25	4.19	1.4
6	2.200	1.28	1.28	0.0
7	2.800	1.24	1.25	0.8
8	3.115	2.55	2.46	3.5
9	3.400	1.30	1.25	3.8
10	4.000	1.05	1.06	0.9
11	4.365	1.82	1.68	7.6
12	4.800	0.94	0.90	4.3

Table 5.1: FEM-analysis compared to theory

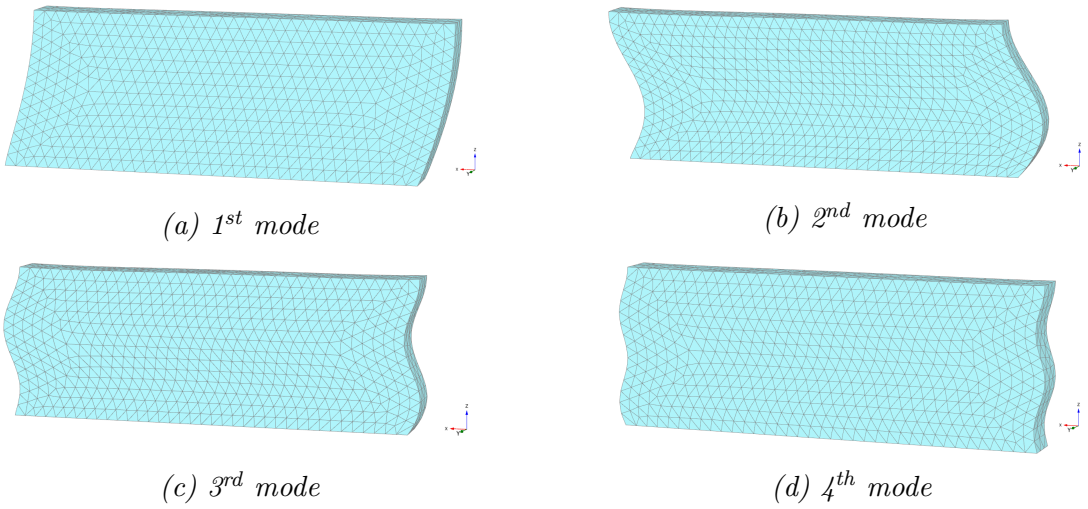

(a) 1st mode *(b) 2nd mode*

(c) 3rd mode *(d) 4th mode*

Figure 5.2: Mode shapes of soil layer at natural frequencies

Earthquake Results

Earthquake acceleration was applied to the bottom of the output soil model. Accelerations recorded at the surface node are plotted on top the input motion in figure 5.3. Maximum accelerations were amplified from 0.245 g in the input motion to 0.374 g at the surface.

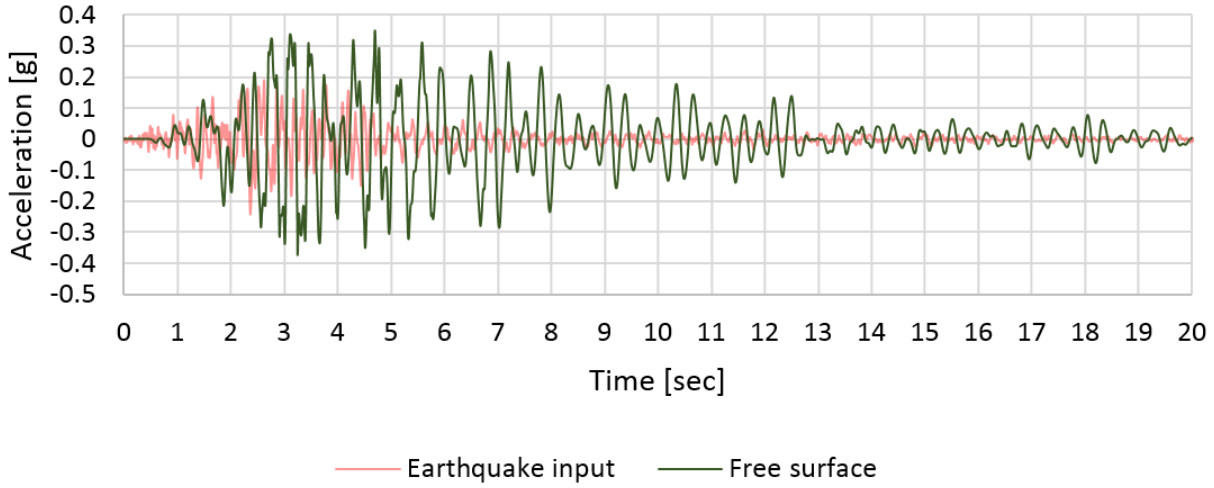

Figure 5.3: Acceleration time series from free-surface recordings on top of the input acceleration time series.

Discussion of Free-Field Results

The harmonic analyses generally gave a very good compliance with theoretical response. At the lower frequencies high amplification are recorded with low error. Although there is seen a slightly increasing error ratio at the higher frequencies, a maximum error of 7.6% are satisfactory to verify the amplification properties within the bandwidth of interest. The mode shapes illustrated that the pre-calculated natural frequencies show a well defined deformation according to theory. These results show that the soil model is able to deform freely in the x-direction and at the same time being fixed from deforming in y-direction, which suggest that proper boundary conditions are used.

From the acceleration plot 5.3 it is seen that the soil layer filters out some of the high frequencies from the input motion. This is even clearer in the Fourier spectres in figure 5.10, where the input energy at 6-10 Hz are completely gone in the surface recordings. This is expected behavior due to the stiffness proportional effect of Rayleigh damping which over-damps high frequencies.

It is seen an increase in peak acceleration from 0.245 g to 0.374 g from input to surface. This suggest a max amplification of 1.53. Between the $\xi = 5\%$ calibrated Rayleigh frequencies at $f_1 = 0.4\ Hz$ and $f_2 = 7\ Hz$ an even higher amplification could have been expected due to under-damping of the soil. Additional hysteric damping at high strain ratios most likely affect the result and cause decreased amplification.

5.1.2 Kinematic Interaction Analyses

Results

The acceleration recorded on top of the caisson is plotted in figure 5.4. The maximum acceleration recorded is 0.310 g after 3.0 seconds.

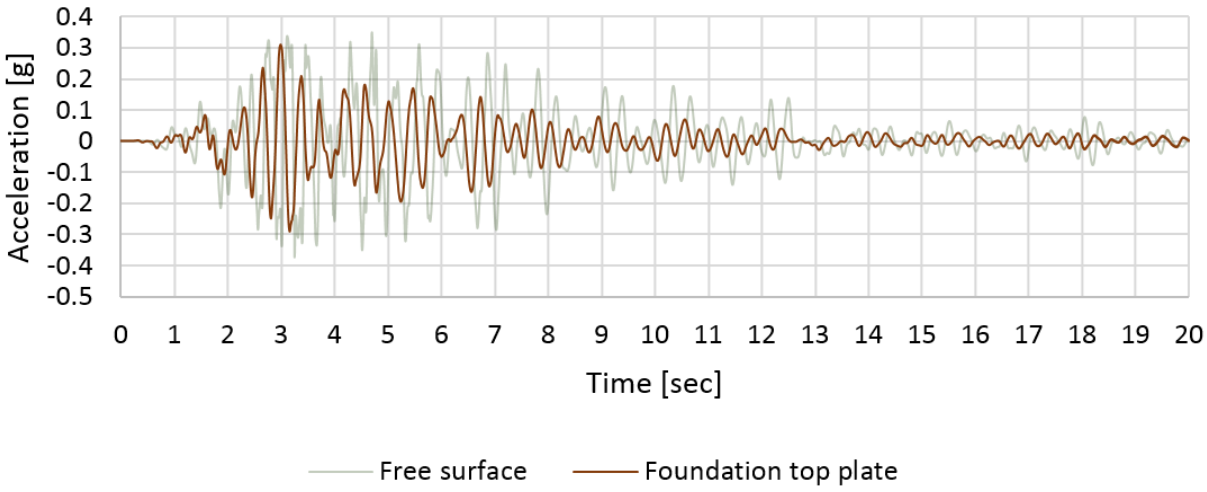

Figure 5.4: Acceleration at top of the closed caisson.

Discussion

Soil-structure interaction theory suggest that the embedded foundation restricts soil from moving freely and gives an approximately averaging of the free field motion in the adjacent soil. The results from the analyses clearly show that the foundation cannot follow the highest frequencies of the free-surface motion and filters out even more of the high frequencies, see figure 5.10. The motion averaging also results in reduced amplitudes, which are confirmed by the results. Peak acceleration at the foundation top plate was measured to be 0.310 g which is significant reduction from the free-field results. This motion represents which motion the structure "feels" during the earthquake and was used for the foundation input motion in the SMNA-analyses.

5.1.3 Manifold Analysis

Manifold Response Results

All relevant time series from the dynamic analyses including the full structure geometry are presented in this section. In figure 5.8 the model are shown in early and late stage of the analysis. A compilation of the frequency content of all acceleration time series from

the FEM-analyses are plotted in the Fourier spectra 5.10. Essential maximum response values from all FEM-analyses are presented in table 5.2 and 5.3. At the end the maximum equivalent dynamic loads on the structure are calculated from the ultimate parameters, presented in table 5.4.

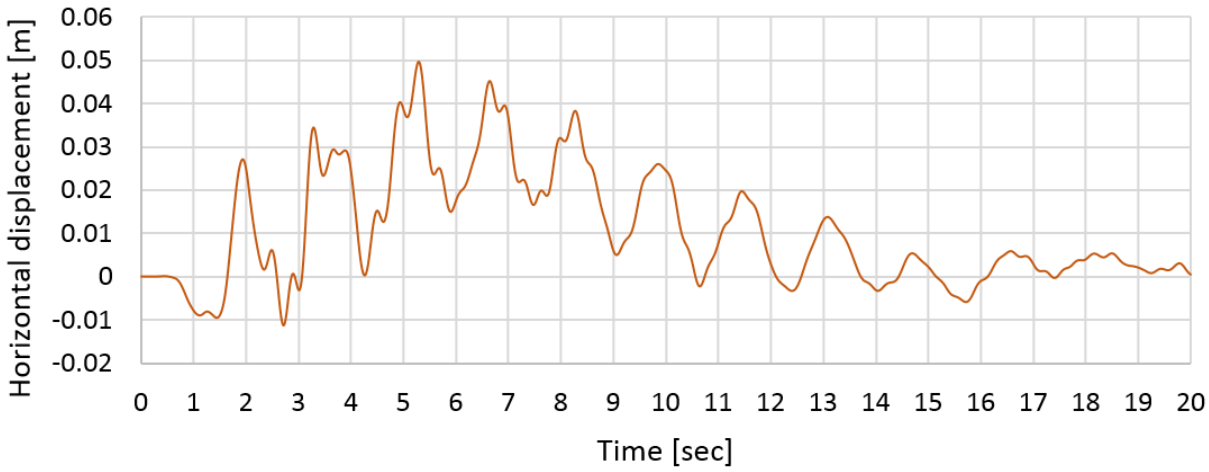

Figure 5.5: Recorded horizontal displacement at the base of the manifold structure from PLAXIS 3D

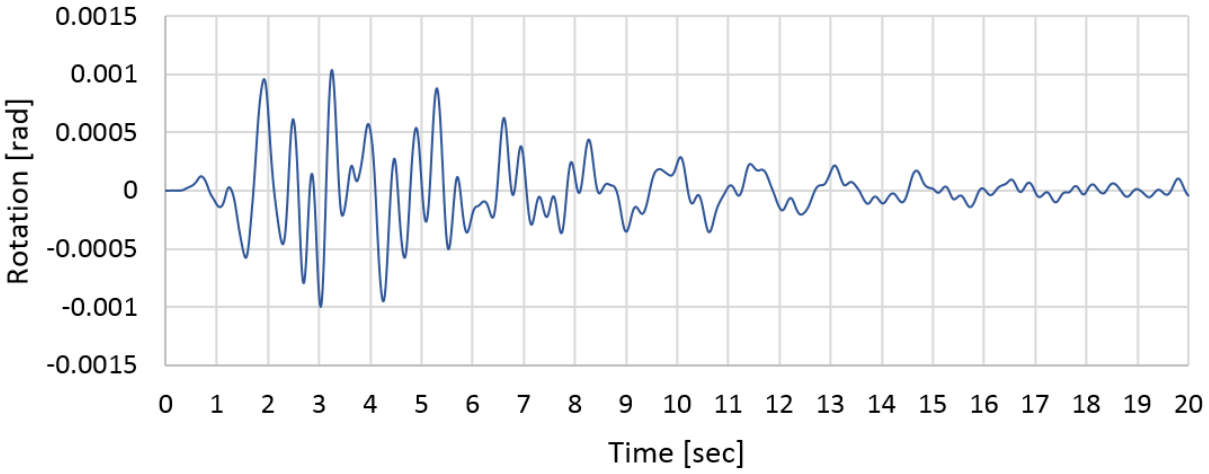

Figure 5.6: Recorded rotation at the base of the manifold structure from PLAXIS 3D

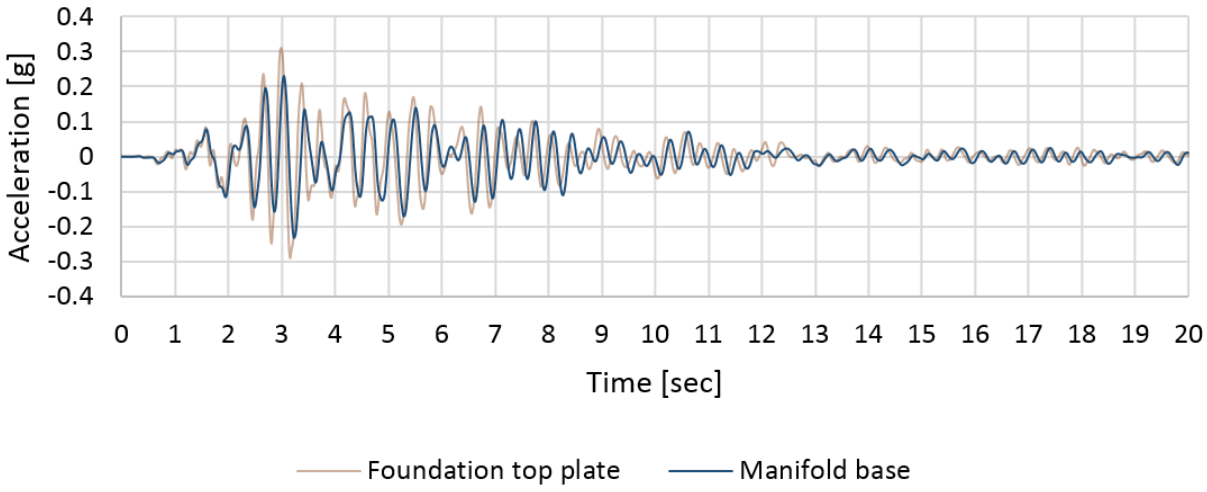

Figure 5.7: Recorded horizontal acceleration at the base of the manifold structure from PLAXIS 3D

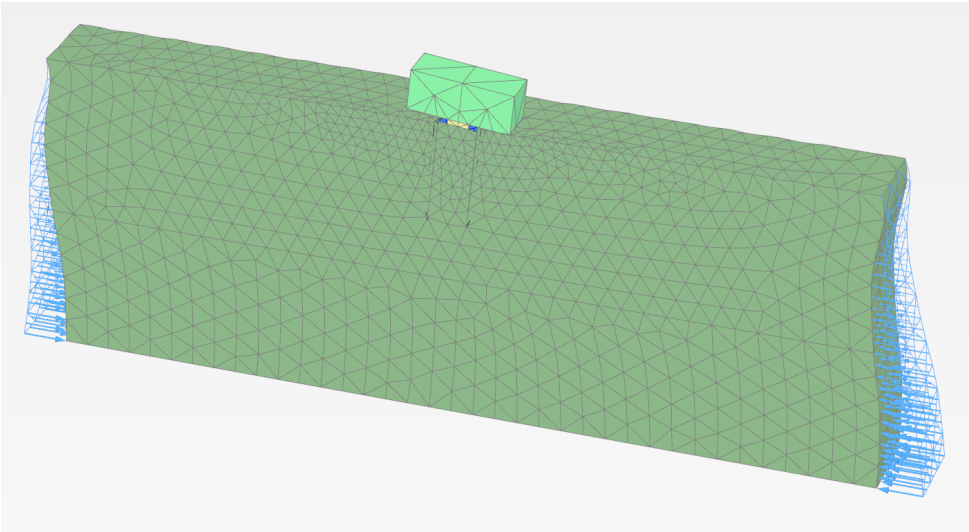

(a) Early stage

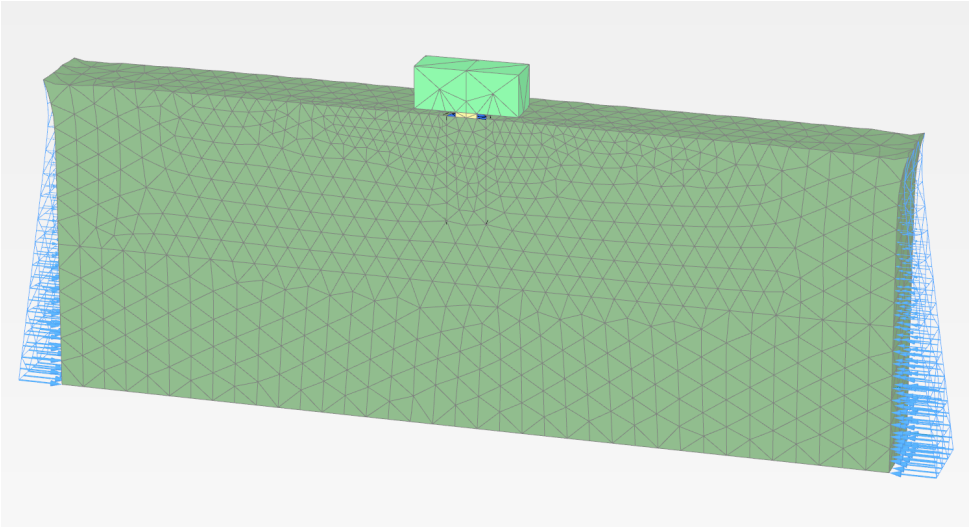

(b) Late stage

Figure 5.8: Deformed mesh scaled by a scaling factor of 50, from the dynamic PLAXIS 3D analysis.

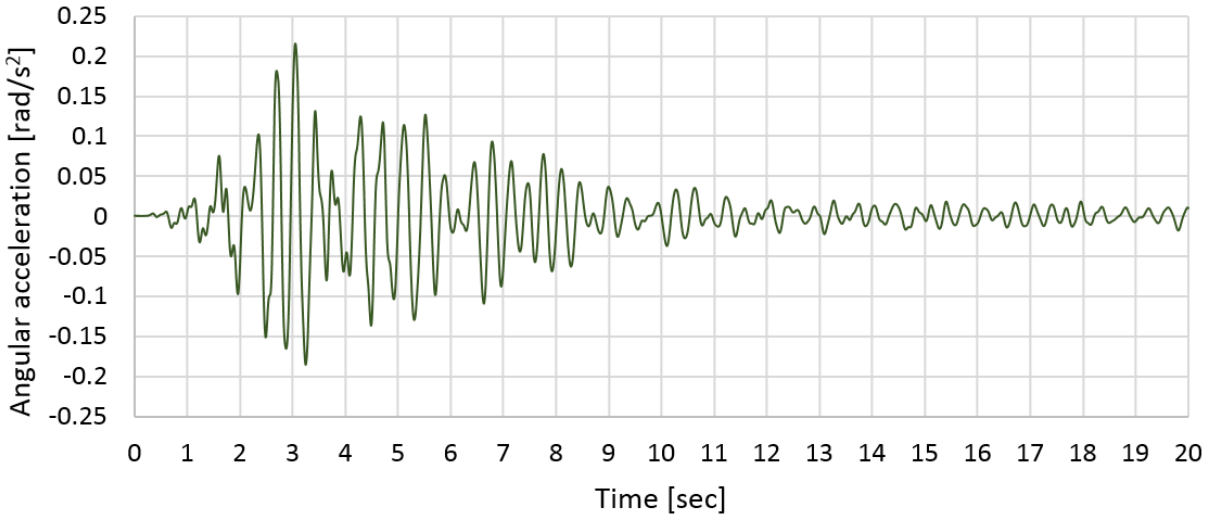

Figure 5.9: Recorded angular acceleration at the base of the manifold structure from PLAXIS 3D.

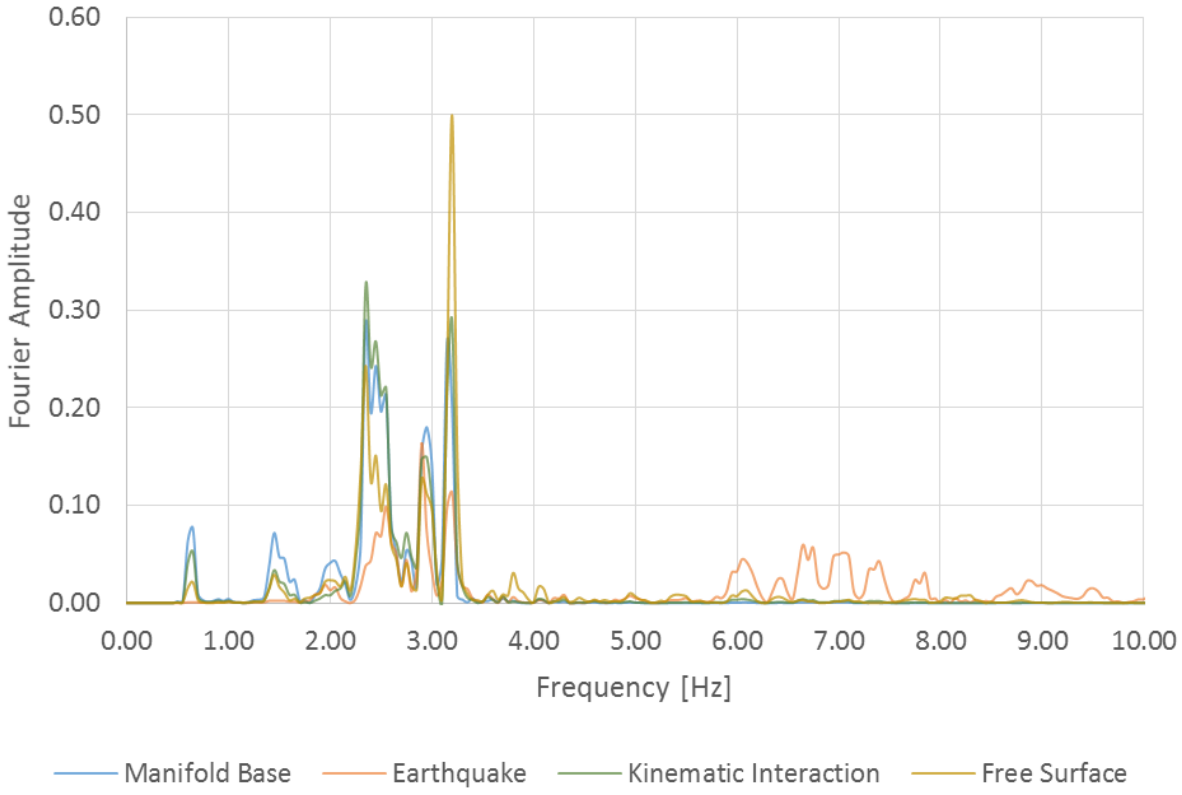

Figure 5.10: Compilation of the Fourier spectres of all output time series from PLAXIS 3D.

Ultimate Accelerations	
Analysis	**Ultimate Value**
Earthquake input	$\ddot{\delta}_{max} = 0.245\ g$
Free surface	$\ddot{\delta}_{max} = 0.374\ g$
Kinematic interaction	$\ddot{\delta}_{max} = 0.310\ g$
Manifold acceleration	$\ddot{\delta}_{max} = 0.232\ g$
Manifold angular acceleration	$\ddot{\theta}_{max} = 0.215\ rad/s^2$

Table 5.2: Compilation of the results from PLAXIS 3D analyses.

Ultimate horizontal displacement and rotation of the structure are found directly from the analysis and are presented in table 5.3.

Ultimate Dynamic Displacement and Rotation		
Horizontal displacement	$\delta_{ult} =$	4.9 cm
Rotation	$\theta_{ult} =$	0.0010 rad

Table 5.3: Ultimate response from PLAXIS 3D Analyses.

From the accelerations a set of ultimate dynamic loads working on the structure are approximated from the equations below.

$$Q_{dyn} = m \cdot \ddot{\delta} \qquad M_{dyn} = I \cdot \ddot{\theta} \tag{5.1}$$

The resulting loads are found from structure data in appendix B and are presented in the table below.

Ultimate Dynamic Loads and Displacements		
Inertial Mass Parameters	**Acceleration**	**Dynamic Load**
$m_{tot} = 534.4$ t	$\ddot{\delta}_{ult} = 0.232$ g	$Q_{dyn} = 1\ 227.9$ kN
$I_{tot} = 39\ 904.9$ tm^2	$\ddot{\theta}_{ult} = 0.215$ rad/s^2	M_{dyn}= 8 598.1 kNm

Table 5.4: Ultimate results from PLAXIS 3D Analyses.

Discussion of Manifold Results

The response of the manifold suggest a maximum lateral displacement of 4.9 cm and a maximum rotation of 0.0012 radians at the base of the structure. Maximum rotation occurs after 2.7 seconds which is a critical time period with high accelerations seen from both free-surface and kinematic interaction analyses. Maximum displacement occurs after 6.2 seconds which may seem a little late. Both displacement and rotations indicate that

there is a slight displacement drift towards the positive x-direction. Whether this is caused by accumulation of numerical error from integration operations or caused randomly by plastic deformations may have been determined using smoothing techniques. However, by inspecting the exaggerated deformed mesh in figure 5.8, it is seen that some plastic strains accumulates at shallow depths during the analysis. This sideways collapse is small but could cause some permanent deformation around the caisson. A more sophisticated horizontal boundary support would in this case be desirable.

Maximum lateral acceleration at the base was recorded to be 0.232 g and maximum angular acceleration is recorded to be 0.215 rad/s^2. Both ultimate accelerations are recorded in the critical phase of the analysis which is reasonable.

The decrease in accelerations from the kinematic interaction analysis was expected due to inertial effects. These effects cause a more mass dependent response unlike free surface and kinematic interaction analyses. The effect is clearly seen in the Fourier spectres (figure 5.10), where the analysis respond lowest of all in high frequencies but dominate the low frequency motions.

The dynamic loads was in this thesis determined with respect to inertial effects due to mass and accelerations. For comparison reasons and probably more accurate results other consideration could have been done. This may include measuring relative soil displacement around the caisson and calculate loads with respect to the soil stiffness. Or integrate the stress distribution over the caisson at critical stages during the analyses. However, there was not found any straight forward solution to this problem, nor was a lot of effort devoted to establish these alternative considerations.

5.2 SMNA-analyses

5.2.1 MODAN-input

Static Soil-Caisson Analysis

Results from the static soil-caisson interaction analyses are plotted in figure 5.11 and 5.12 on the next page. Essential ultimate values and stiffness parameters are presented in table 5.5. Figure 5.13 show how the static PLAXIS-model deformed at ultimate state.

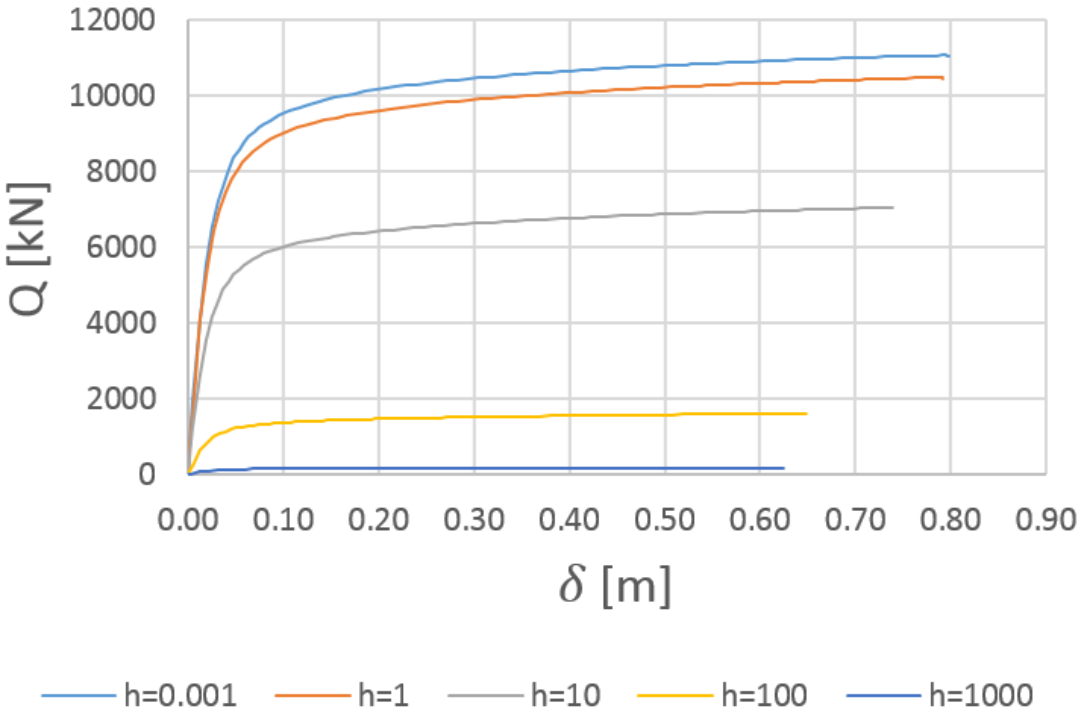

Figure 5.11: Back-bone curves for force-displacement relations.

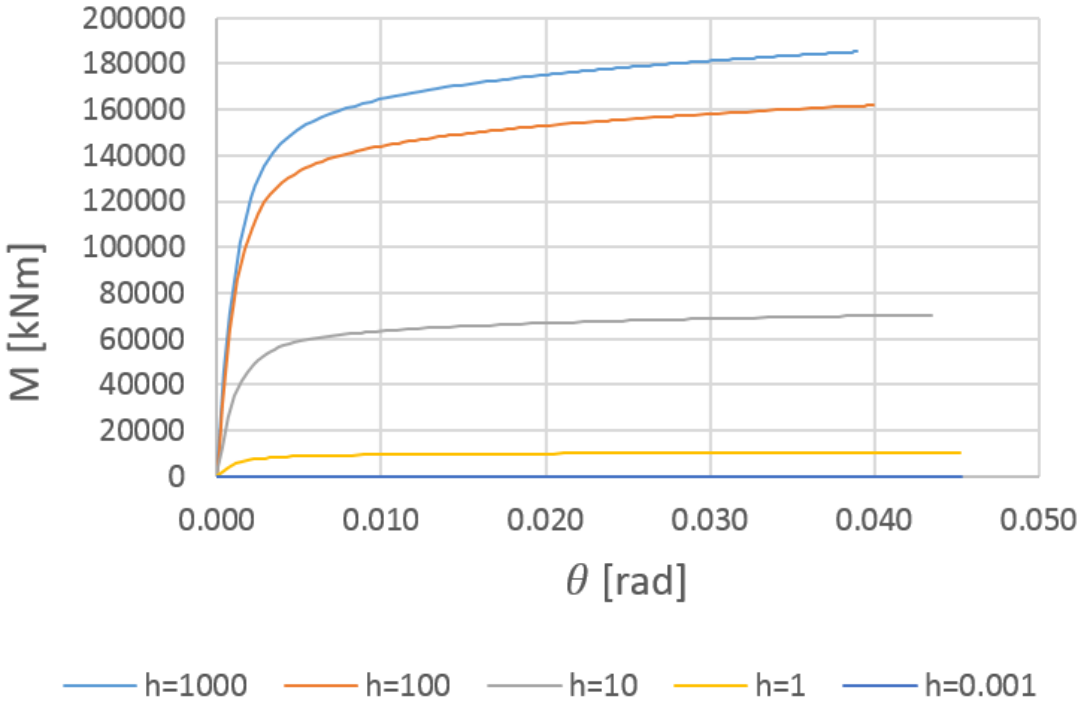

Figure 5.12: Back-bone curves for moment-rotation relations.

Back-Bone Parameters		
$K_{x,max,max}$	375 189.7	kN/m
$K_{\theta,max,max}$	99 852 984.0	kNm/rad
$Q_{ult,0}$	11 075.7	kN
$M_{ult,0}$	185 245.0	kNm
$\delta_{ult,max}$	0.793	m
$\delta_{ult,min}$	0.624	m
$\theta_{ult,max}$	0.045	rad
$\theta_{ult,min}$	0.039	rad

Table 5.5: Ultimate parameters used in MODAN analyses

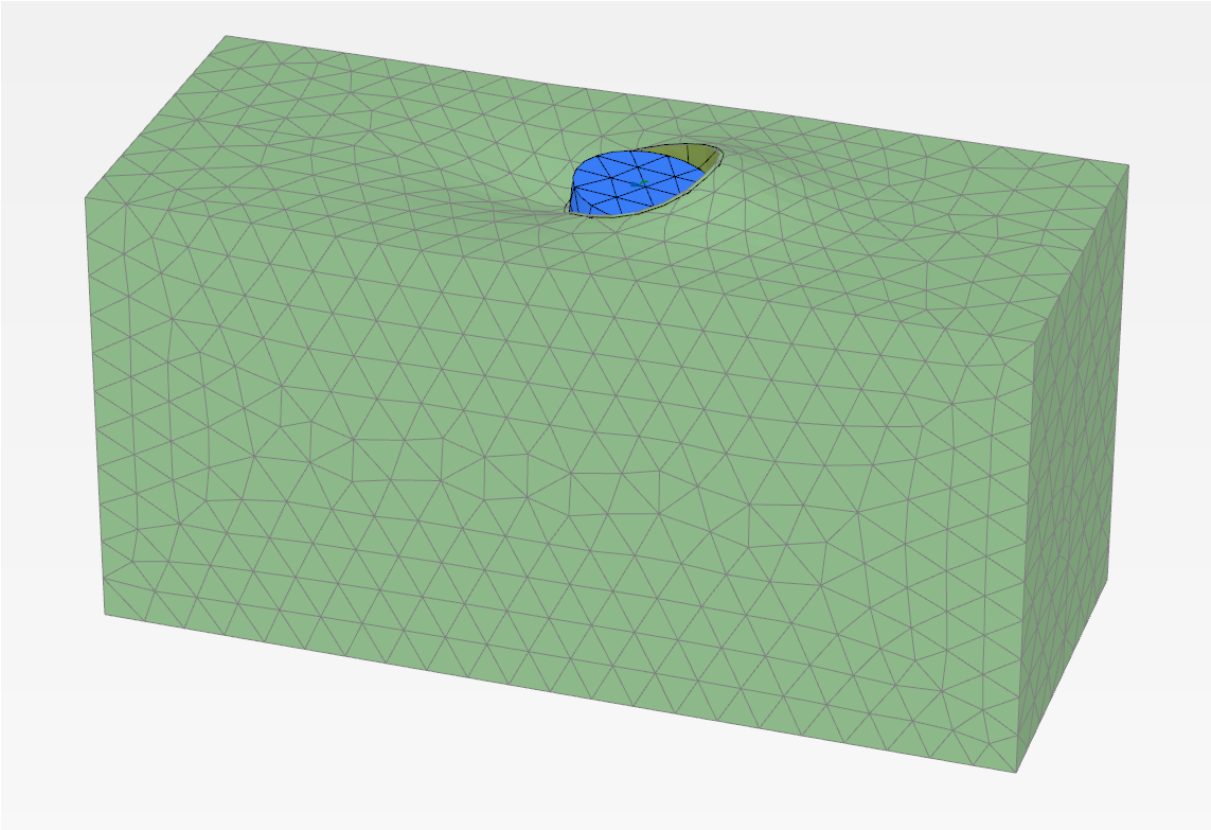

Figure 5.13: Deformed mesh from static analyses.

Failure Surface

The ultimate loads from the static analyses are plotted in the $Q - M$ diagram and compared to the proposed yield surface by Kay and Palix (2011), see figure 5.14. Since the failure criteria was manually defined the overshoot seen in the figure is not of importance in these analyses.

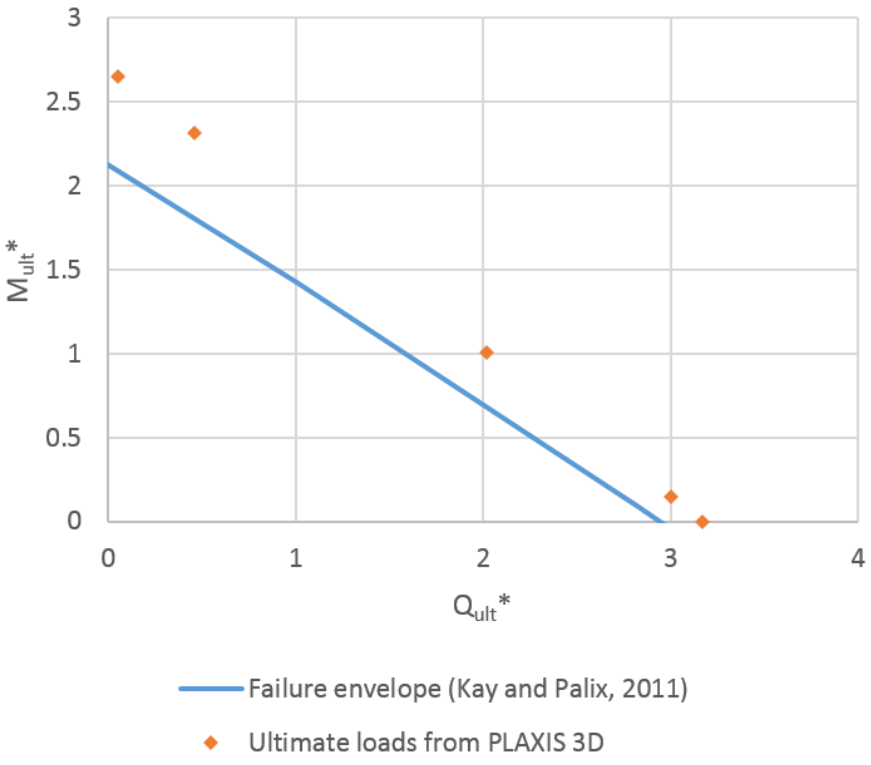

Figure 5.14: Failure surface.

Foundation Input Motion

The response spectra representing the equivalent foundation input motion, was constructed from the kinematic interaction recordings (figure 5.4). Pseudo spectral accelerations (PS_A) were generated in the curves manager in PLAXIS 3D. According to Newmark and Hall (1982) the response spectrum should be reduced if the PS_A exceed PGA over a certain period range. Accordingly, in the range $T = 0.28 - 0.44$ seconds the PS_A was scaled by the factor of $\alpha = 0.231$ multiplied by PGA. Both normalized and generated response spectres are plotted in figure 5.15.

$$PS_A = \alpha \cdot PGA = 3.21 \cdot 0.31 \ g = 0.995 \ g \tag{5.2}$$

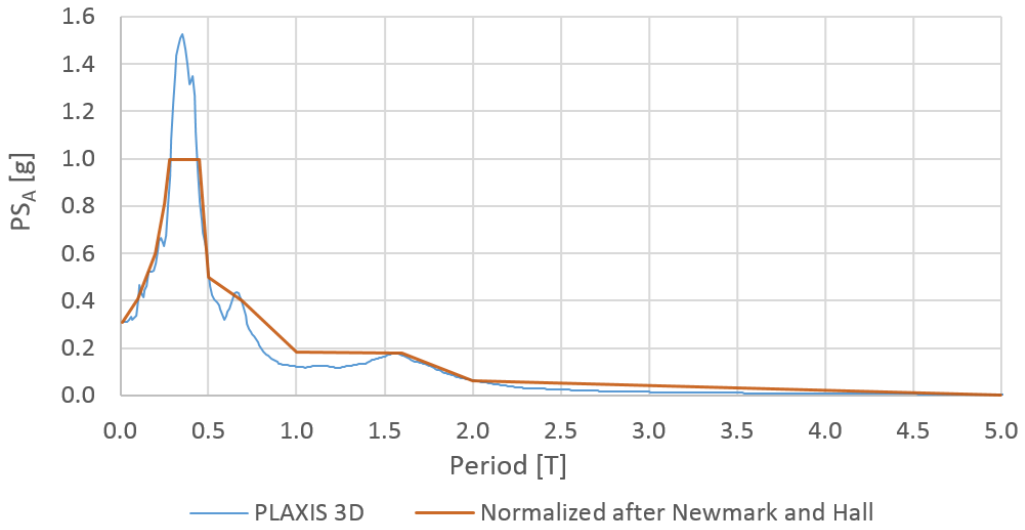

Figure 5.15: Real and normalized pseudo spectral response spectrum constructed from PLAXIS 3D

5.2.2 MODAN-analysis

Five initial analyses were conducted in MODAN. The first analysis was performed with inertial effects from the superstructure alone. The following analyses were done adding foundation mass, and increasing amount of soil added mass inside the caisson.

Three series of additional analyses were conducted in order to further study the effects of selected parameters. Accelerations, spring stiffness and mass moment of inertia were reduced aiming at a better consistency with previous results. A compilation of the input parameters, reduction factors and resulting output from initial and additional analyses is presented in table 5.6 on the next page.

MODAN-Results											
Mass Components		**Input**			**Reduction**				**Results**		
		m $[t]$	I_θ $[tm^2]$	h_c $[m]$	PS_A	K_δ	K_θ	I_θ	Q_{dyn} $[kN]$	M_{dyn} $[kNm]$	δ_{dyn} $[m]$	θ_{dyn} $[rad]$
Initial Analyses												
1	Manifold	411.9	15599.3	4.93					2392.0	63480.0	0.049	0.0028
2	Manifold+Caisson+1/7 soil	749.0	52132.0	0.81					7.3	164159.0	0.700	0.0280
3	Manifold+Caisson+3/7 soil	1171.0	65796.0	-1.54					11.5	174593.0	0.730	0.0339
4	Manifold+Caisson+5/7 soil	1593.0	98302.0	-4.16					16.0	175524.0	0.730	0.0360
5	Manifold+Caisson+7/7 soil	2016.0	156719.0	-6.87					22.0	182480.0	1.200	0.0740
Additional Analyses 1												
6	Manifold+Caisson	538.0	38947.9	2.03	0.8				5.0	164205.0	0.710	0.0213
7	Manifold+Caisson	538.0	38947.9	2.03	0.5				422.00	92152.0	0.045	0.0022
8	Manifold+Caisson	538.0	38947.9	2.03	0.2				195.0	37261.0	1.100	0.0005
Additional Analyses 2												
9	Manifold	411.9	15599.3	4.93	0.5				3400.0	34593.0	0.035	0.0022
10	Manifold	411.9	15599.3	4.93	0.7				2764.0	45615.0	0.037	0.0022
Additional Analyses 3												
11	Manifold	411.9	15599.3	4.93		1	1	0.10	4504.0	19106.0	0.035	0.0022
12	Manifold	411.9	15599.3	4.93		1	1	0.01	4111.0	16523.0	0.028	0.0017
13	Manifold	411.9	15599.3	4.93		1	0.33	0.01	3737.0	15095.0	0.024	0.0042
14	Manifold	411.9	15599.3	4.93		1	0.33	1.00	1315.0	93342.0	0.067	0.0092
15	Manifold	411.9	15599.3	4.93		1	0.1	1.00	6164.0	37735.0	0.140	0.0025
16	Manifold	411.9	15599.3	4.93		1	0.33	0.10	4114.0	18091.0	0.029	0.0051
17	Manifold	411.9	15599.3	4.93		0.25	0.33	0.10	2003.0	9749.0	0.039	0.0019

Table 5.6: Results from initial and additional MODAN-analyses.

Discussion of MODAN-Results

All the initial analyses gave abnormally high dynamic moments. At the same time the lateral force dropped to very low values when adding soil mass. Increasing the mass will normally cause increased natural periods, hence lower input accelerations for low rise structures. However, these results suggest that the variable spring stiffness cause an unbalanced response. Initial max spring stiffness ratio of $\frac{K_{\theta,max}}{K_{\delta,max,max}} = 266$ was noted to be rather large and may affect the load ratio to grow during the iterations. This causes low lateral stiffness and high rotation stiffness. Increasing inertial parameters then rapidly cause excessively large moments on the structure while forces degrade, as shown by the results.

The analyses show divergent tendencies and indicate that adding soil mass to the model cause an unstable effect in the dynamic system. Based on this, additional parametric analyses were conducted, in order to study other effects that may provide a more stable behavior.

First series of additional analyses was conducted with inertial effects from manifold and caisson. Reducing input accelerations was not sufficient to give proper results (test 6, 7 and 8). Only considering the inertial effects of the manifold and reducing accelerations (2^{nd} series) gave more adequate dynamic forces, but still excessive dynamic moments (tests 6, 9 and 10).

In the 3^{rd} series of additional analyses the mass moment of inertia and initial stiffness parameters was reduced. Scaling the mass moment of inertia by a factor of 0.1 (test 11) gave a significant reduction of about 60% in dynamic moments. Further reduction of 0.001 gave less significant changes (test 12). Test 13 only gave a small reduction in loads reducing rotation stiffness by a factor of 0.33, rotation was doubled. Test 14 and 15 first show an large increase in moment when reducing the rotation stiffness by a factor of 0.33. Further reduction to 0.1 gave a significant reduction in moments and rotations.

Best consistency with previous results was obtained using 10% of the I_θ and scaling the K_δ and K_θ by 0.25 and 0.33 respectively (test 17).

In modal analyses the added mass is considered to act together with the structure as a rigid body, while the flexibility of the structure and of the soil inside and outside the caisson may reduce the "acting" mass moment of inertia. This is shown by the fact that the closest results PLAXIS/MODAN were obtained when the chosen ratio I_θ/m was a minimum.

The additional parametric analyses suggest that the spring stiffness ratio are too high causing unstable responses. Reducing mass moment of inertia and rotational spring stiffness provided better stability in the system. A factor of 1.32 between rotational and translational stiffness gave best fit with previous results.

5.2.3 Comparing PLAXIS 3D and MODAN

Results from the case study proved that obtaining compliance between the two approaches could not be obtained from adding soil added mass alone. These analyses gave peculiar results not suitable for proposing any parameter values. For this purpose the model need to be further developed.

Better compliance was obtained by manipulating a set of parameters, including spring stiffness and inertial effects in MODAN. The best results were obtained by neglecting foundation mass and soil added mass, reduce mass moment of inertia and reduce both stiffness parameters. A comparison between the analyses are presented in the table below.

Compared Results				
Analysis	Q_{dyn} $[kN]$	δ_{dyn} $[m]$	M_{dyn} $[kNm]$	θ_{dyn} $[rad]$
PLAXIS 3D	1227.9	0.059	8 598.1	0.0010
MODAN	2003.0	0.039	9 749.0	0.0019
Ratio PLAXIS/MODAN	0.613	1.51	0.882	0.579

Table 5.7: Comparison of PLAXIS 3D and MODAN results.

The parametric study shows that MODAN results are generally more conservative than PLAXIS. The earthquake loads and displacements from MODAN (except horizontal translation) are about 15%- 60% higher than those from PLAXIS.

Comparing the two models proved to be more intricate than initially assumed. Apart from known differences between time-domain and frequency-domain solutions, the discrepancy between the two models can be attributed to the following facts:

- Static soil-caisson interaction analyses conducted in PLAXIS 3D, provides too high stiffness values to be used in MODAN.
- The effect of the two modes of vibration may not be equally contributing to the earthquake loading. Deviations may occur as the MODAN caisson is completely rigid, while PLAXIS caisson are modeled as a steel structure with soil inside.
- Retrieving static loads from inertial considerations in dynamic time domain analyses may not give an adequate representation of actual loads working on the structure.
- The depth of application of the soil motion to MODAN is not necessarily best at the top plate of the foundation.

It is difficult to determine from the field of displacements during earthquake loading in PLAXIS how the soil movements are transmitted to the caisson. In modal analysis the response acceleration spectrum is applied at the end of soil-structure springs (seabed level) which may differ from the soil-caisson movement transfer simulated by PLAXIS. This issue must be further studied.

Chapter 6

Conclusions and Further Work

6.1 Summary and Conclusions

In this thesis two fundamentally different models of dynamic analyses were compared. A comprehensive numerical FEM-model provided indicative results. Then a parametric study was conducted to calibrate mass parameters in a simplified method based on non-linear modal analysis. Both models analyzed the dynamic response of a subsea manifold structure on a closed caisson foundation, founded on soft North Sea clay.

Numerical analyses were carried out in PLAXIS 3D and conducted in three stages. Initial free-field analyses gave results within small error from site response theory in harmonic analyses. Free-surface earthquake response showed proper frequency filtering and amplification, according to theory. No significant boundary issues was observed. Next, kinematic interaction was analysed introducing a massless caisson into the soil. Accelerations was recorded at the top of the foundation during an earthquake, and showed realistic soil-structure interaction effects.

The primary FEM-analysis involved installing the manifold structure on the foundation and apply mass. Response was recorded at the base and top of the manifold during the same earthquake as in the preliminary analyses. Maximum response was observed to be 4.9 cm and 0.0010 radians in lateral displacement and rocking. In order to compare the two models inertial considerations were done to obtain equivalent loads from the numerical results. Maximum accelerations gave $Q_{dyn} = 1\ 227.9\ kN$ and $M_{dyn} = 8\ 598.1\ kNm$. Although some simplifications in material model and damping properties provide some uncertainties to the realistic behavior, the results gave sufficiently accuracy to be used in the parametric study.

The simplified SMNA-method was used to analyse the same manifold structure. The analyses were conducted in MODAN, a code developed at Multiconsult, executing the SMNA-procedure. Secant stiffness relations was obtained through static soil-caisson analyses in PLAXIS 3D and used as MODAN-input. A normalized pseudo spectral response spectrum from the kinematic analysis was used as dynamic input.

First five initial tests was carried out, gradually increasing added soil mass inside the caisson. The results gave unstable results including excessively large dynamic moments and very low lateral forces. The analyses clearly showed that adding soil added mass to the system alone, was not applicable in this case.

Based on initial tests 17 additional analyses was conducted. The analyses was set up as an effort to stabilize and study selected parameters. Reducing accelerations gave convergence, but still unsatisfactory high load ratio. In further tests reducing both spring stiffness and mass moment of inertia gave results within realistic magnitudes. Best compliance was achieved by neglecting soil added mass, reducing mass moment of inertia by a factor of 0.1, and reducing soil stiffness by factors of 0.25 and 0.33 in translation and rotation respectively. Best estimate predicted $\delta_{dyn} = 0.039\ m$, $\theta_{dyn} = 0.0019\ radians$, $Q_{dyn} = 2003\ kN$ and $M_{dyn} = 9749\ kNm$. Thus, in the range of -50% to +40% compliance to the numerical model.

According to this study the simplified SMNA-method is currently not applicable to handle soil added mass, based on the considerations done in this study. Uncertainties are especially associated with too high ratios between rotational and translational soil stiffness acquired from numerical analyses.

In order to obtain results within a reasonable range, three measures needs to be adopted. (1) A reduced mass moment of inertia, only including the manifold structure must be used. (2) Reduced stiffness of soil support must be used. (3) The ration between rotation and translation stiffness must be increased by a factor of 1.32.

6.2 Further Work

Further research is needed to fully understand the differences between the two methods and to evaluate the level of conservatism associated with analyses, using the SMNA-approach.

During this work the writer and supervisors have realized that the study involve effects other than those considered from the start. Particularly the soil stiffness considerations must be better adapted to represent dynamic conditions. A proposal for further work would be to study how the static stiffness parameters evolve under dynamic loading, in order to determine which reduction to consider in a modal analysis.

More effort should also be done studying the modal contributions in the frequency analysis. These are not necessarily equally contributing to the overall response and may have a significant impact on dynamic behavior related to added mass in a completely rigid structure.

Bibliography

Athanasiu, C., Bye, A., Tistel, J., Ribe, A., Arnesen, K., Feizikhanhandi, S., and Sørlie, E. (2015). Simplified earthquake analysis for wind turbines and subsea structures on closed caisson foundations. *Frontiers in Offshore Geotechnics III*, page 221.

Brandt, M. (2014). Earthquake analysis of subsea structure on caisson foundation using 3d finite element solution.

BuildingResearchInstitute (2015). Dynamic behavior of soil.

Chopra, A. K. (2007). *Dynamics of structures : theory and applications to earthquake engineering*. Prentice-Hall international series in civil engineering and engineering mechanics. Prentice Hall, 3th ed. edition.

Dobry, R. (2014). Simplified methods in soil dynamics. *Soil Dynamics and Earthquake Engineering*, 61:246–268.

Elsabee, F. (1975). *Static stiffness coefficients for circular foundations embedded in an elastic medium.* PhD thesis, Massachusetts Institute of Technology.

Gerolymos, N. and Gazetas, G. (2006). Winkler model for lateral response of rigid caisson foundations in linear soil. *Soil Dynamics and Earthquake Engineering*, 26(5):347–361.

Hashash, Y. M. and Park, D. (2002). Viscous damping formulation and high frequency motion propagation in non-linear site response analysis. *Soil Dynamics and Earthquake Engineering*, 22(7):611–624.

Ishihara, K. (1996). *Soil behaviour in earthquake geotechnics*. Clarendon Press; Oxford University Press.

Kausel, E., Whitman, R. V., Morray, J. P., and Elsabee, F. (1978). The spring method for embedded foundations. *Nuclear Engineering and Design*, 48(2):377–392.

Kay, S. and Palix, E. (2011). Caisson capacity in clay: Vhm resistance envelope: Part 3—extension to shallow foundations. In *ASME 2011 30th International Conference on Ocean, Offshore and Arctic Engineering*, pages 789–798. American Society of Mechanical Engineers.

Kramer, S. L. (1996). *Geotechnical earthquake engineering*, volume 80. Prentice Hall.

Lindman, E. (1975). "free-space" boundary conditions for the time dependent wave equation. *Journal of computational physics*, 18(1):66–78.

Liu, G.-R. and Quek, S. S. (2013). *The finite element method: a practical course*. Butterworth-Heinemann.

Luco, J. E. and Wong, H. L. (1987). Seismic response of foundations embedded in a layered half-space. 15(2):233–247.

Lysmer, J. and Kuhlemeyer, R. L. (1969). Finite dynamic model for infinite media. 95(4):859–878.

Meyer, V. (2015). *Frontiers in Offshore Geotechnics III*. CRC Press.

Newmark, N. M. (1959). A method of computation for structural dynamics. *Journal of the engineering mechanics division*, 85(3):67–94.

Newmark, N. M. and Hall, W. J. (1982). Earthquake spectra and design. *Earth System Dynamics*, 1.

Norge, S. (2004). Ns-en 1998-1: 2004+ na: 2008 eurokode 8: Prosjektering av konstuksjoner for seismisk pavirkning del 1: Allmenne regler, seismiske laster og regler for bygninger. *Standard Norge*.

Offshore Center Danmark (2016). Offshore wind farms.

QuakeManager (2015). What is a response spectrum.

Richart, F. E., Hall, J. R., and Woods, R. D. (1970). Vibrations of soils and foundations.

Senpere, D., Auvergne, G. A., et al. (1982). Suction anchor piles-a proven alternative to driving or drilling. In *Offshore Technology Conference*. Offshore Technology Conference.

SubseaWorldNews (2015). Rorewind to use innovative met masts foundation design for dogger bank.

Tjelta, T., Guttormsen, T., Hermstad, J., et al. (1986). Large-scale penetration test at a deepwater site. In *Offshore Technology Conference*. Offshore Technology Conference.

Tjelta, T. I. (2001). Suction piles: Their position and application today. International Society of Offshore and Polar Engineers.

Transparency Market Research (2015). Subsea manifolds market - global industry analysis, size, share, growth, trends, and forecast 2014 - 2020.

Wolf, J. P. (1985). *Dynamic soil-structure interaction*. Prentice Hall int.

Wolf, J. P. (1994). *Foundation Vibration Analysis Using Simple Physical Models*. Pearson Education.

Nomenclature

Greek Letters

α	Mass proportional Rayleigh coefficient
β	Stiffness proportional Rayleigh coefficient
δ	Lateral degree of freedom
γ	Volumetric unit weight
ν	Poisson's ratio
ω	Angular frequency
ω_n	Angular natural frequency
ρ	Volumetric mass density
σ	Normal stress
τ	Shear stress
θ	Rotational degree of freedom
ξ	Damping ratio

Latin Letters

$\ddot{u}$	Horizontal acceleration
$\ddot{u}_g$	Ground acceleration
$\tilde{K}_n$	Modal stiffness
$\tilde{M}_n$	Modal mass
$\tilde{Q}_n$	Modal force
A_n	Fourier amplitude
c	One degree of freedom damping coefficient
E	Young's Modulus
F	Force
f	Frequency
$F(\omega)$	The site response transfer function

f_n	Natural frequency
G	Shear modulus
g	Gravitational acceleration
G_{max}	Maximum shear modulus for small strains
G_{sec}	Secant shear modulus
G_{tan}	Tangential shear modulus
H	Height
h_c	Center of gravity
i	The imaginary unit
I_θ	Mass moment of inertia
k	One degree of freedom stiffness coefficient
K_δ	Lateral stiffness coefficient
K_θ	Rotational stiffness coefficient
$K_{\delta,\theta}$	Coupled stiffness coefficient
M	Overturning moment
m	One degree of freedom mass coefficient
PS_A	Pseudo spectral acceleration
q_n	Modal degree of freedom
S_A	Acceleration response spectrum
S_u	Undrained shear strength
T	Period
t	Time in seconds
T_n	Natural period
u	Horizontal displacement
V_p	Primary or compressional wave velocity
V_s	Secondary or shear wave velocity
W	Weigth

Matrices and Vectors

$\boldsymbol{\varphi_n}$	The system mode shape
$\boldsymbol{l}$	Unit vector
$\mathbf{C}$	Damping matrix
$\mathbf{K}$	Stiffness matrix
$\mathbf{M}$	Mass matrix

Q	Load vector
Others	
det	The matrix determinant
Im	Imaginary part of an imaginary number
Re	Real part of an imaginary number
Abbreviations	
CCF	Closed Caisson Foundation
CPU	Central Processing Unit
FEM	Finite Element Method
PGA	Peak Ground Acceleration
PS_A	Pseudo Spectral Acceleration
$SDOF$	Single Degree Of Freedom
$SMNA$	Simplified Modal Non-linear Analysis
SSI	Soil-Structure Interaction

List of Figures

List of Tables

Appendix A

Soil Profiles

The soil parameters are provided by Multiconsult ASA and have been used in preliminary research. The material properties represent a soft North Sea clay.

Soil Model	
General	
Depth	0-60 meters
Water Table	0 m
Material Model	Mohr-Coulomb
Drainage	Undrained B
Unit Weight	$\gamma = 16.4$ kN/m^3
K_0'	$K_{0,x} = K_{0,y} = 0.6$
Stiffness	
Youngs Modulus	E' = 2575 kPa
	E'$_{\text{inc}}$ = 2788 kPa/m $\cdot$ z
Poisson's Ratio	$\nu' = 0.35$
Shear Modulus	G = 953.7 kPa
Initial shear wave velocity	$V_s = 23.9$ m/s
Strength	
Shear Strength	S$_{\text{u}}$ = 1.87 kPa
	S$_{\text{u,inc}}$ = 2.025 kPa/m $\cdot$ z
Tensile strength	0 kPa
Damping	
Rayleigh Damping	ξ=5%
	$f_1 = 0.4$ Hz
	$f_2 = 7.0$ Hz
	$\alpha = 0.2377$
	$\beta = 2.151 \cdot 10^{-3}$

Table A.1: Soil parameters

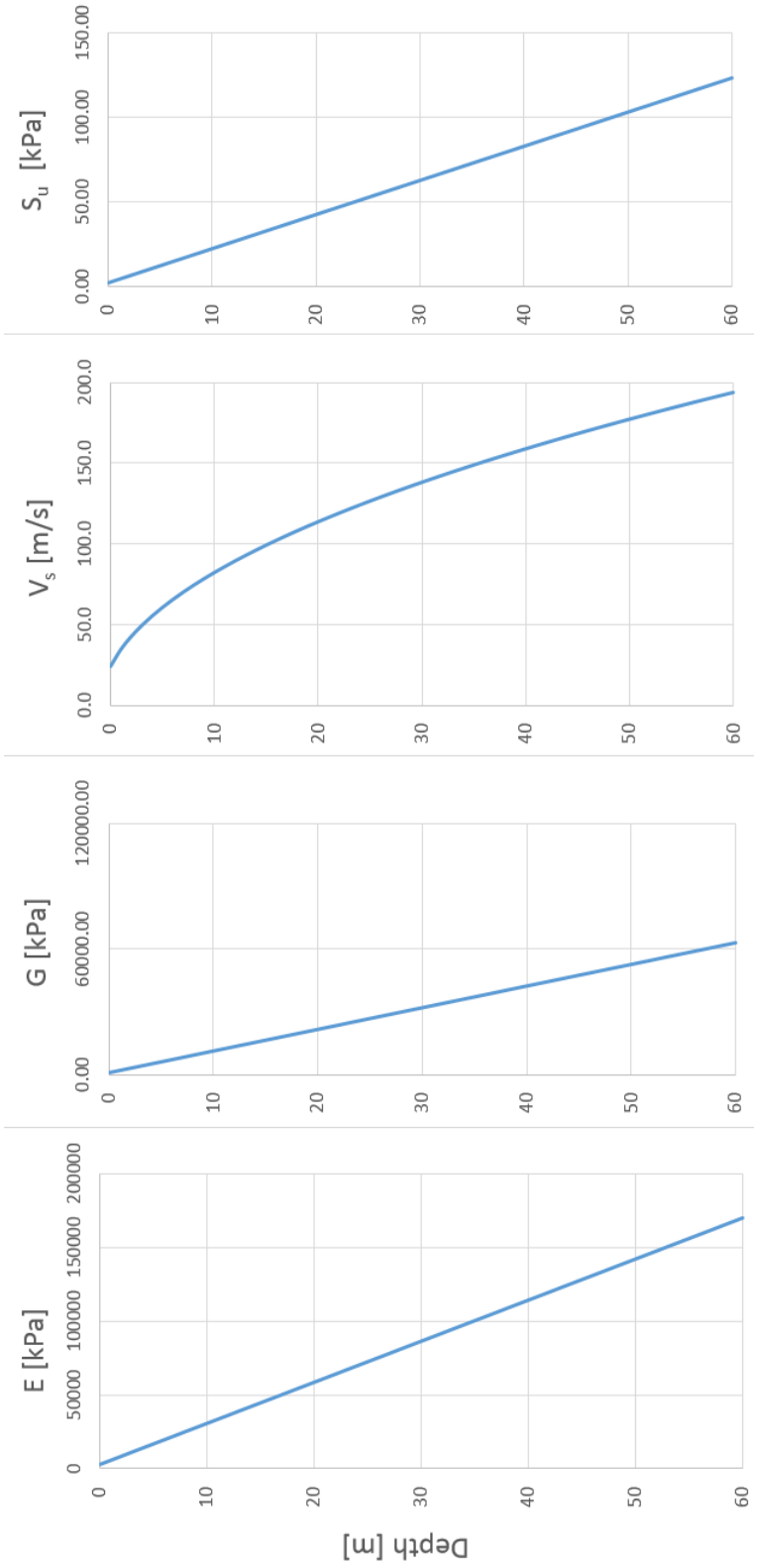

Figure A.1: Soil profile of PLAXIS 3D model

Appendix B

Structure Data

B.1 Structure Measurements

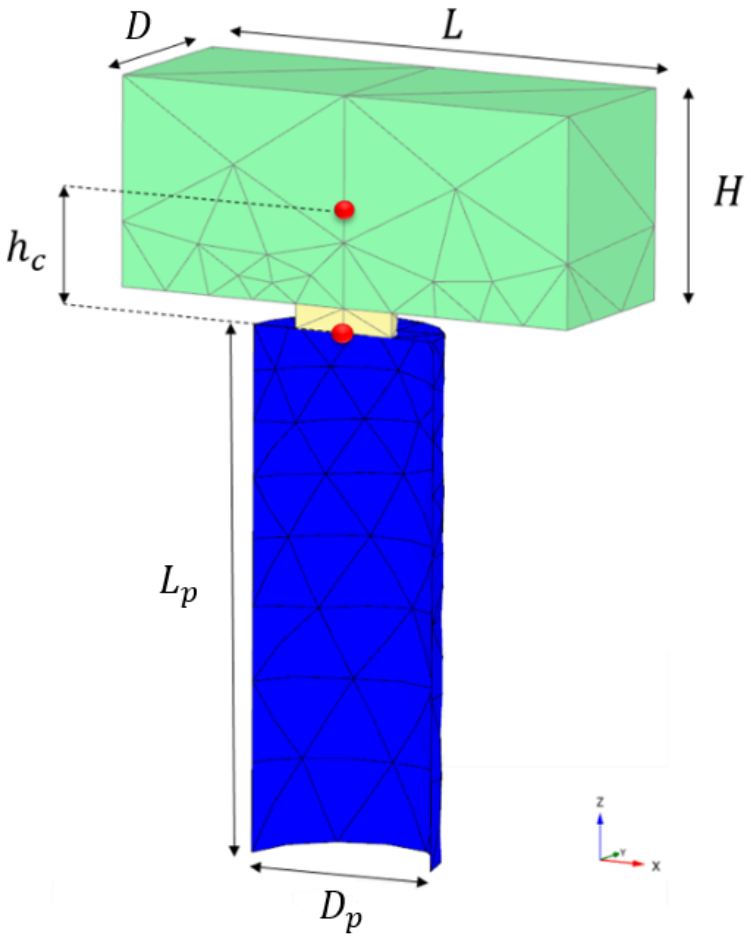

Figure B.1: Geometric measurements of structure.

B.2 Real Structure

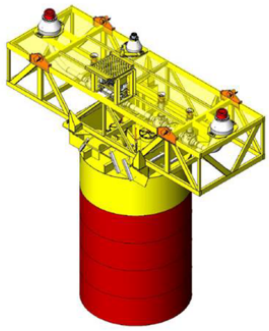

Real Structure	Length (m)	Depth (m)	Height (m)	Dp (m)	Lp (m)	Skirt thickness (m)	Top plate thickness (m)	Volume (m^3)	Υ (kN/m^3)	Weight (kN)	Center of gravity (m)	Mass (t)	I_θ (tm^2)
Manifold	18.90	14.20	9.86	-	-	-	-	2497.14	1.62	4040.99	4.93	411.93	15599.28
Foundation Skirt	-	-	-	7.50	20.00	0.03	-	14.14	78.00	1102.70	-10.00	112.41	4530.91
Top plate	-	-	-	7.50	-	-	0.04	1.77	78.00	137.84	0.00	14.05	49.40
Total	-	-	-	-	-	-	-	2511.28	-	5281.53	1.68	538.38	39881.10

Figure B.2: Real structure geometry and physical parameters.

B.3 PLAXIS 3D Structure

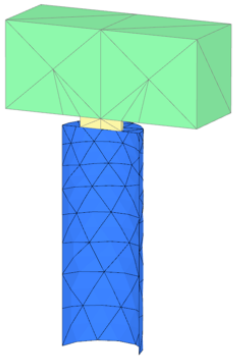

PLAXIS Structure	Length (m)	Depth (m)	Height (m)	Dp (m)	Lp (m)	Skirt thickness (m)	Top plate thickness (m)	Volume (m^3)	Υ (kN/m^3)	Weight (kN)	Center of gravity (m)	Mass (t)	I_θ (tm^2)
Manifold	18.90	14.20	8.00	-	-	-	-	2497.14	1.62	4040.99	4.93	411.93	15599.28
Foundation Skirt	-	-	-	7.50	20.00	0.03	-	14.14	78.00	1102.70	-10.00	112.41	4530.91
Top plate	-	-	-	7.50	-	-	0.04	1.77	78.00	137.84	0.00	14.05	49.40
Total	-	-	-	-	-	-	-	2511.28	-	5281.53	1.68	538.38	39904.84

Figure B.3: PLAXIS 3D equivalent geometry and physical parameters.

Appendix C

PLAXIS 3D Setup

General setup information for the different PLAXIS 3D analyses are presented here.

C.1 Harmonic Free-Field

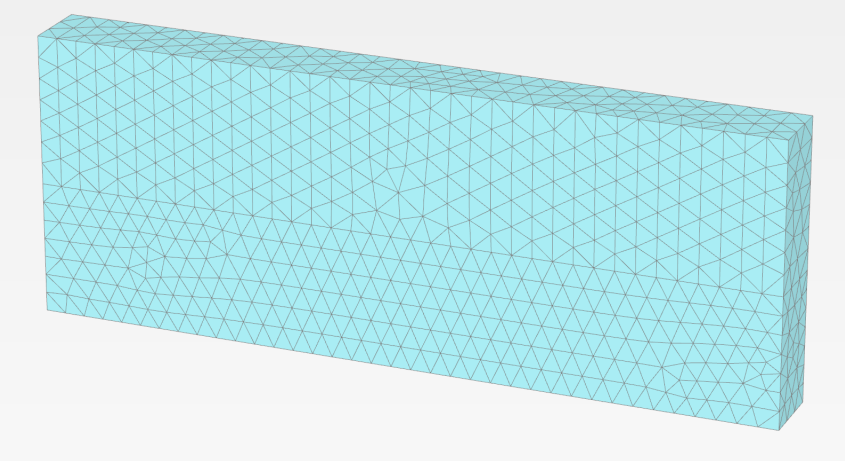

Figure C.1: Linear elastic soil model used in harmonic free field analyses

Model Information	
Material model	Linear Elastic
Mesh refinement	Medium
Coarseness factor	0.70
Number of elements	8738
Elements	10-noded tetrahedral
Average element size	4.05 m

Table C.1: Elastic soil model

Phases			
Identification	Phase	Start from	Calculation type
Initial phase	Initial phase	-	K_0'
Dynamic loading	Phase 0	Initial phase	Dynamic

Table C.2: Calculation phases in harmonic free-field analyses.

C.2 Free-Field Earthquake

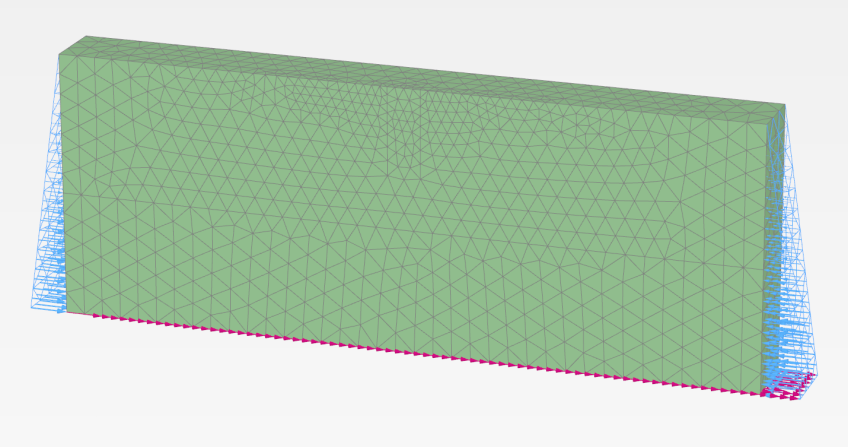

Figure C.2: Mohr-Coulomb soil model used in free field analyses.

Model Information	
Material model	Mohr-Coulomb
Mesh refinement	Medium
Coarseness factor	0.70
Number of elements	10756
Elements	10-noded tetrahedral
Average element size	3.92 m

Table C.3: Mohr-Coulomb free-field model

Phases			
Identification	Phase	Start from	Calculation type
Initial phase	Initial phase	-	K_0'
Apply side support	Phase 0	Initial Phase	Plastic
Dynamic loading	Phase 1	Phase 0	Dynamic

Table C.4: Calculation phases in earthquake free-field analyses.

C.3 Kinematic Interaction Analysis

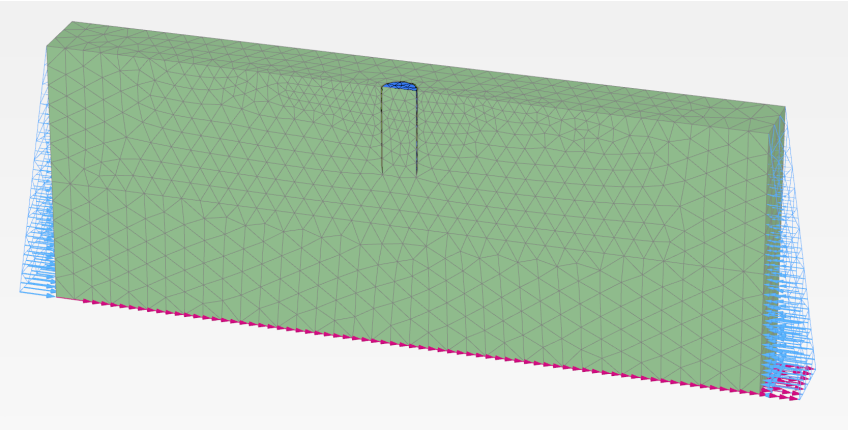

Figure C.3: Mohr-Coulomb soil model used in kinematic interaction analysis.

Model Information		
	Soil	Closed Caisson
Material model	Mohr-Coulomb	Linear Elastic
Mesh refinement	Medium	Medium
Coarseness factor	0.70	0.50
Number of soil elements	10756	-
Elements	10-noded Tetrahedral	6-noded Plate
Average element size	3.92 m	-

Table C.5: Mohr-Coulomb kinematic interaction model information.

Phases			
Identification	Phase	Start from	Calculation type
Initial phase	Initial phase	-	K_0'
Caisson installation	Phase 0	Initial phase	Plastic (drained)
Apply side support	Phase 1	Phase 0	Plastic
Dynamic loading	Phase 2	Phase Phase 1	Dynamic

Table C.6: Calculation phases in kinematic interaction analyses.

C.4 Manifold Analysis

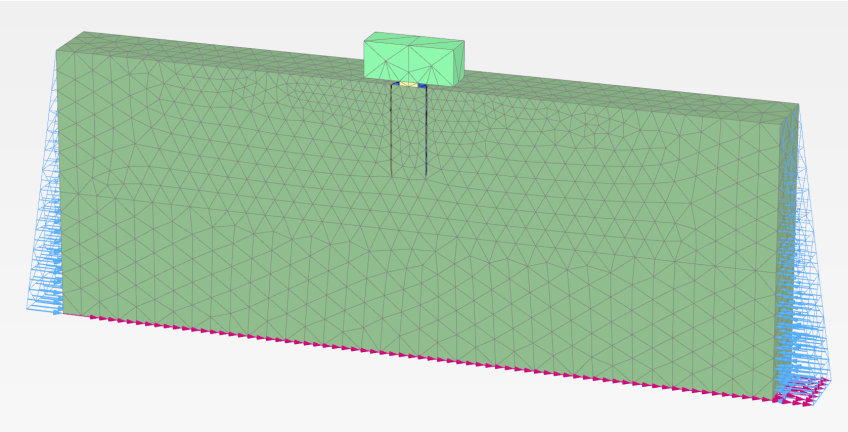

Figure C.4: Mohr-Coulomb soil model used in manifold analysis.

Model Information			
	Soil	Closed Caisson	Manifold
Material model	Mohr-Coulomb	Linear Elastic	Linear Elastic
Mesh refinement	Medium	Medium	Medium
Coarseness factor	0.70	0.50	4.0
Number of soil elements	10756	-	-
Elements	10-noded Tetrahedral	6-noded Plate	10-noded Tetrahedral
Average element size	3.92 m	-	-

Table C.7: Mohr-Coulomb manifold model information.

Phases			
Identification	Phase	Start from	Calculation type
Initial phase	Initial phase	-	K_0'
Structure installation	Phase 0	Initial phase	Plastic (drained)
Apply side support	Phase 1	Phase 0	Plastic
Dynamic loading	Phase 2	Phase Phase 1	Dynamic

Table C.8: Calculation phases in kinematic interaction analyses.

C.5 Static Analysis

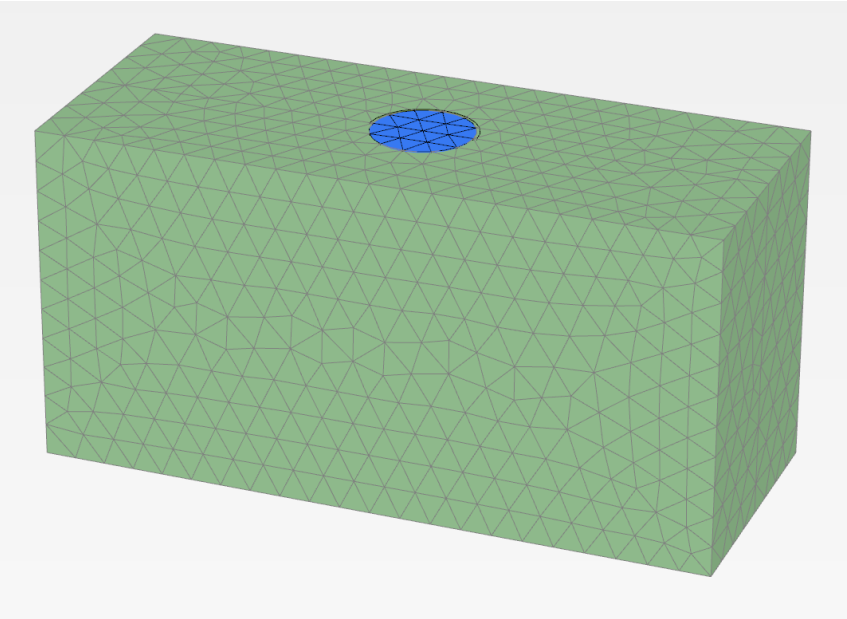

Figure C.5: Mohr-Coulomb soil model used in static analysis.

Model Information		
	Soil	Closed Caisson
Material model	Mohr-Coulomb	Linear Elastic
Linear Elastic		
Mesh refinement	Medium	Medium
Coarseness factor	0.50	0.45
Number of soil elements	13006	-
-		
Elements	10-noded	6-noded
	Tetrahedral	Plate
Average element size	1.39 m	-

Table C.9: Mohr-Coulomb static model information.

Phases			
Identification	Phase	Start from	Calculation type
Initial phase	Initial phase	-	K_0'
Structure installation	Phase 0	Initial phase	Plastic (drained)
Apply loads	Phase 1	Phase 0	Plastic

Table C.10: Calculation phases in static analyses.